UNDERSTANDING UNEXPECTED REACTIONS OF HYDROXYBENZYLTHIAMIN

By

John Francis Lam

A Thesis Submitted in Conformity with the Requirements
for the Degree of Doctor of Philosophy,
Graduate Department of Chemistry, in the
University of Toronto

Abstract

Understanding Unexpected Reactions of Hydroxybenzylthiamin

Doctor of Philosophy, 1995
John Francis Lam
Department of Chemistry, University of Toronto

2-(1-Hydroxybenzyl)-thiamin (HBzT) is the first covalent adduct formed in the thiamin-catalyzed formation of benzoin. HBzT is the conjugate acid of the product of the reversible reaction of the thiamin ylid and benzaldehyde in weakly basic solutions.

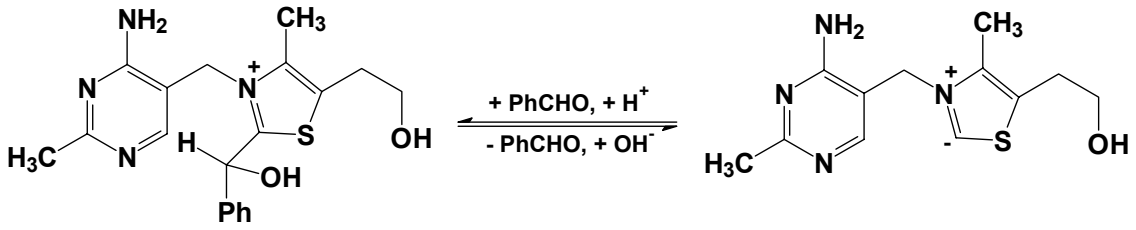

HBzT **Thiamin ylid**

However, in neutral and acidic solutions, reaction of HBzT does not produce benzaldehyde and thiamin. Instead, an unexpected fragmentation reaction produces 2-benzoyl-4-methyl-5-(2-hydroxyethyl)-thiazole (PTK) and 4-amino-3,5-dimethyl-pyrimidine (DMP). This is an undesirable reaction because it destroys the thiamin catalyst in the process.

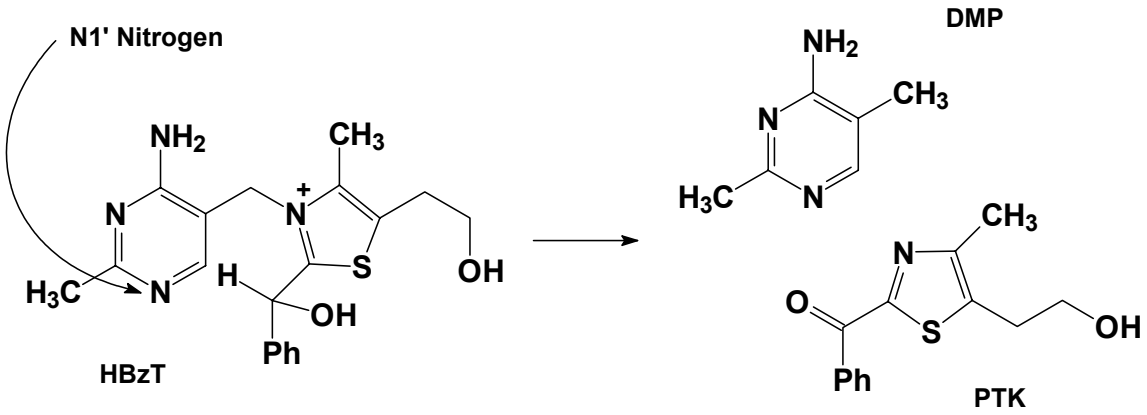

The mechanism of fragmentation was analyzed by product and kinetic studies. pH-Rate profiles for the fragmentation of HBzT reveal thermodynamic and kinetic pK_a's.

N_1'-Methyl-2-(1-hydroxybenzyl)-thiamin (NMHBzT) is a related derivative that has an undissociable positive charge on N_1'. It lacks a thermodynamic pK_a in the range of our study, and fragments with a linear pH-rate profile. From analysis of these data, propose that HBzT fragments by two low barrier pathways with the pyrimidine protonated, and by a single higher barrier pathway from the unprotonated species.

The key intermediate **1** in all the fragmentation pathways has a proton on N_3 which adds to the carbanionic site generated by cleavage of the carbon-N_3 bond.

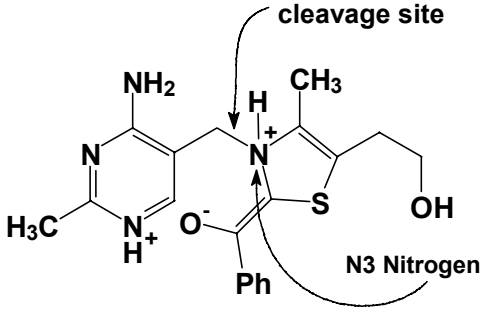

1

Since the concentration of **1** relative to the reactant increases with increasing pH, the rate of fragmentation of HBzT also increases with pH. The higher barrier pathway involves the intermediate lacking a proton on the pyrimidine, producing a higher energy leaving group.

Other factors control the fragmentation pathway in thiamin derivatives. Increased acidity of the $C_{2\alpha}$ proton of the substrate promotes fragmentation relative to elimination. 2-(1-Hydroxyalkyl)-thiamin derivatives eliminate aliphatic aldehydes rather than undergoing fragmentation, consistent with their $C_{2\alpha}$ protons being less acidic than those of 2-1-(hydroxybenzyl)-thiamin derivatives.

In enzymic reactions that produce 2-1-(hydroxybenzyl)-thiamin diphosphate, fragmentation is avoided. It is proposed that the enzymic environment could control the conformation of the thiamin diphosphate derivative and prevent fragmentation. Alternately, the enzyme could specifically catalyze elimination by its array of functional groups.

Acknowledgments

Table of Contents

List of Figures

List of Tables

Abbreviations

HBzT	2-(1-hydroxybenzyl)-thiamin
cHBzT	cyclized HBzT
rHBzT	rearranged HBzT
NMHBzT	N_1'-methyl-2-(1-hydroxybenzyl)-thiamin
HET	2-(1-hydroxyethyl)-thiamin
BFD	benzoylformate decarboxylase
5nT	5-nor-thiamin
5nHBzT	2-(1-hydroxybenzyl)-5-nor-thiamin
PTK	phenyl thiazole ketone (2-benzoyl-5-(2-hydroxyethyl)-4-methylthiazole
DMP	dimethyl pyrimidine (4-amino-3,5-dimethyl-pyrimidine)
TMP	trimethyl pyrimidine (4-amino-1,3,5-trimethyl-pyrimidinium chloride)
BT	2-benzoylthiamin

Chapter One : INTRODUCTION

Purpose and Scope of this Thesis

2-(1-Hydroxybenzyl)-thiamin (HBzT) is the adduct generated by reaction of thiamin and benzaldehyde in weakly basic solutions. However, under more acidic conditions, instead of reverting to the starting materials, HBzT undergoes a novel fragmentation reaction[1] to produce 2-benzoyl-5-(2-hydroxyethyl)-4-methylthiazole (phenyl thiazole ketone or PTK) and 4-amino-3,5-dimethyl-pyrimidine (DMP) (the "fragmentation set") (Figure 1-1). Under weakly basic conditions, HBzT reacts to produce the expected products, benzaldehyde and thiamin (the "elimination set"). The product distribution changes from the fragmentation set to the elimination set, with both product sets produced at equal rates at pH 7.3. Based on these observations, we recently proposed a minimal mechanism.[1] This thesis reports the first detailed mechanistic study of the novel fragmentation reaction of C_2 thiamin adducts and related model compounds.

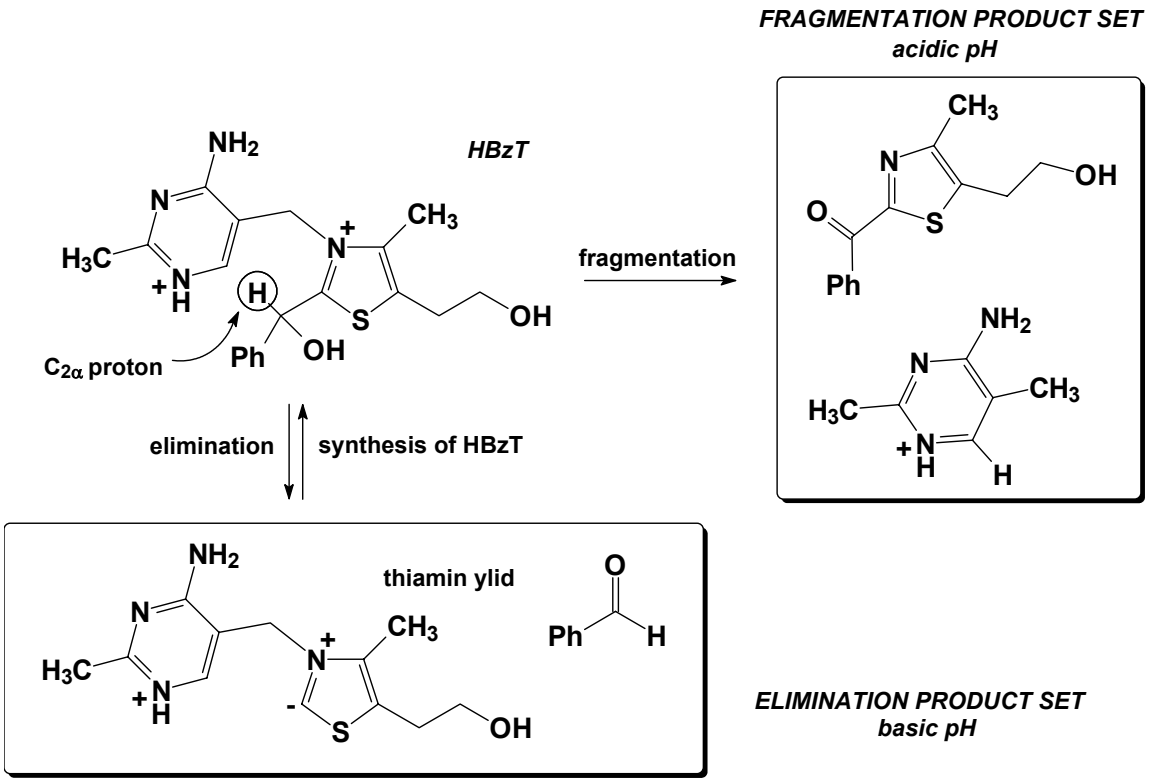

Figure Chapter One -1: Products from HBzT reaction

Our analysis of HBzT's product distribution shows that the fragmentation set dominates at pH's where the pyrimidine N_1' nitrogen is protonated. If protonation controls the course of the reaction, its effects can be modeled by studying an analogue (N_1'-methylated HBzT, NMHBzT) where a methyl group replaces the N_1' proton, thereby removing possible ambiguity regarding the site of protonation.

Both sets of products cannot arise from a common reaction intermediate because there is a change in the product distribution as pH increases. In addition, because both fragmentation and elimination are accelerated by increasing pH. The addition of the thiamin ylid to benzaldehyde produces, after protonation, HBzT (Figure 1-1).[2,3] Microscopic reversibility requires that the elimination mechanism is the reverse of this

process and would involve removal of the hydroxyl proton of the C2 adduct. Therefore, the fragmentation reaction must proceed by a different conjugate base, or by a complex route from the same base. From analysis of the structure of the products and possible pathways to them, a likely route involves loss of the $C_{2\alpha}$ proton (Figure 1-1). To investigate whether the loss of this proton is the rate-limiting step in the fragmentation reaction, we studied the fragmentation of HBzT and NMHBzT using ^{1}H NMR.

Role of Thiamin as a Catalyst

Chemical reactions can be grouped into those that proceed via 'normal polarity', and those that require a reversal of polarity. A normal polarity reaction is one that proceeds as would be expected by inspection of the dipoles of the reactants. For example, the addition of an anionic carbon nucleophile to an aldehyde is a normal polarity reaction (Figure 1-2). The carbon nucleophile, bearing a negative charge, attacks the carbonyl carbon of the aldehyde, which bears a partial positive charge. The carbonyl group's dipole is consistent with the carbonyl oxygen being more electronegative than the carbonyl carbon. Therefore, the nucleophile and electrophile react as predicted by the polarity of their dipoles. Thiamin, however, catalyzes reactions that require a 'reversal of polarity.'

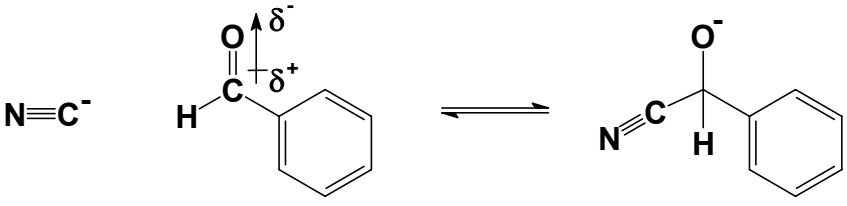

Figure Chapter One -2: Example of a normal polarity reaction

In the corresponding reversal of polarity reaction, the carbonyl carbon of the

aldehyde acts as a nucleophile to attack another electrophile, as in the benzoin condensation (Figure 1-4). In order for the carbonyl carbon to act as a nucleophile, it must be able to donate a pair of electrons. However, an aldehyde lacks a lone pair of electrons on the carbonyl carbon. To reverse the polarity of the carbonyl group, an electrophilic catalyst is normally required. The catalyst adds to the carbonyl group, and its electronegative character makes the carbinol proton more acidic. Removal of this proton generates the nucleophilic species. Such a species is commonly referred to as an acyl carbanion equivalent. Perhaps the most notable reversal-of-polarity (or "umpolung") catalyst is the cyanide ion that is used extensively in organic synthesis[11]. Thiamin is the biological equivalent to cyanide, but lacks cyanide's toxicity to heme-containing proteins.

Thiamin performs its catalytic functions by catalyzing the formation of acyl carbanion equivalents. These acyl carbanion equivalents are referred to in the thiamin literature as the 'second carbanion' of thiamin or the thiamin enamine. Therefore, thiamin catalyzes reactions that involve the generation of the thiamin enamine as a reaction intermediate. These reactions can be divided into carbon-carbon bond formation and cleavage groups.[5,9,45] Representative members of the carbon-carbon bond formation group are the benzoin condensation, the transketolase reaction, and the biosynthesis of acetolactate. Examples of the carbon-carbon bond cleavage group include the decarboxylation of pyruvate and benzoylformate. As exemplified by the benzoin condensation (Figure 1-4), all of these reactions require the generation of the thiamin enamine as a reaction intermediate, at some stage of the catalytic cycle.

Overview

The benzoin condensation is a typical reaction catalyzed by thiamin[4,5] (Figure 1-4). It produces benzoin from two equivalents of benzaldehyde by creating acyl carbanion equivalents via an apparent benzoyl carbanion.[6,7] The catalytic power of thiamin resides in the ability of its thiazolium ring to stabilize two conjugate base intermediates: the ylid of thiamin and the $C_{2\alpha}$ carbanion of its condensation product with various aldehydes (Figure 1-3).[8,9,10] The first step in the thiamin catalyzed benzoin condensation is addition of the thiamin ylid to benzaldehyde's carbonyl group to give the conjugate base of HBzT (Figure 1-4). Tautomerization via loss of the $C_{2\alpha}$ proton (Figure 1-4) generates an enamine with carbanion character, which is an acyl carbanion equivalent[11]. Condensation of this enamine with another molecule of benzaldehyde, followed by regeneration of the thiamin catalyst by elimination, results in the production of benzoin.

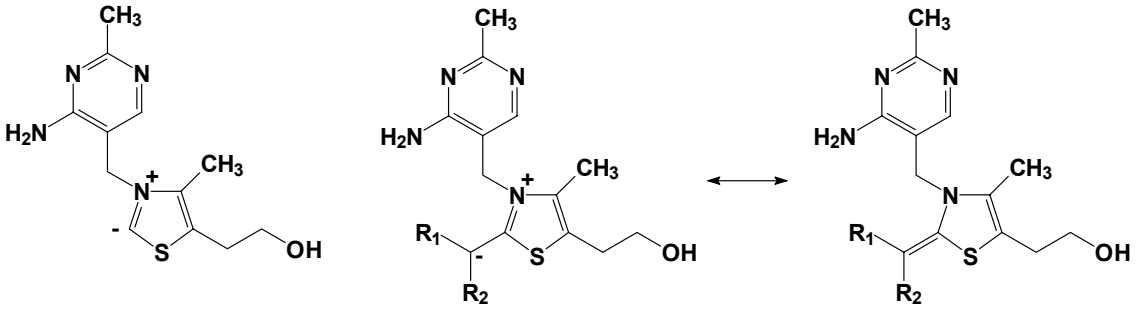

Figure Chapter One -3: Thiamin ylid and hydroxyalkyl thiamin enamine in dipolar and neutral forms

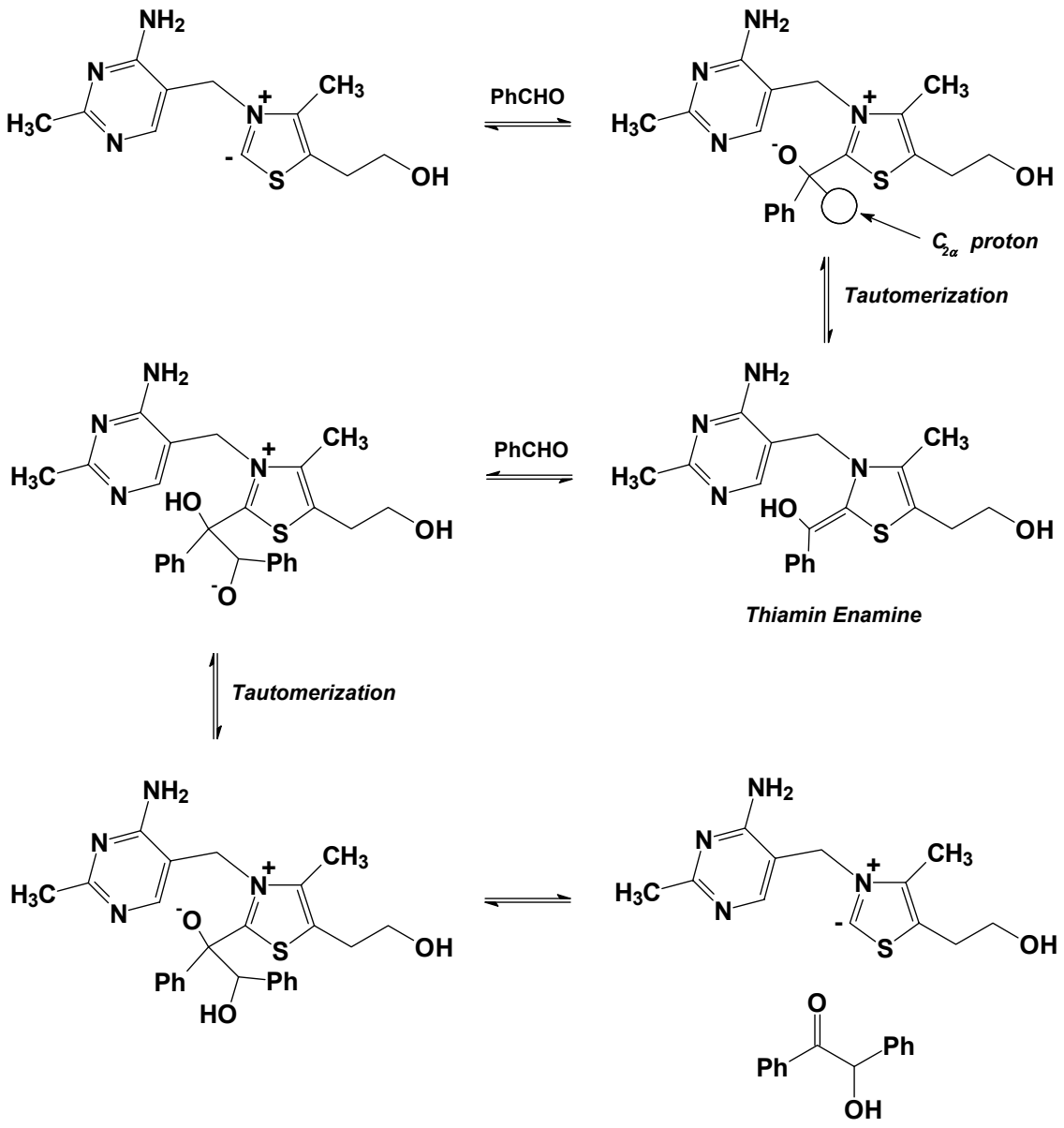

Figure Chapter One -4: Thiamin-catalyzed benzoin condensation

The acidity of the $C_{2\alpha}$ proton of C_2 thiamin adducts has been the subject of controversy[12,13,14], because this proton's acidity cannot be measured directly in water, and extrapolations are necessary.[15] By using proton-deuteron exchange experiments[12] and the kinetic study of model compounds,[14] various workers have attempted to measure the

acidity of this proton. Their results suggest that the pK_a of the $C_{2\alpha}$ proton is anywhere between 12 and 18. A common feature in all of these studies is that they assumed diffusion-controlled rates of protonation of the conjugate base. However, these studies also introduced complications.

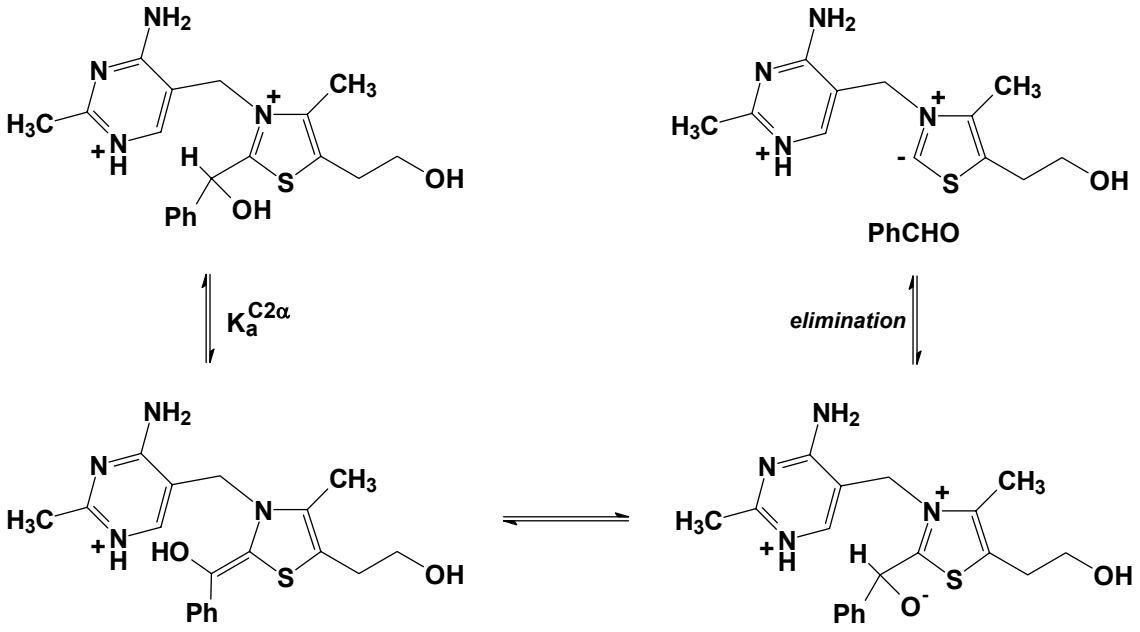

Figure Chapter One -5: Competing elimination during enamine studies

During a recent study of the acidity of the $C_{2\alpha}$ proton of 2-(1-hydroxybenzyl)-3,4-dimethyl thiazolium ion, Stivers and Washabaugh observed that elimination of benzaldehyde also occurs (Figure 1-5).[16] Benzaldehyde elimination from HBzT can be expected in any study of the $C_{2\alpha}$ proton's acidity (Figure 1-5). Removal of this proton to generate the thiamin enamine should also be accompanied by tautomerization to produce the less basic alkoxide. This alkoxide can readily undergo elimination to yield the thiamin ylid and benzaldehyde.

Crane and Washabaugh studied the elimination reaction in detail using initial rate methods and indirect detection.[17] Unexpectedly, they observed general base catalysis of the elimination reaction. They interpreted this observation as a reaction involving Brönsted acid catalysis of the conjugate base of HBzT. Since Brönsted acid catalysis must be concerted with carbon-carbon bond cleavage in such a reaction, Jencks' rules require that the stepwise alternative involves an intermediate that is too unstable to exist.[18] Moreover, to interpret the elimination reaction as a Brönsted acid catalyzed process, their mechanism avoids a known, stable intermediate–the thiamin ylid. Figure 1-6 shows a simple More-O'Ferrall reaction coordinate analysis of the possible pathways that can lead from reactants to products. For a concerted pathway to exist, both corners along the disparity axis of the reaction coordinate must be too unstable to exist. However, the thiamin ylid in the lower right of Figure 1-6 should have a significant lifetime in water, with a pK_a of ~18.[19] Although this is a high pK_a, it is within the range of carbon bases that have been found to exist in other reactions.[20,21] Since we could not see a role for Brönsted acid catalysis in such a reaction, we began our investigations in this area.[1,39]

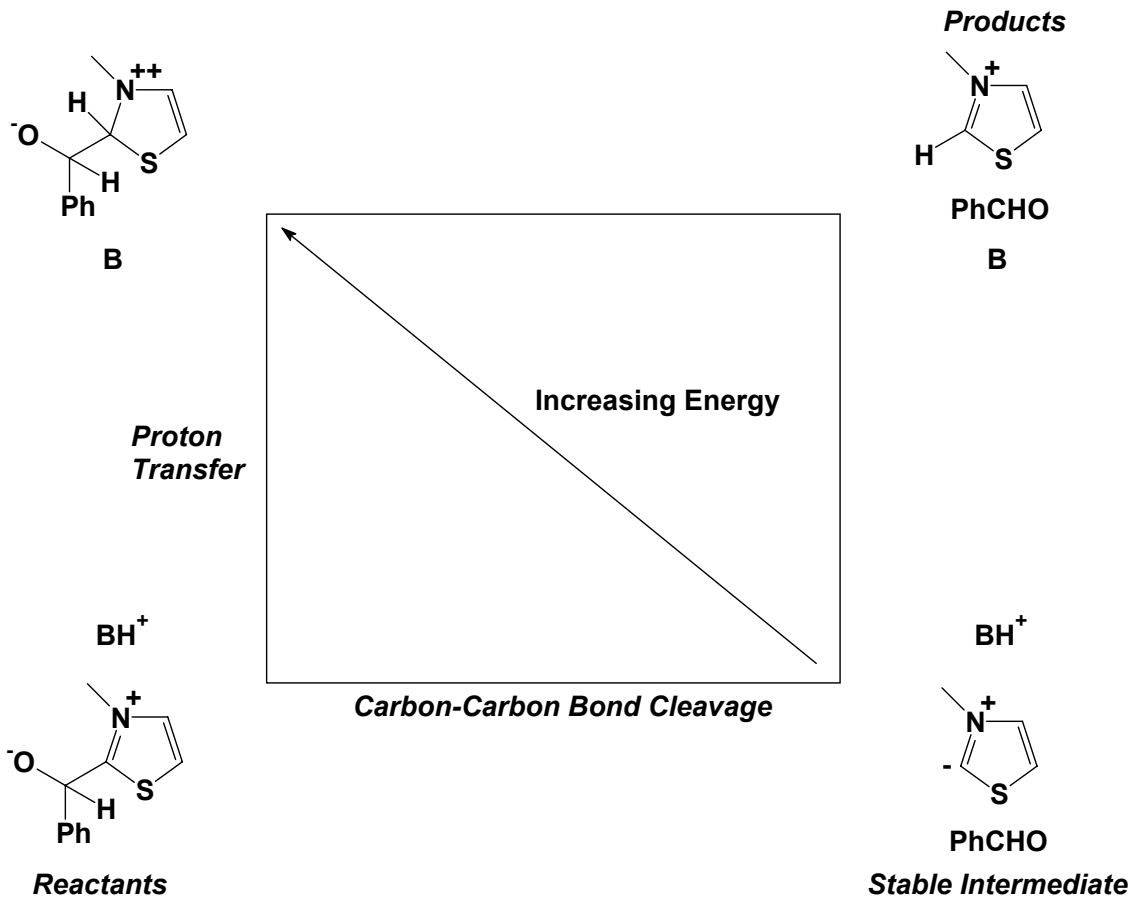

Figure Chapter One -6: Reaction coordinate diagram for elimination reaction

Unexpected Products: HBzT Fragments

Crane and Washabaugh measured the rate of benzaldehyde release from HBzT by trapping it with hydrazine or semicarbazide.[2] Since we suspected that their observed catalysis might be associated with the trapping reaction, we followed the UV spectra for HBzT reaction without using any trapping reagents.

Surprisingly, a peak at 328 nm appeared (Figure 1-7). If one molecule of HBzT produces one molecule of product, the molar extinction coefficient of the 328 nm compound would be approximately 1.0×10^4 M^{-1} cm^{-1}. From our control experiments,

we knew that neither HBzT, thiamin nor benzaldehyde absorbed significantly at this wavelength (Figure 2-3). Furthermore, such a large molar extinction coefficient is characteristic of a π–π* transition, and benzaldehyde is known to undergo only a weak n–π* transition ($\varepsilon = 10\ M^{-1}\ cm^{-1}$) at 320 nm.

We had to isolate the reaction products because the expected reaction products could not be responsible for the 328 nm peak. We then ran the reaction on a preparative scale and found that the products were neither benzaldehyde nor thiamin. Below pH 7.3, analysis showed that the products were PTK and DMP. The same products were found in an earlier study by Oka and coworkers in which they refluxed thiamin and benzaldehyde in methanolic triethylamine.[22,23] Upon examining the PTK isolated from reaction mixtures, we found that its absorption spectrum exhibited the characteristic intense peak at 328 nm (Figure 2-3).

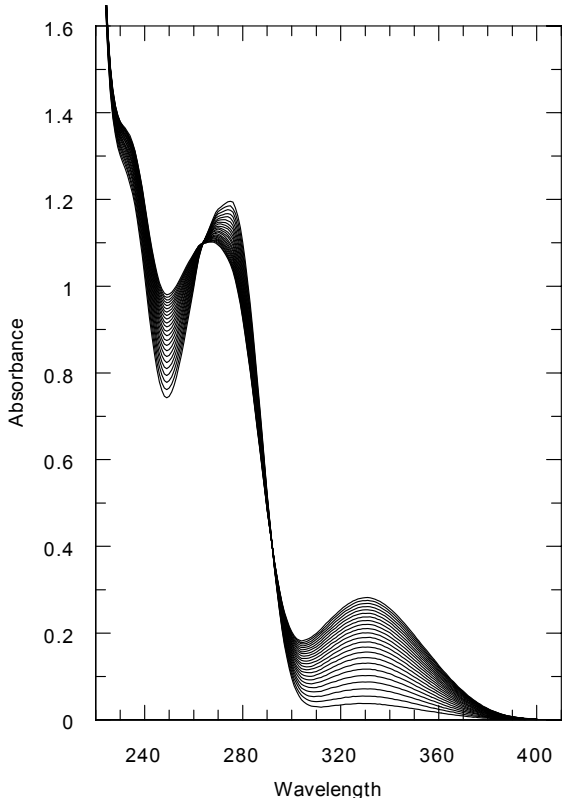

Figure Chapter One -7: Overlaid scans (each scan is 1 hour apart) of HBzT reaction in aqueous solutions

In our preliminary kinetic studies, we also observed general base catalysis.[1] Since the general base catalysis might be explained in terms of the formation of this alternative set of products, it became the subject of our detailed kinetic analysis.

Expected Products are Also Present

Our preliminary investigations also revealed that thiamin and benzaldehyde were the major products in solutions with a pH above 7.3. We found that the product distribution changes from the fragmentation products to the elimination products as a function of pH. Figure 1-8 shows this change in the product distribution in the form of absorbance vs. time plots of PTK production conducted at different pH's. As pH is increased, we found

that less PTK was produced and that the balance of the products were benzaldehyde and thiamin. This change in product distribution provides valuable information for us to consider when we propose our mechanism.

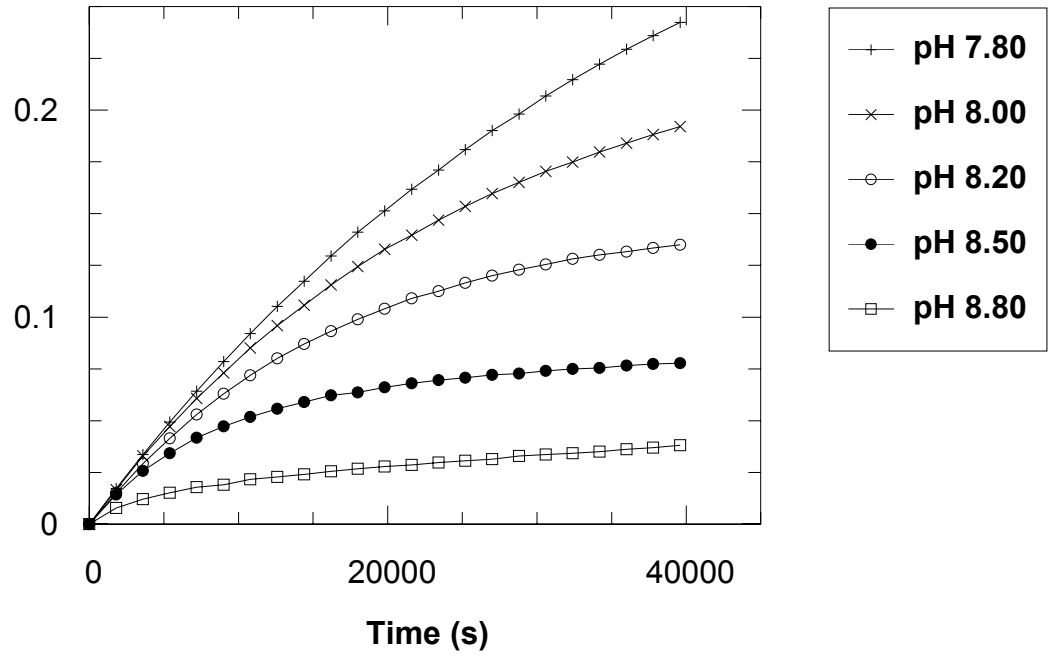

Figure Chapter One -8: Plots of absorbance vs. time for solutions of HBzT reacting at different pH's. The absorbing species is PTK.

The Williams Fragmentation: A Prototype Mechanism:

The other well-known fragmentation reaction of thiamin is the Williams fragmentation. In this reaction, sulfite cleaves the bond between the bridging methylene carbon and the nitrogen of the thiazolium ring (Figure 1-9). This reaction was discovered during the isolation of thiamin in the 1930's, when Williams and coworkers bubbled sulfur dioxide through aqueous extracts of rice husks in an attempt to suppress bacterial growth.[24] A white precipitate appeared quickly, which upon analysis proved to be the

sulfonic acid of the pyrimidine species. The discovery of this product led him to deduce the structure of thiamin by comparing the fragmentation products with known pyrimidines and thiazoles.[25] Williams attempted to elucidate the mechanism of the fragmentation reaction,[24,26] but it was not until much later that Zoltewicz and coworkers unraveled the details of the fragmentation reaction mechanism.

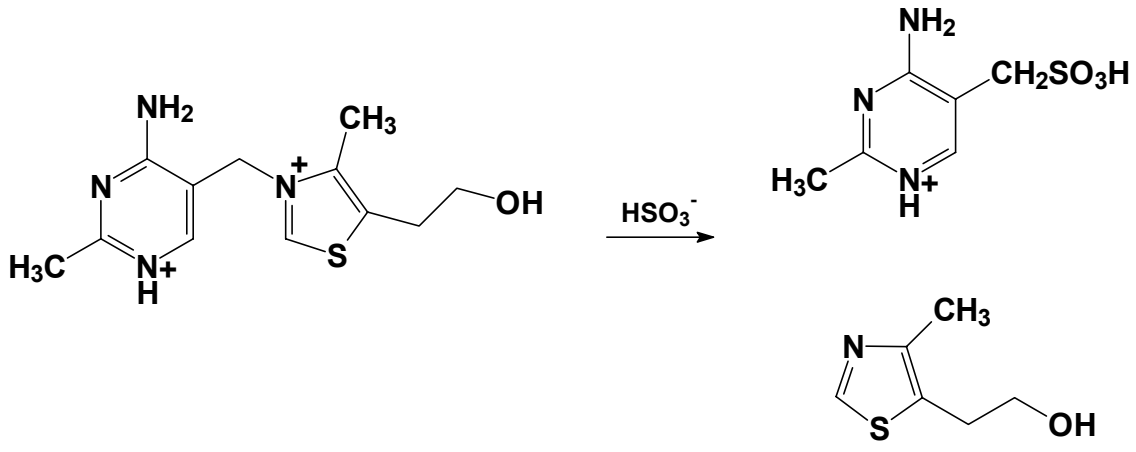

Figure Chapter One -9: The Williams fragmentation

Zoltewicz and coworkers presented in 1977 what is now the generally accepted mechanism for the Williams fragmentation.[27] Their mechanism requires two equivalents of sulfite. The first sulfite is catalytic, and adds to the C6' carbon of the N_1'-protonated pyrimidine to form intermediate **2** in Figure 1-10. The thiazole departs, leaving the resonance-stabilized carbocation (**3** in Figure 1-10) which is rapidly trapped by a second molecule of sulfite, or other nucleophile. In the presence of exogenous nucleophiles, this is a convenient method for synthesizing substituted pyrimidines.[28] Finally, the first sulfite is regenerated in an elimination step. Where there is an excess of sulfite, the second molecule of sulfite is not involved in a kinetically significant process and the overall

reaction is first order in sulfite.

Zoltewicz also addresses the rate-limiting step of the reaction: is it the nucleophilic addition of the first molecule of sulfite, or is it the departure of the thiazole? By studying kinetic isotope effects, Zoltewicz provides evidence that addition of sulfite ion to the pyrimidine is reversible, and that the loss of the thiazole group is rate-limiting.[28,29]

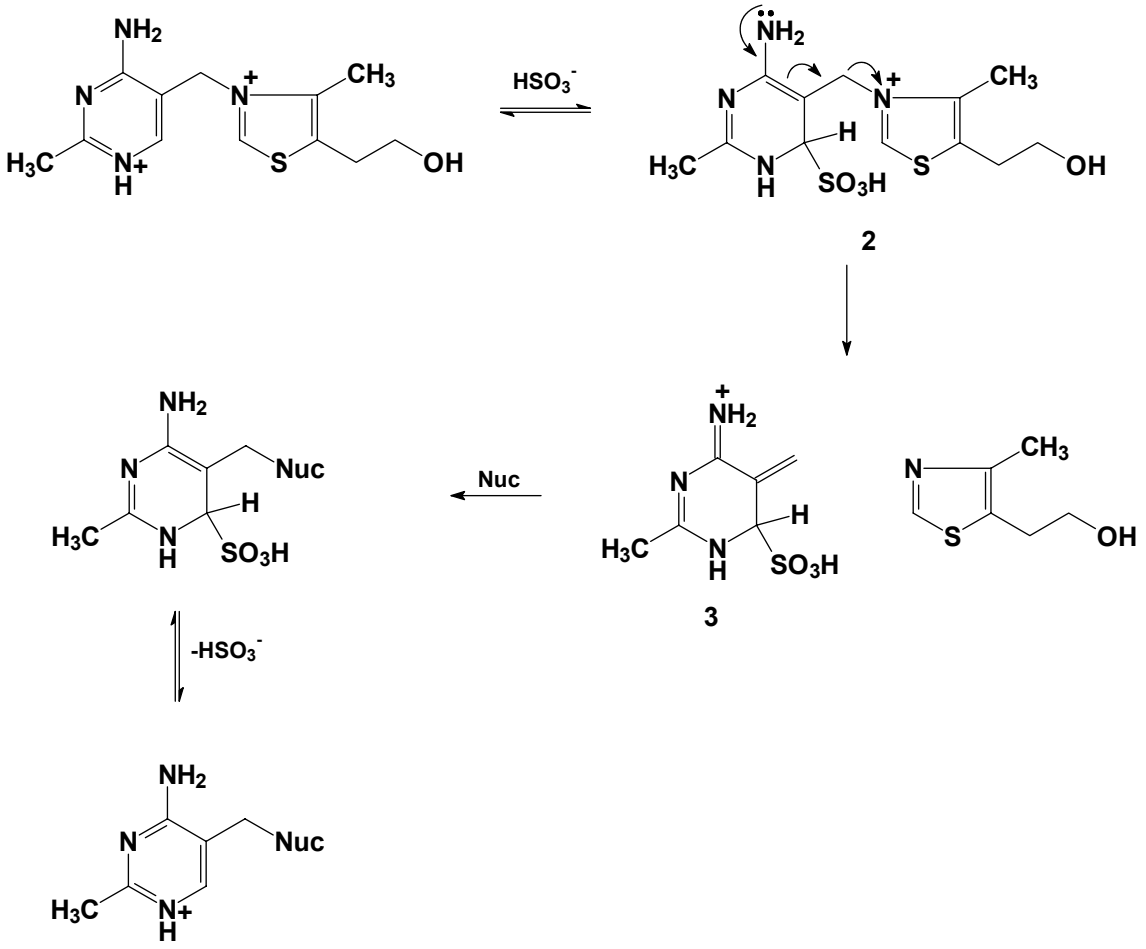

Figure Chapter One -10: Zoltewicz's mechanism for thiamin fragmentation

N_1' Nitrogen Controls Product Distribution

Our product analysis shows that fragmentation is the dominant reaction at pH's where

the N_1' nitrogen is protonated. During fragmentation, the bond between the bridging methylene carbon and the thiazolium ring is cleaved. Heterolytic cleavage could involve transfer of electrons from the cleaved bond to the thiazolium nitrogen, as in the Williams fragmentation. Instead, however, we suggest that the methylpyrimidine rather than the thiazolium, is the nucleofuge. In this case, methyl-pyrimidine would be a better nucleofuge if it left as a neutral rather than anionic species.[30] If the pyrimidine ring were protonated on the N_1' nitrogen, it would bear a positive charge prior to cleavage, and would allow the pyrimidine ring to depart as a neutral species. This idea is consistent with the observation that the fragmentation reaction is suppressed at high pH, above the pK_a of the N_1' nitrogen of the pyrimidine.

A positively charged pyrimidine can accelerate the fragmentation reaction. The inductive effect of a positive charge on N_1' could be the stabilizing factor since the carbanion that forms during fragmentation on the bridging methylene carbon cannot be resonance stabilized by a positive charge on N_1'. When the concentration of protonated pyrimidine falls, inductive stabilization of the methylene carbanion is not possible. We concluded that this would result in fragmentation not occurring, and elimination occurring instead. A minimal mechanism consistent with these ideas is presented in Figure 1-11.

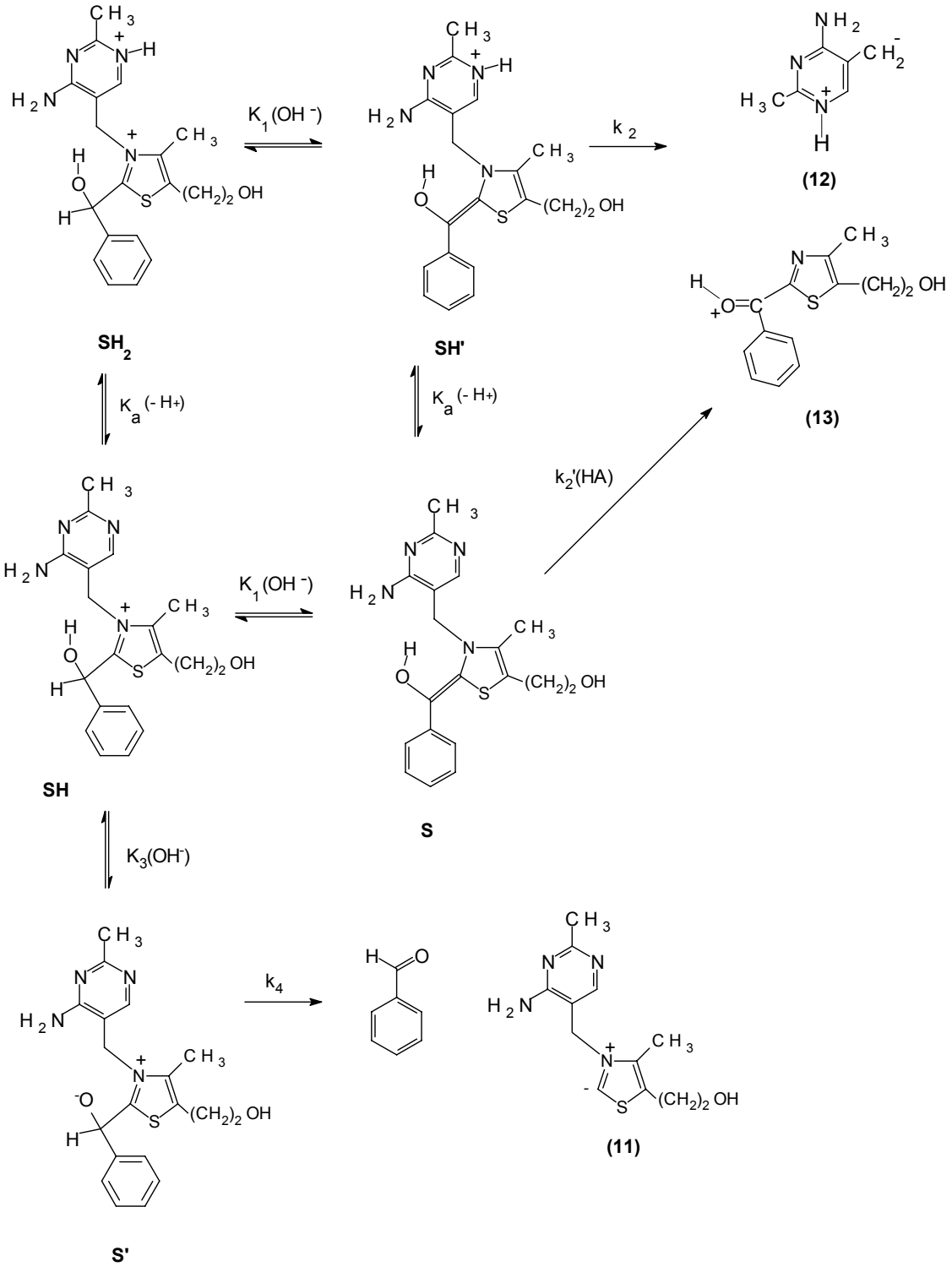

Figure Chapter One -11: Mechanistic proposal for fragmentation

Kinetic Ambiguity and the Assignment of the Site of Catalysis

Jencks states the obvious problem concerning sites of protonation: "it [the proton] is mobile, and its position on one or another atom in the transition state cannot be decided from the rate law of a reaction".[31] By following his suggestion of using a methyl group as a "proton equivalent", we avoid this ambiguity. Therefore, we synthesized N_1'-methyl-2-(1-hydroxybenzyl)-thiamin (NMHBzT) in order to test our hypothesis that the protonation state of the N_1' nitrogen controls the product distribution. Since the N-methylated compound always has a positive charge on N_1' within the pH range that we are studying, we can make two important predictions about the outcome of this structural modification:

1. The pH-Rate profile for the fragmentation of NMHBzT should no longer show the curvature characteristic of the N_1' nitrogen pK_a in the HBzT fragmentation reactions since the N_1' site is occupied by a methyl group.

2. Only the fragmentation products should be generated since protonation of the N_1' nitrogen controls the product distribution between the fragmentation products and the elimination products.

3. It is protonation on N_1' that is responsible for the fragmentation reaction, and not a minor C-protonated tautomer.

Chapter Two : EXPERIMENTAL AND RESULTS

General Methods and Procedures

Materials

Thiamin chloride hydrochloride was a gift from Novopharm. All general chemicals were purchased from Fisher, Aldrich or Eastman Kodak and were the highest quality reagent grade. They were used without further purification. Buffer substances were purchased from Sigma or Fisher, and were lyophilized overnight prior to preparation of the buffer solutions. Water used in kinetic studies was doubly distilled and deionized using a Corning AG-1b water purification system.

Equipment

UV-visible measurements were taken in the thermostatted cell holder of a Perkin Elmer Lambda 2 or Lambda 19 spectrophotometer. Data were collected using an IBM-PC compatible computer running Perkin-Elmer PECSS or UVCSS data acquisition software.

200 MHz ^{1}H and 50 MHz ^{13}C NMR spectra were recorded on a Varian Gemini-200 spectrometer. 400 MHz ^{1}H and 100 MHz ^{13}C NMR spectra were recorded on a Varian Unity-400 spectrometer. Spectra run in D_2O were referenced against DSS as an internal standard. Spectra run in $CDCl_3$ were referenced against TMS as an internal standard.

FAB-MS spectra were recorded by Dr. Henrianna Pang on a ZAB-SE spectrometer at the Mass spectrometry laboratory of the Carbohydrate Research Centre, Faculty of Medicine, University of Toronto.

Kinetic Methods

Kinetic studies were run in buffered solutions in 1-cm quartz cuvettes kept at 40 °C with a Haake D8L recirculating water bath in the thermostatted cell holder of a Perkin-Elmer Lambda 2 or Lambda 19 UV/Visible spectrophotometer. Reactions were followed by monitoring absorbance changes at 328 nm, or by repetitive scans of the UV-VIS spectrum between 220 and 400 nm. Data were collected with an interfaced computer using Perkin-Elmer PECSS software. Rate constants were calculated by nonlinear regression fitting of the UV-VIS data to the integrated first order rate equation using GraFit V3.0 (Erithacus Software) on an IBM-compatible computer (MS Windows 3.1) or by initial rate methods, as indicated.

Buffer solutions were prepared in a constant temperature water bath maintained at 40°C with a Haake D8L recirculating water bath. A glass calomel electrode (Fisher Scientific) was standardized against reference buffer solutions (BDH) at 40°C. pH readings were obtained from a Radiometer PHM-82 pH meter. The ionic strength of all buffer solutions was maintained at 0.10 by the addition of sodium chloride.

When HBzT fragmentation reactions were followed under first-order conditions, a different technique was used. A large recirculating water bath was fitted with an alloy vessel that was capable of holding 66 20 mL vials, the reaction vessels. To each vial was added 10 mL of buffer solution and 100 μL of an 8.06×10^{-3} M HBzT stock solution, to make the final concentration of HBzT in the vial 8.00×10^{-5} M. Periodically, 3 mL aliquots were transferred from the vial to a 1 cm path quartz cuvette, and an absorbance reading taken at 328 nm. The aliquot was transferred back to the cell which was then

returned to the water bath. The total time for each reading was 2 minutes. Since the reactions were very slow, the minor cooling effect of bringing each solution out into room temperature for the duration of the reading was taken as being insignificant. The experimental technique generates good first-order kinetic plots, as seen in Figure 2-1.

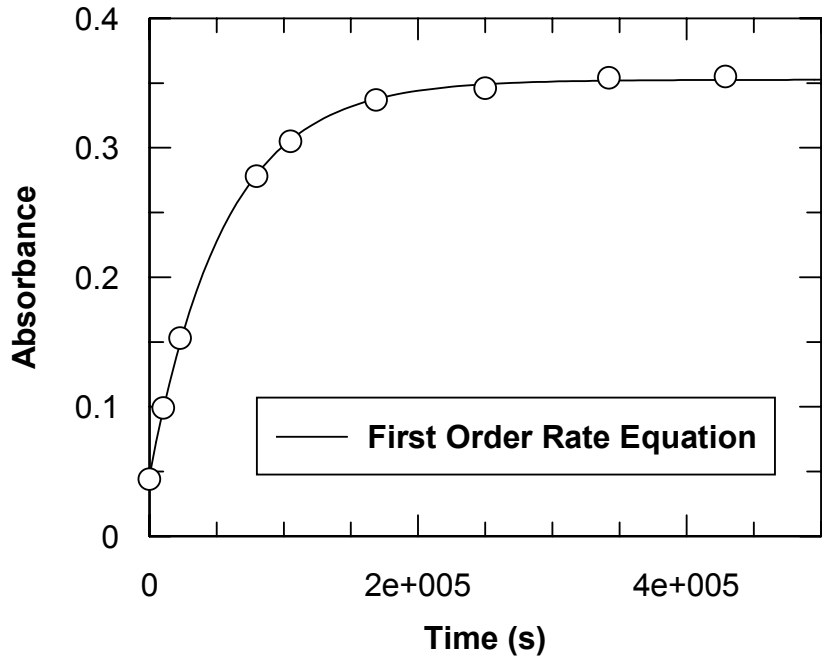

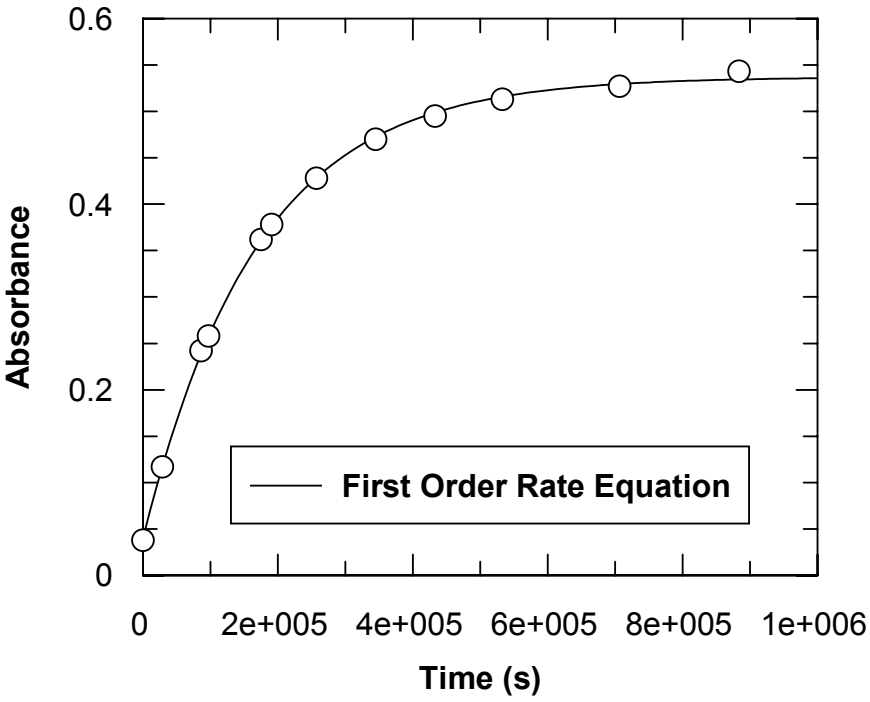

Figure Chapter Two -1: Representative first-order kinetic plots that show the effectiveness of the water bath kinetic technique. The upper plot is the reaction of HBzT in pH 7.70 36 mM POPSO buffer, and the lower plot is the reaction of HBzT in pH 6.92 35 mM PIPES buffer

Syntheses

N_1'-Methyl-2-(1-hydroxybenzyl)-thiamin

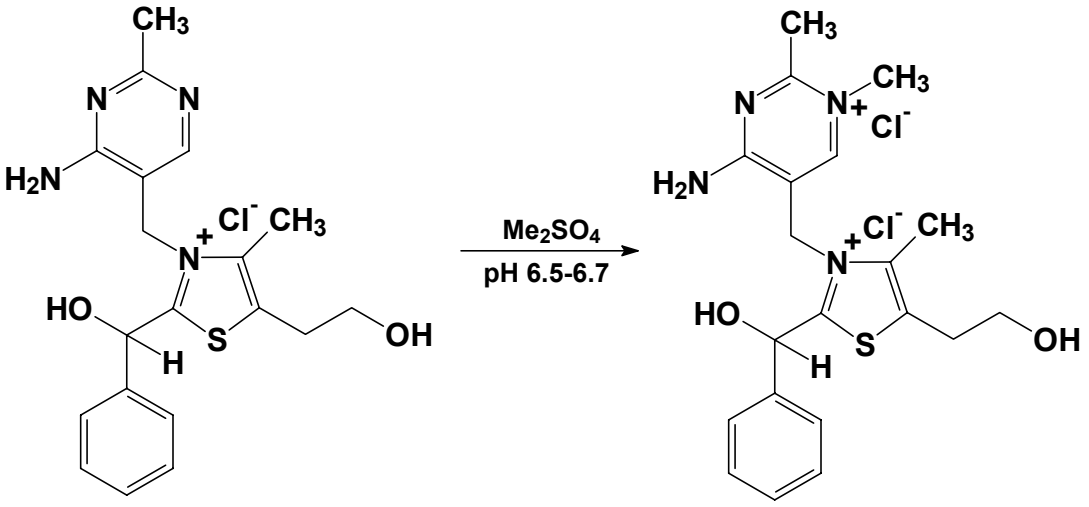

2-(1-Hydroxybenzyl)-thiamin chloride hydrochloride (**1**) was prepared by the condensation of benzaldehyde and thiamin.[2,3,23,32] **1** (1.0 g, 2.3 mmol) was dissolved in distilled water (2.8 mL). $NaHCO_3$ (0.25 g, 3 mmol) was added in small portions, and the reaction mixture was warmed slightly so that a clear solution resulted. $CaCO_3$ (0.15 g, 1.5 mmol) was added to the reaction mixture and the pH was adjusted to 6.5 by the addition of HCl. Dimethyl sulfate (0.70 mL, 7.4 mmol) was added by syringe in three portions over a period of 1.5 hours. The pH was monitored by a pH meter throughout the addition of dimethyl sulfate, and was maintained between 6.5 and 6.7 by the addition of $NaHCO_3$. The reaction mixture was filtered and washed with distilled water (1 mL). A solution of $NaClO_4$ (1.5 g in 2 mL distilled water) was added to the filtrate. The resultant white suspension was stirred for 2 hours, filtered and washed with 1% $HClO_4$ (2 × 1 mL). The white powder was then recrystallized from 5 mL of 1% $HClO_4$ to yield 0.93g (74 %

from **1**) **4** as white crystals: m.p. 122-123°C; UV (1% $HClO_4$) λ_{max} 262 (ε = 15500); FABMS for $M^{2+}(ClO_4)_2$: 487 ($M^{2+}(^{37}ClO_4)$, 12.9), 485 ($M^{2+}(^{35}ClO_4)$, 42); high resolution FABMS: Calculated MH^+ peak for NMHBzT ($C_{20}H_{24}N_4O_2S$): 385.1698, Observed: 385.1691.;

^{1}H NMR (200 MHz, D_2O)	δ 7.30-7.46 (m, 5H), 6.51 (s, 1H), 6.41 (s, 1H), 5.33 (dd, 2H, J = 18.2, 29.6 Hz), 3.96 (t, 2H, J = 5.8 Hz), 3.52 (s, 3H), 3.22 (t, 2H, J = 5.8 Hz), 2.53 (s, 3H), 2.38 (s, 3H);
^{13}C APT NMR (50 MHz, D_2O)	δ 162.4 (-), 144.0 (-), 141.8 (+), 134.1 (-), 136.0 (-), 129.4 (+), 129.3 (+), 127.5 (+), 107.5 (-), 81.0 (+), 75.7 (-), 71.3 (+), 59.7 (-), 46.1 (-), 41.5 (+), 28.9 (-), 20.5 (+), 10.5 (+).

***5-Nor-thiamin*[33]**

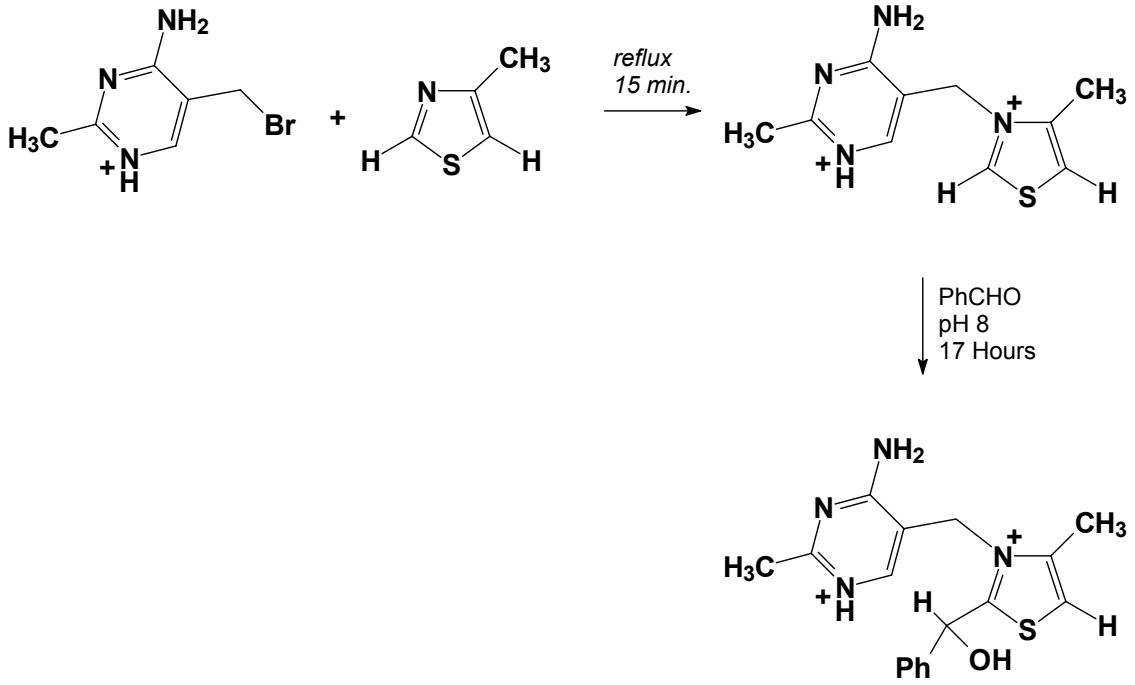

Scheme Chapter Two -1: Preparation of 5-nor-HBzT (5nHBzT)

To 4-methyl-thiazole (1.22 g, 12.3 mmol) in a 25 mL round bottom flask was added 4-amino-5-bromomethyl-2-methylpyrimidine (378 mg, 1.05 mmol). The reaction mixture was briefly heated to reflux, and a light brown precipitate appeared on the walls of the flask. The reaction mixture was diluted with diethyl ether (15 mL), and the precipitate (which is 4-methyl-thiazole hydrochloride) was removed by filtration. The diethyl ether was evaporated, and the residue dissolved in water (20 mL). The pH was adjusted to 4.0 using 0.5 M potassium hydroxide. This solution was extracted with ethyl acetate (2 × 20 mL) to remove the unreacted 4-methyl-thiazole, and the aqueous phase was lyophilized to yield 5-northiamin (447 mg) (5nT) as a white powder.

^{1}H NMR (200 MHz, D_2O): δ 9.70 (d, 1H, J = 2.6 Hz), 7.99 (s, 1H), 7.92 (d, 1H,

J = 2.6 Hz), 5.51 (s, 2H), 2.56 (s, 3H).

^{13}C NMR (50 MHz, $CDCl_3$): δ 15.55, 24.15, 52.60, 125.01, 148.38.

2-(1-Hydroxybenzyl)-5-nor-thiamin (5nHBzT)

To a solution of 5-nor-thiamin (191 mg, 0.5 mmol) in methanol (2 mL) and water (1 mL) was added benzaldehyde (501 mg, 5.4 mmol, 10 equivalents). The pH was adjusted to 7.8, and maintained by the automated addition of a 0.5 M potassium hydroxide solution using a pH-stat apparatus. After 17 hours, the reaction was quenched by the addition of 1 M hydrochloric acid, until the pH was below 2. The reaction mixture was washed with ethyl acetate (2 × 20 mL), and the aqueous phase was evaporated to yield an inseparable mixture (171 mg) of 5nHBzT and 5nT as a white powder.

^{1}H NMR (200 MHz, D_2O): δ 7.47-7.21 (m, 5H), 6.58 (s, 1H), 6.38 (s, 1H), 5.34 (d, 1H, J = 16.9 Hz), 5.19 (d, 1H, J = 17.1 Hz), 2.57 (s, 3H), 2.39 (s, 3H).

Determination of HBzT Concentration by Chloride Ion Conductivity Measurements

First-order kinetic measurements do not ordinarily require accurate determinations of the absolute concentrations of the reactants. However, our studies require us to use the absorbance limits of reactions allowed to run to completion to determine the stoichiometry of the HBzT reaction. Therefore, we independently measured the concentration of HBzT in solution by measuring the amount of chloride ion present in a solution of HBzT chloride hydrochloride in deionized water.

The chloride ion concentration determinations were performed with the assistance of Mr. Dan Mathers in the undergraduate physical chemistry laboratories at the University of Toronto. We measured the chloride ion concentrations with a Perkin-Elmer HPLC fitted with a cation exchange column and a conductivity cell. By integration of the conductivity signal received from the detector, we were able to determine the concentration of chloride ion present in the sample, as measured against a series of sodium chloride standard solutions. The results of these measurements are presented in Figure 2-2.

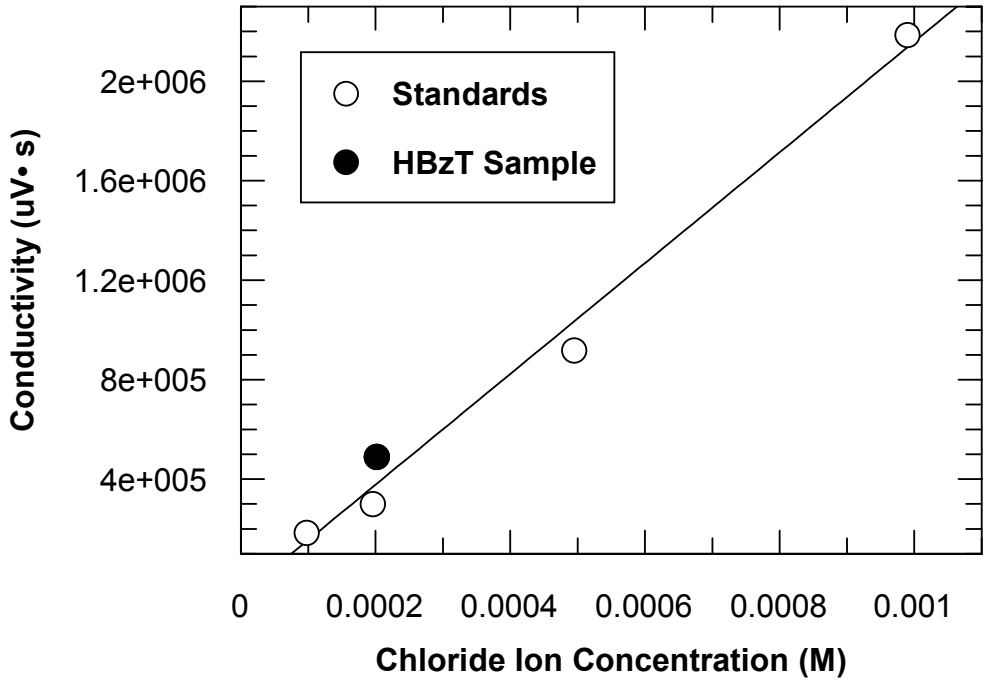

Figure Chapter Two -2: Chloride ion conductivity versus concentration plots showing calibration curve

Preparative-Scale Product Isolation from the NMHBzT Fragmentation

To confirm the structure of the fragmentation products, we ran a preparative scale reaction of NMHBzT. In this reaction, 170 mg NMHBzT diperchlorate was dissolved in 5 mL of doubly distilled water, and the pH was adjusted to 8.0. The pH was maintained at 8.0 by the addition of a 0.5 M potassium hydroxide solution from an autoburette. The reaction was continued for approximately two hours at room temperature, and was quenched by the dropwise addition of a 1 M hydrochloric acid solution until the pH was below 2.0.

The acidic reaction mixture was then extracted using two 50 mL portions of ethyl acetate. The organic phase was dried over anhydrous magnesium sulfate, and the ethyl

acetate was evaporated. The residue was purified by column chromatography on silica gel (1:1 ethyl acetate:hexanes) to give 51 mg of PTK as a yellow oil:

^{1}H NMR (200 MHz, $CDCl_3$): δ 2.44 (s, 3H), 3.03 (t, 2H, J = 6.3 Hz), 3.84 (t, 2H, J = 6.3 Hz), 7.43-7.62 (m, 3H), 8.35-8.40 (m, 2H).

^{13}C NMR (100 MHz, $CDCl_3$): δ 15.4, 30.2, 62.6, 128.2, 131.0 133,2, 135.3, 137.3, 152.1, 163.4, 184.0.

The aqueous phase was lyophilized to yield 0.12 g of TMP and potassium chloride as white crystals. The white crystals were analyzed by ^{1}H and ^{13}C NMR:

^{1}H NMR (200 MHz, D_2O): δ 7.90 (s, 1H), 3.79 (s, 3H), 2.59 (s, 3H), 2.11 (s, 3H).

^{13}C NMR (100 MHz, D_2O): δ 13.6, 21.9, 42.7, 63.3, 115.0, 146.6, 162.5, 164.4.

Generation of DMP Using the Oka Conditions[23]

Triethylamine (10.5 g, 104 mmol) was added to a suspension of thiamin (16.8 g, 49.8 mmol) in methanol (125 mL). After stirring for 5 minutes, the suspension became a clear, dark-yellow solution. Benzaldehyde (10.5 g, 100 mmol) was added to the solution and the reaction mixture was refluxed for 4 hours. The methanol was evaporated, and the residue suspended in water (200 mL). The pH was adjusted to 1 by dropwise addition of concentrated hydrochloric acid and extracted with ethyl acetate (2 × 200 mL). The aqueous phase was acidified using concentrated hydrochloric acid until the pH was below 5, and rotary evaporated to dryness. The residue was extracted with hot ethanol (40 mL), and the ethanol was evaporated to yield DMP (0.15 g) as white crystals m.p. 195-7 (dec)

^{1}H NMR (200 MHz, D_2O): δ 7.71 (s, 1H), 2.36 (s, 3H), 1.93 (s, 3H).

NMR Kinetic Studies

In a typical kinetic run, HBzT (0.20 g, 46 μmol) was dissolved in a 1 M CD_3CO_2H / CD_3CO_2Na buffer solution (1 mL) and transferred to 5 mm NMR tubes. The temperature of all NMR tubes was maintained at 40°C in a water bath. The NMR tubes were periodically removed from the bath and NMR spectra recorded on Gemini-200 or Unity-400 spectrometers.

Results

Product Studies of the NMHBzT Fragmentation Reaction

Several studies were performed to identify the products of NMHBzT fragmentation. We ran preparative-scale reactions of NMHBzT in unbuffered aqueous solutions to isolate the reaction products. To avoid having to separate the reaction products from buffers, the pH was maintained at 8.0 by the automated addition of a 0.5 M potassium hydroxide solution using a pH-stat apparatus. The ketone product 2-(1-hydroxybenzyl)-5-(2-hydroxyethyl)-4-methylthiazole (PTK) isolated has the same melting point, ^{1}H, ^{13}C NMR spectra and UV spectra as the material reported by Oka.[23] It is also identical to the material that we independently synthesized.[1] The other fragmentation product, TMP, was isolated and characterized by ^{1}H, ^{13}C, UV, MS and melting point.

Overlaid UV spectra of HBzT, and PTK are presented in Figure 2-3. Overlaid UV spectra of NMHBzT, TMP and PTK are presented in Figure 2-4.

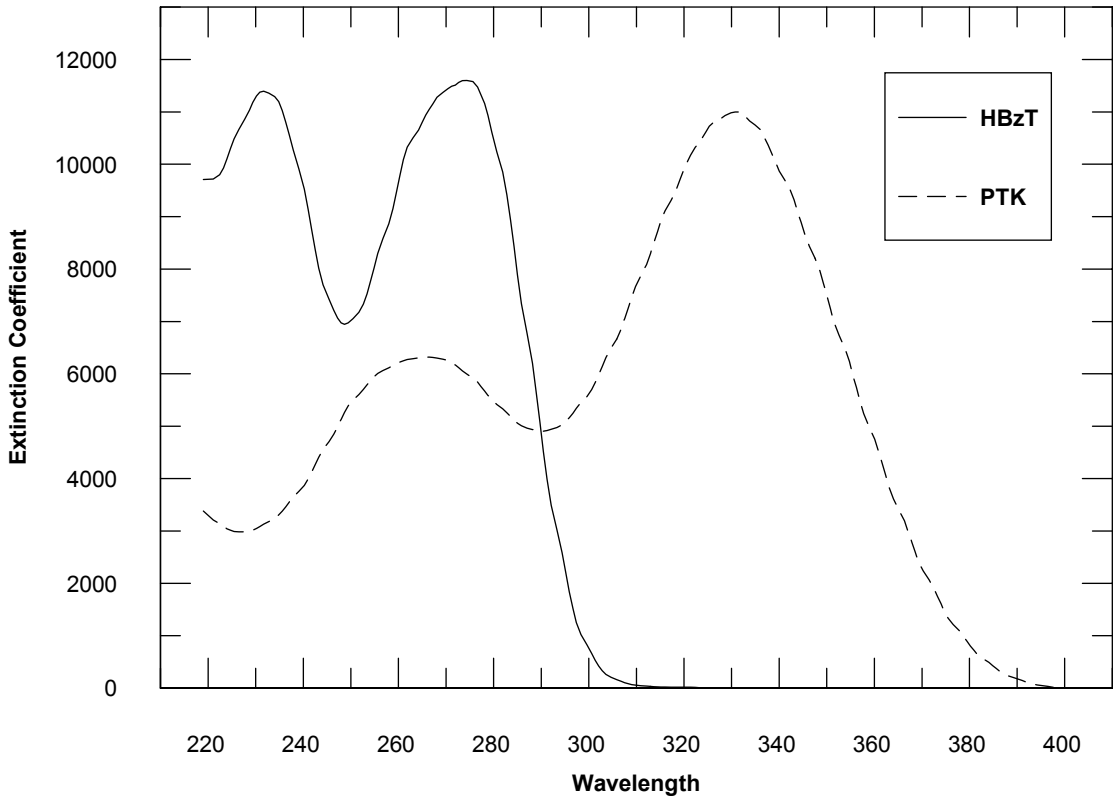

Figure Chapter Two -3: UV Spectra of HBzT and PTK

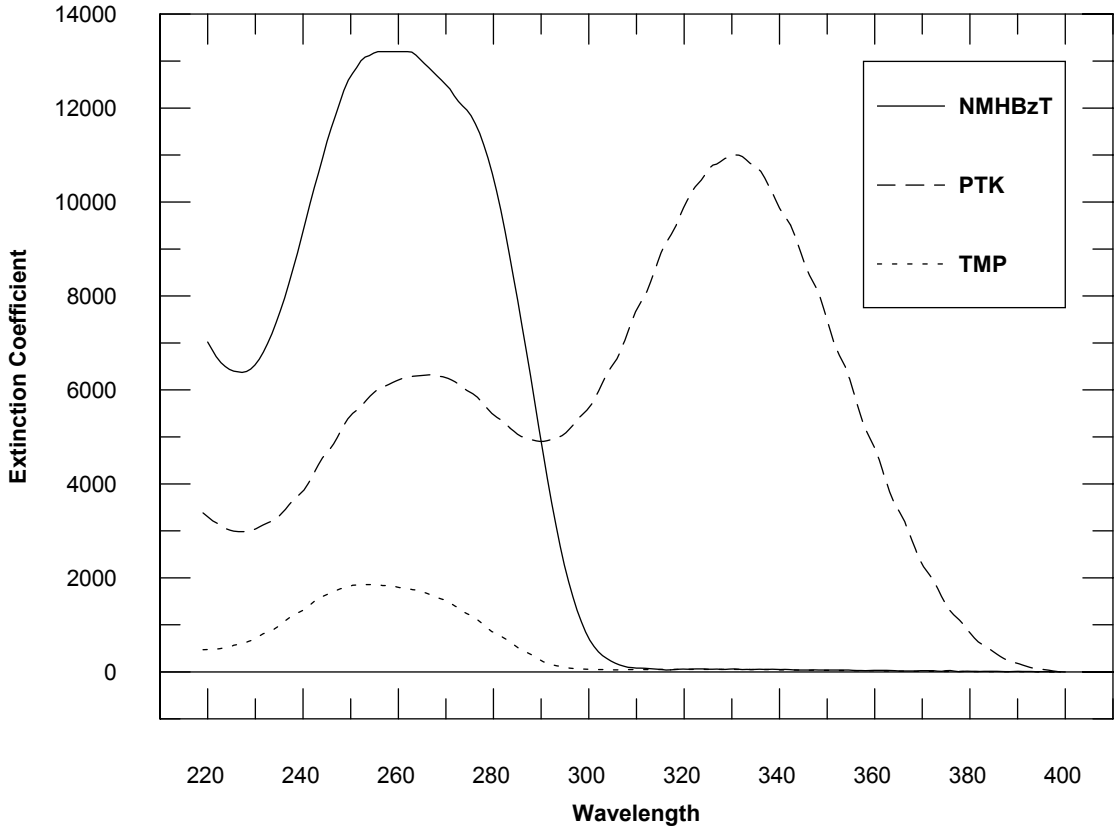

Figure Chapter Two -4: Spectra of NMHBzT, TMP and PTK.

Initial Rate pH-Rate Profile for HBzT

Reactions were run in various buffered aqueous solutions maintained at 40° C. The ionic strength of all buffer solutions was 0.10. The progress of the reaction to the first 2% of completion was followed by monitoring the absorbance changes at 328 nm, characteristic of a π–π^* transition (ε = 8720 M^{-1} cm^{-1}) of the PTK species. Where buffer catalysis was observed, we extrapolated to zero buffer concentration for this pH-Rate profile. These data are reported in Table 2-1.

Table Chapter Two -1: First-order rate constants obtained by initial rate methods and corrected to zero buffer concentration, and second-order buffer rate constants (where catalysis was observable) for HBzT fragmentation at 40 °C.

Buffer	pK_a	pH	Concentrations (mM)	k_0 (s^{-1})	k_B ($M^{-1}s^{-1}$)
Acetate	4.76	4.30	100, 50.2, 10.4	$1.3 \pm 0.3\times10^{-7}$	–
		5.00	104, 50.7, 10.4	$6.8 \pm 0.2\times10^{-7}$	–
Succinate	5.64	5.30	61.5, 30.9, 8.10	$1.2 \pm 0.3\times10^{-6}$	$2.0 \pm 0.6\times10^{-5}$
		5.90	43.5, 21.2, 4.37	$1.6 \pm 0.2\times10^{-6}$	$2.2 \pm 0.7\times10^{-5}$
MES	6.15	5.70	101, 51.0, 10.5	$1.3 \pm 0.1\times10^{-6}$	–
		6.20	100, 51.4, 10.8	$1.9 \pm 0.1\times10^{-6}$	–
PIPES	6.82	6.40	33.1, 16.5, 3.38	$2.2 \pm 0.1\times10^{-6}$	–
		6.90	33.3, 17.2, 3.40	$3.6 \pm 0.1\times10^{-6}$	–
Phosphate	7.15	6.90	58.4, 28.4, 6.07	$3.7 \pm 0.5\times10^{-6}$	$6 \pm 1\times10^{-5}$
		7.40	44.0, 21.6, 4.50	$5.5 \pm 0.3\times10^{-6}$	$6 \pm 1\times10^{-5}$
HEPES	7.27	7.00	100, 51.1, 11.6	$3.7 \pm 0.2\times10^{-6}$	–
		7.60	100, 49.8, 11.7	$6.0 \pm 0.3\times10^{-6}$	–
POPSO	7.59	7.80	38.7, 19.9, 3.96	$7.1 \pm 0.2\times10^{-6}$	$1.4 \pm 0.1\times10^{-5}$
		8.10	39.6, 20.4, 4.32	$8.1 \pm 0.3\times10^{-6}$	$1.4 \pm 0.1\times10^{-5}$
Bicine	7.99	8.30	100, 49.2, 9.97	$7.3 \pm 0.9\times10^{-6}$	–
		8.60	98.6, 50.5, 9.97	$7.9 \pm 0.2\times10^{-6}$	$3.3 \pm 0.1\times10^{-5}$

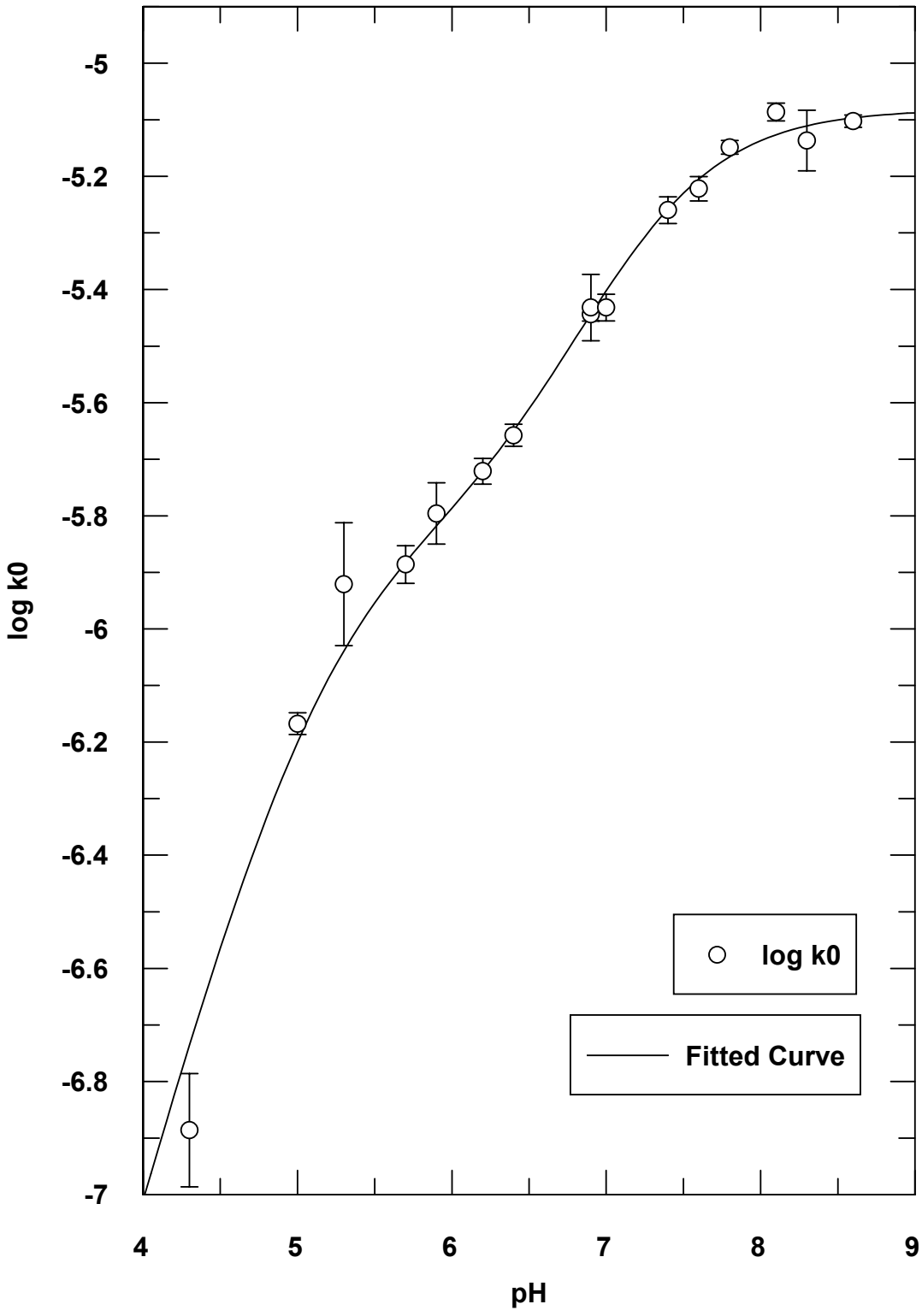

Figure Chapter Two -5: pH-Rate Profile for HBzT fragmentation at 40°C

Derivation of Rate Expressions for HBzT pH-Rate Profile

The HBzT pH-Rate profile (Figure 2-5) resembles a diprotic acid titration curve. By fitting to a two pK_a equation:

$$\log_{10} k_0 = \frac{Lim_1 + Lim_2 10^{(pH-pK_1)}}{10^{(pH-pK_1)} + 1} - \frac{(Lim_2 - Lim_3)10^{(pH-pK_2)}}{10^{(pH-pK_2)} + 1} \qquad \textbf{E- 1}$$

we obtain two apparent pK_a's: 5.2 ± 0.1 and 7.3 ± 0.1. Since it is important in our discussion that follows, we will derive expressions for the concentrations for all major equilibrium species of HBzT as a diprotic acid.

There is a mass balance expression:

$$[HBzT] = [H_3A^{2+}] + [H_2A^{+}] + [HA] \qquad \textbf{E- 2}$$

and two acid dissociation equilibria:

$$H_3A^{2+} \overset{K_a}{\rightleftharpoons} H_2A^{+} + H^{+} \qquad \textbf{E- 3}$$

$$H_2A^{+} \overset{K_a'}{\rightleftharpoons} HA + H^{+} \qquad \textbf{E- 4}$$

These lead to expressions for the two acidity constants:

$$K_a = \frac{[H_2A^{+}][H^{+}]}{[H_3A^{2+}]} \qquad \textbf{E- 5}$$

$$K_a' = \frac{[HA][H^{+}]}{[H_2A^{+}]} \qquad \textbf{E- 6}$$

Adding equations E-3 and E-4 gives:

$$H_3A^{2+} \overset{K_aK_a'}{\rightleftharpoons} HA + 2H^{+} \qquad \textbf{E- 7}$$

and:

$$K_a K_a^{'} = \frac{[HA][H^+]^2}{[H_3A^{2+}]} \qquad \textbf{E- 8}$$

To obtain an expression for the concentration of H_3A^{2+} in terms of the total concentration of HBzT present in solution, we can rearrange equation E-5 to give:

$$[H_3A^{2+}] = \frac{[H_2A^+][H^+]}{K_a} \qquad \textbf{E- 9}$$

Substituting equation E-2 into equation E-9, we obtain:

$$[H_3A^{2+}] = \frac{([HBzT] - [H_3A^{2+}] - [HA])[H^+]}{K_a} \qquad \textbf{E- 10}$$

Substituting equation E-8 into equation E-10, we obtain this expression for the concentration of H_3A^{2+} in terms of the total concentration of HBzT:

$$[H_3A^{2+}] = \frac{[HBzT][H^+]}{K_a + [H^+] + \frac{K_a K_a^{'}}{[H^+]}} \qquad \textbf{E- 11}$$

In a similar series of algebraic manipulations involving equations E-2, E-5, and E-6, we obtain the expression for the concentration of H_2A^+ in terms of the total concentration of HBzT:

$$[H_2A^+] = \frac{K_a[HBzT]}{K_a + [H^+] + \frac{K_a K_a^{'}}{[H^+]}} \qquad \textbf{E- 12}$$

By combining equations E-2, E-6 and E-8, we obtain the expression for the concentration of HA in terms of the total concentration of HBzT:

$$[HA] = \frac{K_a^{'}[HBzT]}{K_a^{'} + [H^+] + \frac{[H^+]^2}{K_a}}$$ **E- 13**

First-Order pH-Rate Profile for HBzT

To measure the concentration of PTK present in the solution at the end of the reaction (the absorbance limit), it is necessary to allow the reactions to run to completion. This is not a feasible experiment because the fragmentation reaction is very slow. In all cases except the pH = 5.10 and pH = 5.50 measurements, the reactions were followed for a minimum of three half lives, or longer. By using a computerized (Levenberg-Marquardt) first-order curve fitting algorithm, the data were extrapolated to completion. These first-order data are presented in Table 2-2.

Table Chapter Two -2: First-order rate constants obtained using an integrated rate equation, corrected to zero buffer concentration for HBzT fragmentation at 40 °C

Buffer	pK_a	pH	Concentrations (mM)	k_0 (s^{-1})
Acetate	4.76	5.10	100, 80, 50, 20, 10	$9.5 \pm 0.9\times10^{-7}$
		5.50	100, 80, 50, 20, 10	$1.06 \pm 0.08\times10^{-7}$
MES	6.15	5.67	100, 80, 50, 20, 10	$1.23 \pm 0.07\times10^{-6}$
		6.17	100, 80, 50, 20, 10	$2.1 \pm 0.1\times10^{-6}$
PIPES	6.82	6.42	58, 46, 29, 12, 5.8	$2.9 \pm 0.2\times10^{-6}$
		6.92	44, 35, 22, 8.7, 4.4	$5.6 \pm 0.3\times10^{-6}$
Phosphate	7.15	6.89	60, 48, 30, 12, 6.0	$7.1 \pm 0.3\times10^{-6}$
		7.52	43, 35, 22, 8.7, 4.3	$1.60 \pm 0.06\times10^{-5}$
HEPES	7.27	6.93	100, 80, 50, 20, 10	$5.1 \pm 0.2\times10^{-6}$
POPSO	7.59	7.70	40, 32, 20, 7.9, 4.0	$1.76 \pm 0.05\times10^{-6}$
		7.94	45, 36, 22, 8.9, 4.5	$2.65 \pm 0.07\times10^{-6}$
Bicine	7.99	8.28	149, 120, 74, 30, 15	$4.1 \pm 0.1\times10^{-6}$
		8.46	125, 100, 63, 25, 13	$6.8 \pm 0.4\times10^{-6}$

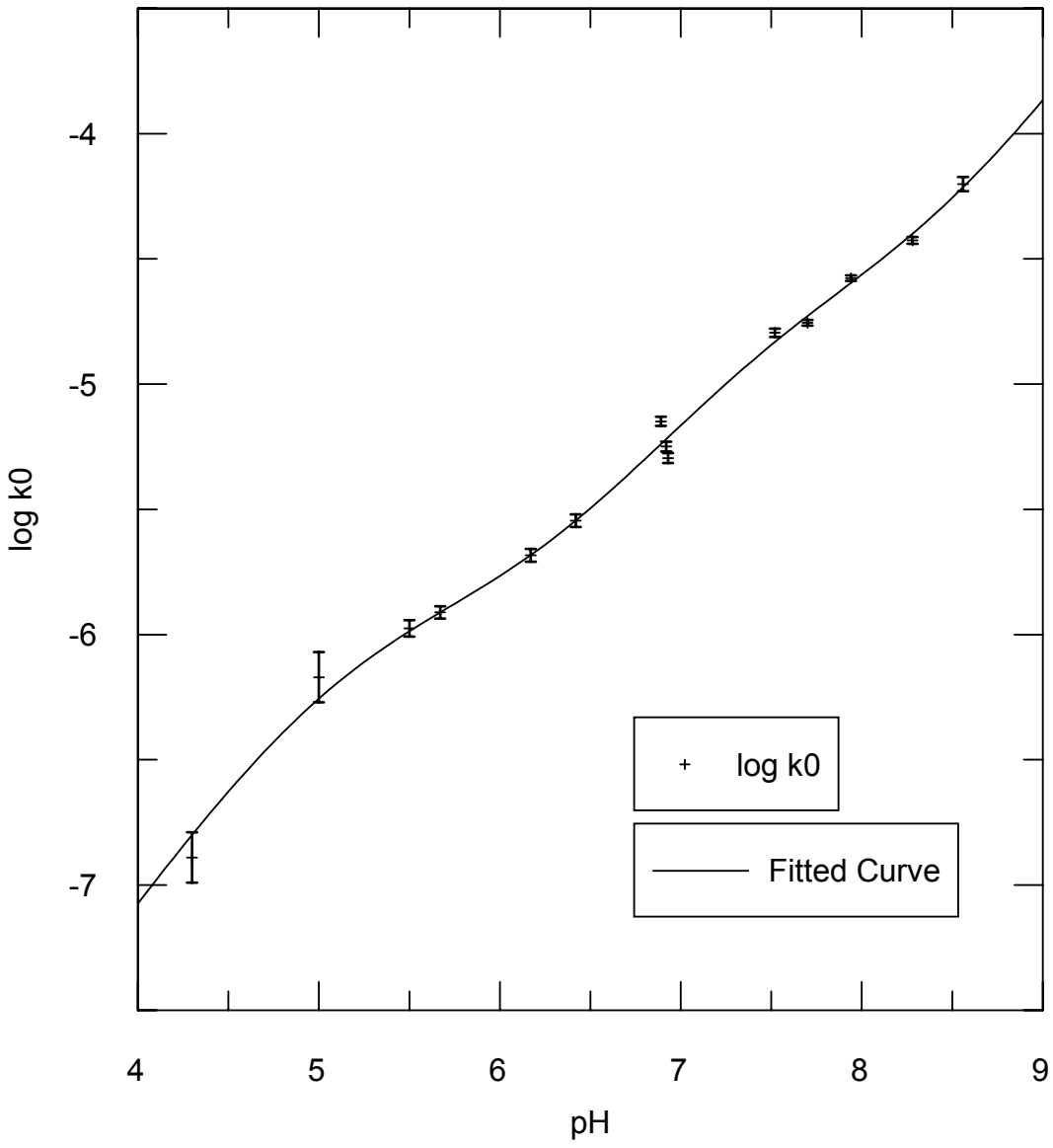

Figure Chapter Two -6: The pH-rate profile for the first order fragmentation of HBzT at 40°C.

Analysis of Production Distribution Change-Over for HBzT:

Between pH 7 and 8, we see a change in the product distribution of the HBzT reaction from the fragmentation product set to the elimination product set (Figure 2-10). Due to the very slow rate of the fragmentation reaction, we originally measured these rate constants by initial rate methods. The initial rate method requires knowledge of the stoichiometry of the reaction, and in cases where a change in product distribution occurs, a correction factor must be applied to the measured rate constants.

A change in the product distribution occurs when the rates of fragmentation and elimination are equal. A simplified model for this change in product distribution is presented in Figure 2-7. The k_f and k_e rate constants represent the observed fragmentation and elimination rate constants respectively.

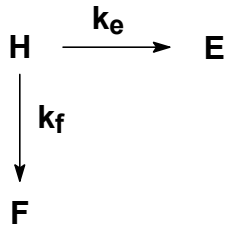

Figure Chapter Two -7: Simplified scheme for the change from fragmentation to elimination

If $[H]_0$ represents the initial concentration of HBzT, the following differential equations describe the rate of formation of the fragmentation products F, and the elimination products E from HBzT:

$$\frac{d[E]_t}{dt} = k_e[H]_t \qquad \textbf{E- 14}$$

$$\frac{d[F]_t}{dt} = k_f[H]_t \qquad \text{E- 15}$$

We have an expression for the rate of disappearance of the reactant:

$$-\frac{d[H]_t}{dt} = k_e[H]_t + k_f[H]_t \qquad \text{E- 16}$$

The solution for equation E-16 is:

$$[H]_t = [H]_0 e^{-(k_e+k_f)t} \qquad \text{E- 17}$$

Expressing $[H]_t$ from equation E-16:

$$[H]_t = \frac{\left(-d[H]_t/dt\right)}{k_e + k_f} \qquad \text{E- 18}$$

Substituting equation E-18 into equation E-14, and solving yields:

$$[E]_t = \frac{k_e}{k_e + k_f}[H]_0(1 - e^{-(k_e+k_f)t}) \qquad \text{E- 19}$$

Similarly, substituting equation E-18 into equation E-15 and solving yields:

$$[F]_t = \frac{k_f}{k_e + k_f}[H]_0(1 - e^{-(k_e+k_f)t}) \qquad \text{E- 20}$$

The ratio of elimination to fragmentation products can be expressed as:

$$\frac{[E]_t}{[F]_t} = \frac{k_e}{k_f} \qquad \text{E- 21}$$

We can use equation E-21 to calculate where the two rates are equal. At completion of the reaction, when $[H]_t = 0$, equation E-20 simplifies to:

$$\frac{[F]_\infty}{[H]_0 - [F]_\infty} = \frac{k_f}{k_e} \qquad \textbf{E- 22}$$

The mole fraction of elimination products generated can be calculated as:

$$\frac{[E]_\infty}{[H]_0} = \frac{k_e}{k_e + k_f} \qquad \textbf{E- 23}$$

By using equation E-23 and the absorbance limits of a series of first-order fragmentation kinetic runs, we can calculate the point at which the curves defined by the k_f and k_e rate constants intersect. A plot of these data is presented in Figure 2-8, and the pH where k_f and k_e are equal is 7.0 ± 0.1.

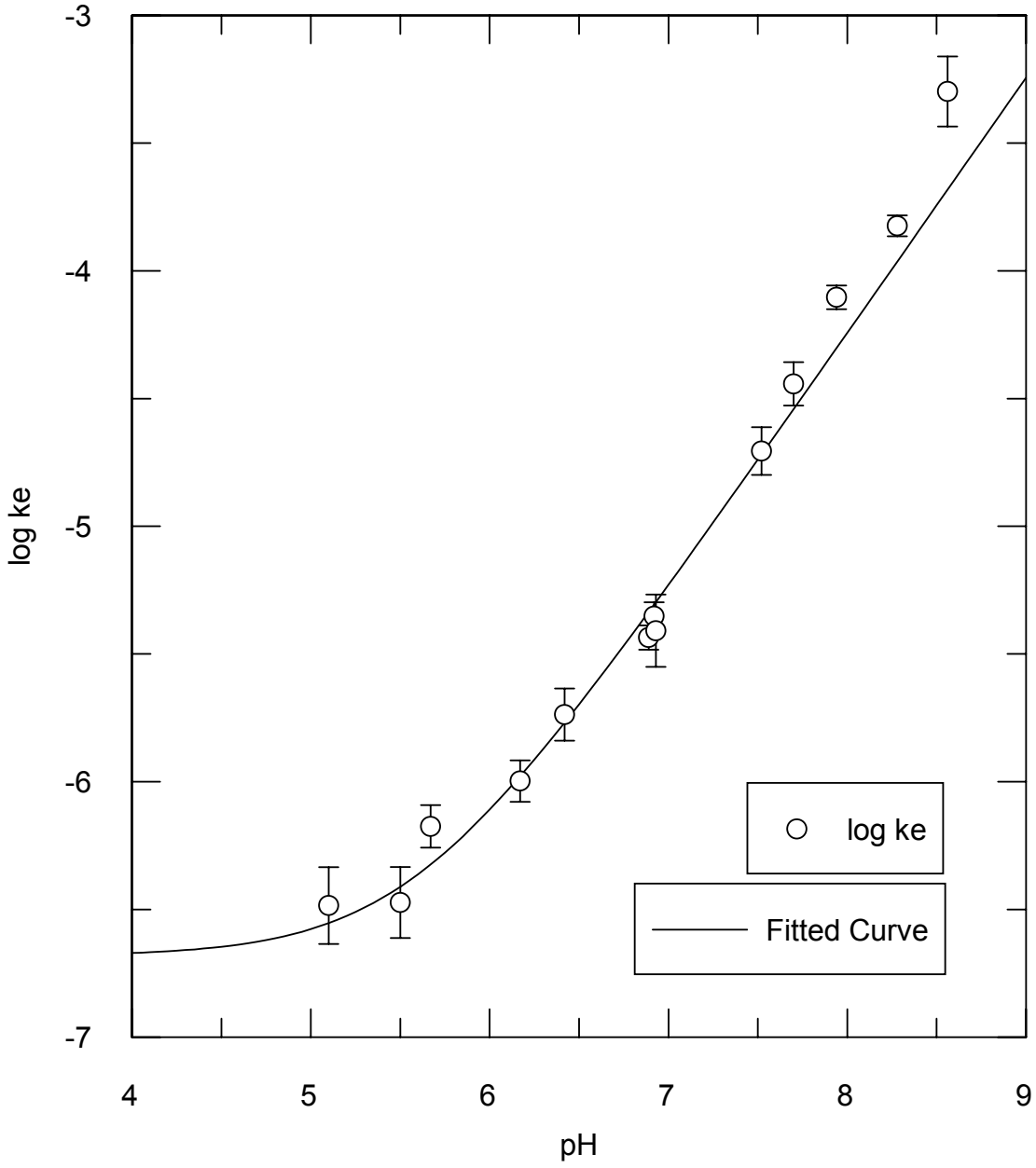

Figure Chapter Two -8: Plot of the logarithm of the calculated elimination rate coefficients versus pH

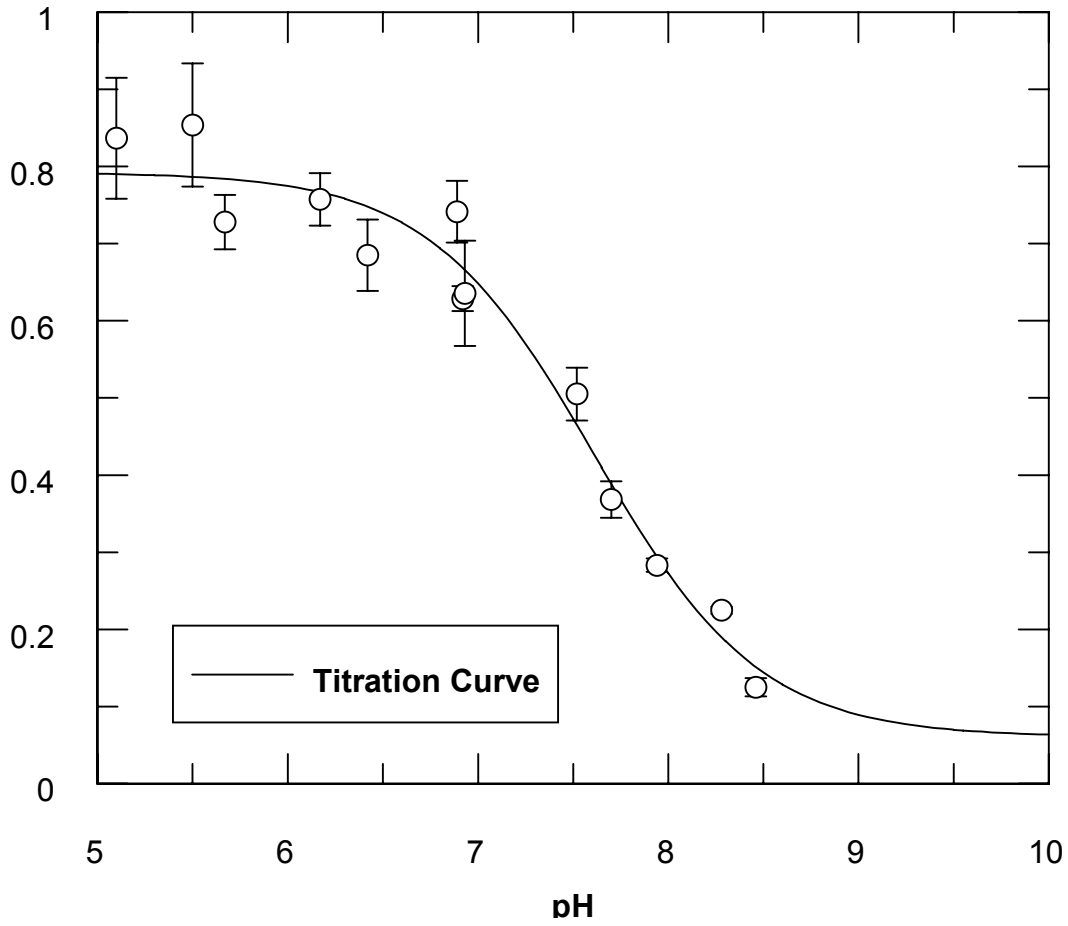

Figure Chapter Two -9: Fraction of products from HBzT fragmentation versus pH.

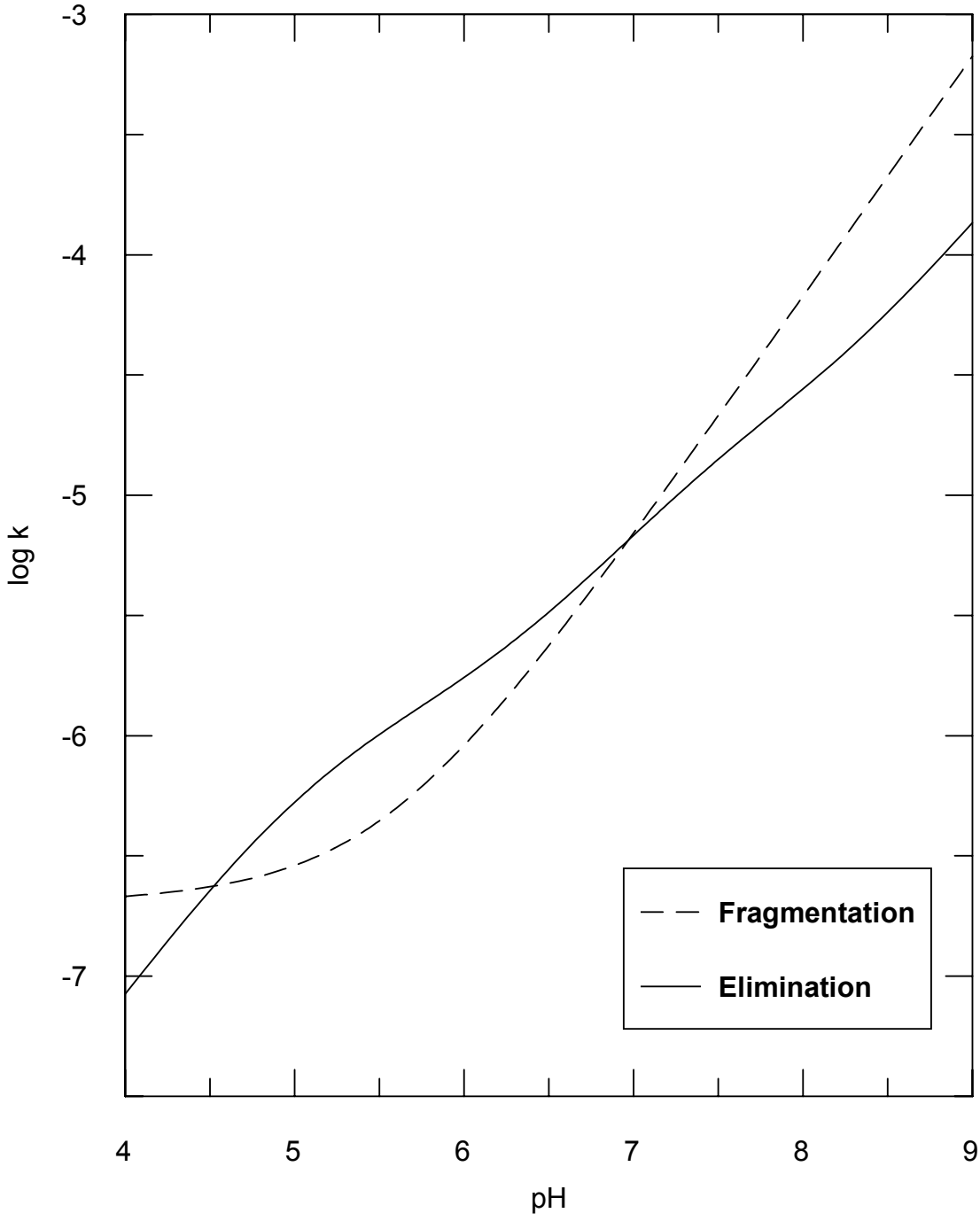

Figure Chapter Two -10: Plots of the rate equations for elimination and fragmentation of HBzT at 40°C

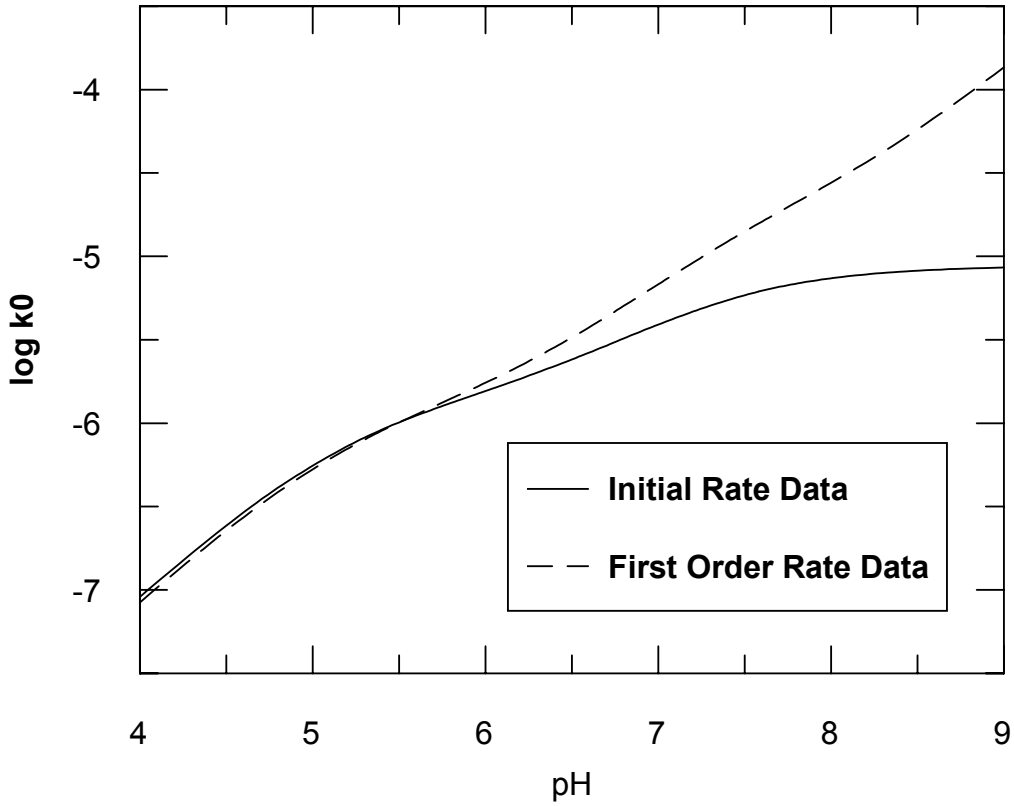

Figure Chapter Two -11: Plots of the initial rate and integrated rate equations for the fragmentation reaction.

pH-Rate Profile for NMHBzT

Kinetic studies of NMHBzT were run under the same conditions as for HBzT. The progress of the fragmentation reaction was followed by monitoring the 328 nm band in the UV spectra, which is characteristic of a π-π* transition ($\varepsilon = 8720\ cm^{-1}\ M^{-1}$) of the PTK species. The rate constants were collected using first-order techniques or by initial rate methods where indicated. The rate constants for reactions extrapolated to zero buffer concentration, and the second order rate constants where buffer catalysis was observed are presented in Table 2-3, and a plot of these rate constants versus pH is shown in Figure 2-12.

Table Chapter Two -3: First-order rate constants (k_0)corrected to zero buffer concentration, and second-order buffer rate constants (k_B) (where buffer catalysis was observable) for NMHBzT fragmentation at 40 °C.

Buffers	pK_a	pH	Concentrations (mM)	k_0 (s^{-1})	k_B ($M^{-1}s^{-1}$)
Acetate	4.76	4.30	100, 50.2, 10.4	$2.7 \pm 0.4\times10^{-7}$	$1.4 \pm 0.2\times10^{-6}$
		5.00	104, 50.7, 10.4	$1.91 \pm 0.02\times10^{-6}$	$9.2 \pm 0.4\times10^{-6}$
Succinate	5.64	5.30	61.5, 30.9, 8.10	$4.0 \pm 0.3\times10^{-6}$	$5.4 \pm 0.6\times10^{-5}$
		5.90	43.5, 21.2, 4.37	$1.1 \pm 0.2\times10^{-5}$	$3.2 \pm 0.7\times10^{-4}$
MES	6.15	5.70	101, 51.0, 10.5	$9.0 \pm 0.4\times10^{-6}$	
		6.20	100, 51.4, 10.8	$2.5 \pm 0.2\times10^{-5}$	
PIPES	6.82	6.40	33.1, 16.5, 3.38	$4.4 \pm 0.2\times10^{-5}$	
		6.90	33.3, 17.2, 3.40	$1.31 \pm 0.02\times10^{-4}$	
Phosphate	7.20	6.90	58.4, 28.4, 6.07	$1.19 \pm 0.08\times10^{-4}$	$2.3 \pm 0.2\times10^{-3}$
		7.40	44.0, 21.6, 4.50	$3.01 \pm 0.06\times10^{-4}$	$4.7 \pm 0.2\times10^{-3}$
HEPES	7.55	7.00	100, 51.1, 11.6	$1.63 \pm 0.02\times10^{-4}$	
		7.60	100, 49.8, 11.7	$5.0 \pm 0.3\times10^{-4}$	
POPSO	7.85	7.80	38.7, 19.9, 3.96	$1.1 \pm 0.1\times10^{-3}$	$4.2 \pm 0.6\times10^{-3}$
		8.10	39.6, 20.4, 4.32	$2.65 \pm 0.03\times10^{-3}$	$1.6 \pm 0.2\times10^{-2}$
Bicine	8.35	8.30	100, 49.2, 9.97	$2.64 \pm 0.03\times10^{-3}$	
		8.60	98.6, 50.5, 9.97	$5.09 \pm 0.04\times10^{-3}$	$4.3 \pm 0.8\times10^{-2}$

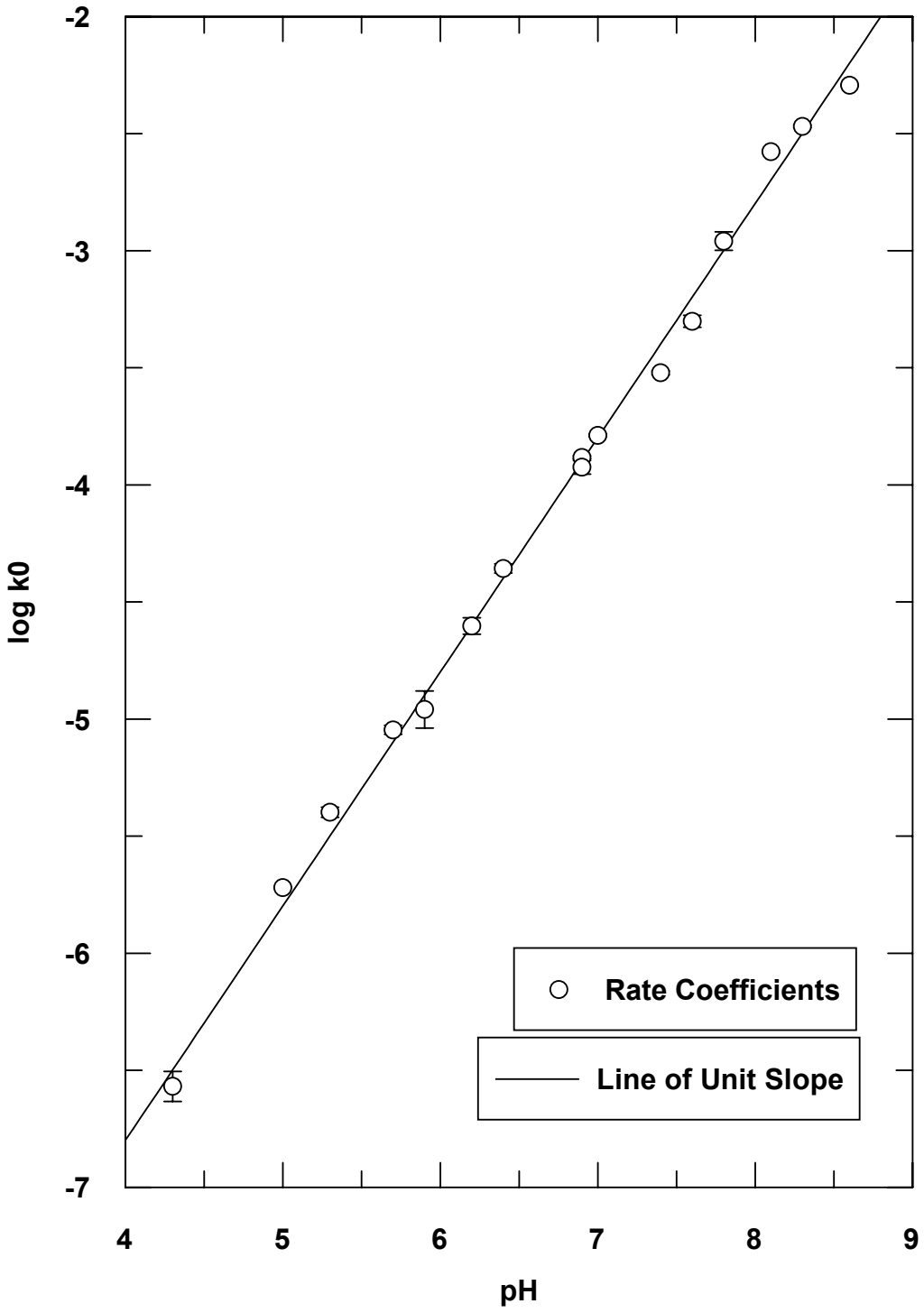

Figure Chapter Two -12: pH-Rate profile for NMHBzT fragmentation 40 °C

Comparison of HBzT and NMHBzT Fragmentation Profiles:

Figure 2-13 is a plot of the NMHBzT and HBzT fragmentation initial rate constants on the same scale. One can see that the rate constants at the low end of the pH-initial rate profile (below pH 5), are very similar, within a factor of 2. As both the HBzT and the NMHBzT fragmentation reactions were carried out in the same series of buffer solutions, ionic strengths and temperature, the similarity in rate constants in this pH region suggests that both HBzT and NMHBzT are fragmenting by the same mechanism.

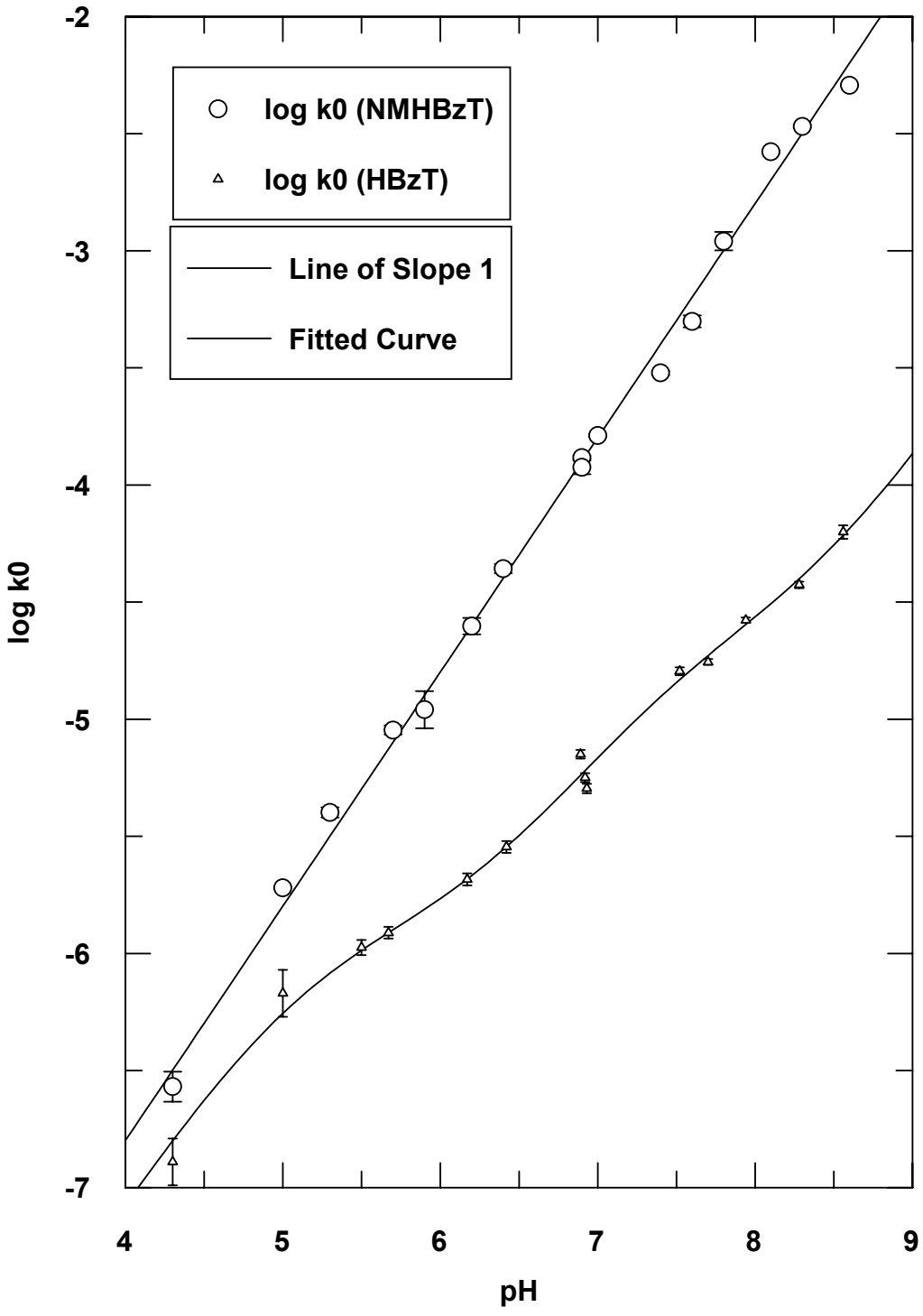

Figure Chapter Two -13: NMHBzT and HBzT fragmentation pH-Rate profiles

Buffer Catalysis of the NMHBzT Fragmentation Reaction

We observe buffer catalysis in the pH-Rate profiles of both HBzT and NMHBzT. The second-order rate constants for buffer catalysis are collected in Tables 2-1 and 2-3. Figure 2-14 is a Brönsted plot for the fragmentation reaction of NMHBzT. The line fitted through the data points has a slope of 0.98.

The fragmentation reaction is accelerated by the basic buffer component and obeys the general rate law:

$$k_{obs} = k_{H_2O} + k_{OH^-}[OH^-] + k_B[B] \qquad \textbf{E- 24}$$

However, buffer catalysis was limited to species with anionic basic components. It is likely that neutral buffer species will catalyze the reaction less effectively than anionic basic buffers which can benefit from an electrostatic interaction with dicationic NMHBzT. Alternately, if a kinetically equivalent specific base-general acid mechanism is involved, anionic bases produce neutral acids while neutral bases produce cationic acids that would be repelled by NMHBzT.

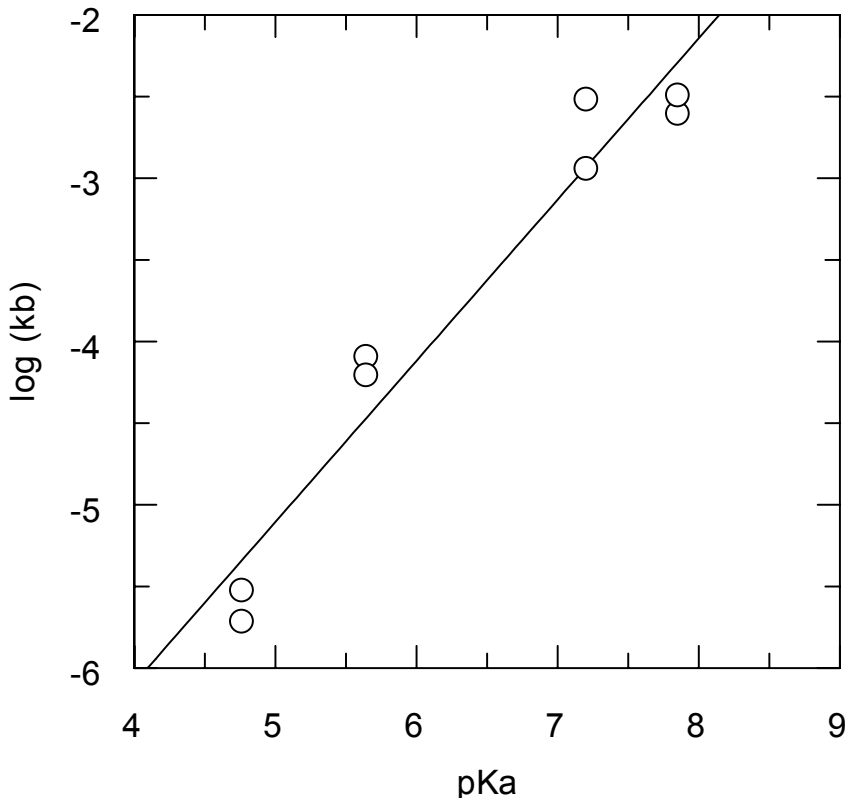

Figure Chapter Two -14: Brönsted plot for the fragmentation of NMHBzT

Cyclization of HBzT Occurs at low pH

The NMR spectra reveal the accumulation of a compound consistent with the structure proposed in Figure 2-15 (cHBzT). Several observations in the NMR spectra support the assignment of the structure in Figure 2-15. They are:

1) The integrated area of the pyrimidine C6' proton of HBzT (δ 6.51) decreases at a rate equal to the rate of appearance of a separate triplet corresponding to the $C_{5'\beta}$ protons of cHBzT.

2) We see the appearance of a singlet in the NMR which we assign as the pyrimidine C6' proton of cHBzT (δ 4.31).

3) The integrated area of the signal for the $C_{5'\alpha}$ protons of HBzT (AB quartet, δ 5.23) decreases at a rate equal to the rate of appearance of the integrated area of a new AB quartet which we assign to the $C_{5'\alpha}$ protons in cHBzT (δ 4.65).

4) The cHBzT $C_{5'\alpha}$ protons are shifted upfield relative to the HBzT $C_{5'\alpha}$ protons. This is consistent with Zoltewicz's suggestion[27] that the product formed by addition of a nucleophile to the pyrimidine ring is a better electron donor than the parent pyrimidine ring.

5) The cHBzT $C_{5\beta}$ protons are shifted upfield (Δδ 0.10) relative to the corresponding protons of HBzT.

6) The $C_{5'\alpha}$ protons, being farther removed from the new carbon-oxygen bond, are shifted upfield by a lesser amount (Δδ 0.04).

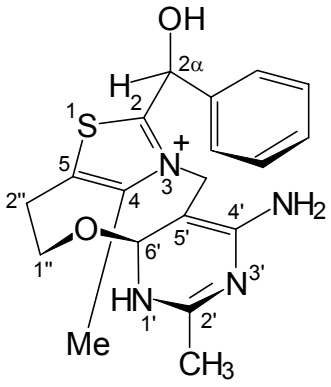

Figure Chapter Two -15: Proposed structure of cyclized HBzT (cHBzT) adduct.

Exchange Studies on NMHBzT

In order to determine if general base catalysis involves ionization of the $C_{2\alpha}$ proton, a study of exchange was performed by John Pezacki as his fourth-year undergraduate project. The pK_a's of the buffers in deuterium oxide were determined by combining equal amounts of acidic and basic forms of the buffer (0.01M) with ionic strength adjusted to 1.0 using potassium chloride in deuterium oxide. The pD value was calculated by adding 0.40 to the pH meter reading at 40° C.[34]

Buffer catalysis of the exchange reaction was observed with phosphate, acetate and formate buffers (Table 2-4). Rate coefficients for exchange of the $C_{2\alpha}$ proton increased with increasing buffer concentration and only in proportion to the base component of the buffer. The second order rate constants for buffer catalysis were determined from the slope of the plots of $k_{obsd.}$ versus buffer concentration. A Brönsted plot of these data (Figure 2-16) shows $\beta \geq 0.9$ for $C_{2\alpha}$ proton removal. Stivers and Washabaugh have discussed the nature of the related proton removal reaction in detail for similar compounds.[35,36,37] For the purposes of the present study it is sufficient to note that this

exchange is faster than the fragmentation. Therefore, buffer catalysis of proton removal is not responsible for the general base catalysis observed during fragmentation.

Table Chapter Two -4: Rate constants for general-base catalyzed exchange of $C_{2\alpha}$ proton of NMHBzT in deuterium oxide buffer solutions at 40°C[a]

Buffer	*pK_a'* [b]	*concentrations, M*	*$k_b / M^{-1} s^{-1}$*
formate	4.24	1.0, 0.75, 0.5	2.7×10^{-6}
acetate	5.05	1.0, 0.75, 0.5	2.6×10^{-5}
phosphate	6.85	0.28, 0.20, 0.15	7.0×10^{-4}

[a] Ionic Strength = 1.0 (KCl)
[b] pK_a of conjugate acid in D_2O (I = 1.0 M) determined as described in experimental section.

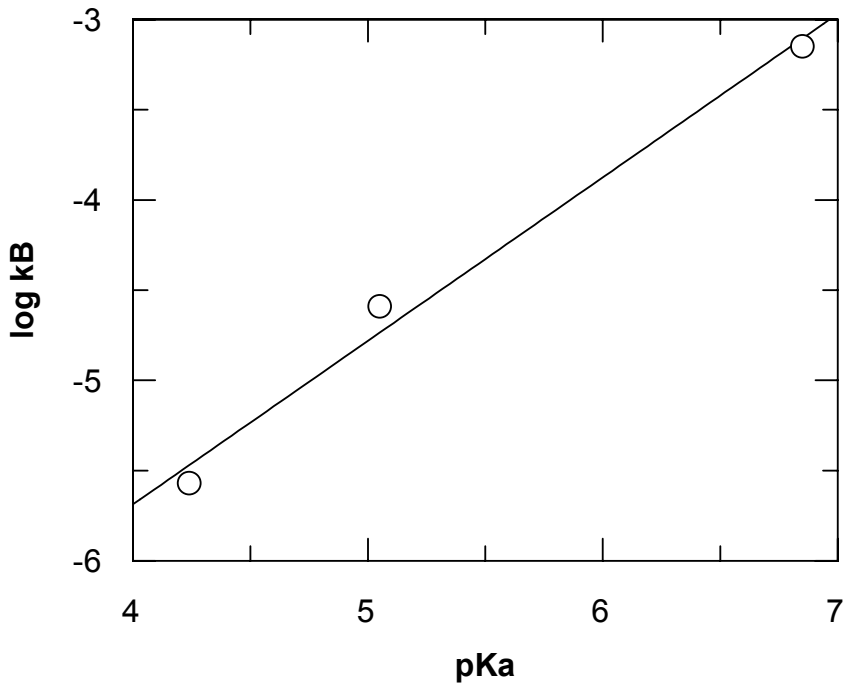

Figure Chapter Two -16: Brönsted plot for exchange of the $C_{2\alpha}$ proton. The slope of the line is 0.90.

Chapter Three : DISCUSSION AND CONCLUSIONS

Overview of the Experimental Results

A mechanism that explains reactivity patterns of HBzT must be consistent with the body of experimental evidence that was gathered. The mechanism must also explain the reactivity of NMHBzT as a subset of that of HBzT. To lay the groundwork for the discussion that follows, we will first review the major experimental results.

1. Two sets of products are generated by reacting HBzT in aqueous solutions. Below pH 7.3, we find mainly the fragmentation products: PTK and DMP. Above pH 7.3, most of the products are from the elimination set: benzaldehyde and thiamin.
2. Only the fragmentation product set is generated from NMHBzT at all acidities.
3. General-base catalysis is observed in both NMHBzT and HBzT fragmentation. Catalysis is only observed with buffers whose basic component is anionic.
4. ^{1}H NMR studies show the $C_{2\alpha}$ proton of HBzT and NMHBzT exchanges with solvent faster than fragmentation occurs. The rate of exchange is proportional to hydroxide concentration.
5. Hydroxyethylthiamin (HET) fragments at least 500 times more slowly than HBzT, and 10000 times more slowly than does NMHBzT.
6. The HBzT pH-Rate profile has two apparent pK_a's. The first is the thermodynamic pK_a of the pyrimidine N_1' nitrogen. The second apparent pK_a is not a thermodynamic pK_a of HBzT.
7. The extent of HBzT cyclization is dependent on the concentration of N_1' protonated pyrimidine. The thiazolium hydroxyethyl side chain cyclizes onto the C6' carbon of the pyrimidine.

pH-Rate Profile of HBzT:

The pH-Rate profile for HBzT fragmentation (Figure 2-5) resembles the titration curve of a diprotic acid. By fitting our fragmentation rate coefficients to equation E- 1, we obtain two apparent pK_a's: 5.2 ± 0.1 and 7.3 ± 0.1. If we assign the first apparent pK_a as the thermodynamic pK_a of HBzT's N_1' nitrogen, we are consistent[38] with earlier observations.[17] But what of the second apparent pK_a?

The simplest explanation of the second apparent pK_a is that it is a thermodynamic pK_a of the $C_{2\alpha}$ proton. We suggested earlier[1,39] that two factors govern whether the reaction gives fragmentation products rather than elimination products. We argued that there must be a positive charge present on the pyrimidine ring, and that it is due to protonation of the N_1' nitrogen. Since the $C_{2\alpha}$ proton must be removed to generate the enamine of HBzT, this ionization could explain the second apparent pK_a.

Thermodynamic pK_a of the $C_{2\alpha}$ Proton?

Figure 3-1 treats the second apparent pK_a as a thermodynamic pK_a, giving a simple scheme for the generation of the fragmentation products. Fragmentation is rate-limiting from the monoprotic and unprotonated species in Figure 3-1. We can derive expressions for the concentrations at time *t* for HA and A in terms of the total concentration of HBzT (H_2A^+ and HA from Equations E-12 and E-13).

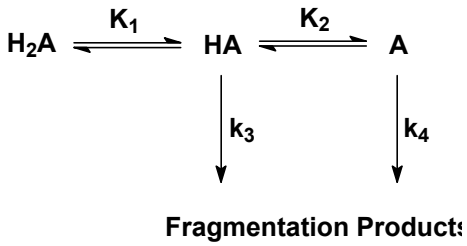

Figure Chapter Three -1: Treatment of both apparent pK_a's as Thermodynamic pK_a's

The rate of formation of the fragmentation products P is given by:

$$\frac{dP}{dt} = k_3[HA] + k_4[A] \qquad \textbf{E- 25}$$

We obtain an expression for k_{obs} by substituting equations E-12 and E-13 into equation E-25:

$$k_{obs} = \frac{k_3 K_1}{K_1 + [H^+] + \frac{K_1 K_2}{[H^+]}} + \frac{k_4 K_2}{K_2 + [H^+] + \frac{[H^+]^2}{K_1}} \qquad \textbf{E- 26}$$

Since the K_1K_2 and $[H^+]^2$ terms are small, we can simplify equation E-26 to:

$$k_{obs} = \frac{k_3 K_1}{K_1 + [H^+]} + \frac{k_4 K_2}{K_2 + [H^+]} \qquad \textbf{E- 27}$$

By fitting equation E-27 to the rate coefficients for fragmentation, we can obtain values for all rate and equilibrium constants in the simplified reaction scheme. How does this translate into reactions of chemical species?

Figure 3-2 is a mechanism that shows the chemical species involved in rate-determining fragmentation or elimination steps. The figure is arranged by decreasing protonation states from left to right. Within each protonation state, all reasonable

tautomeric equilibria are shown, along with estimates of the magnitude of the tautomeric equilibrium constants, based upon pK_a estimates.

Figure Chapter Three -2: Protonation states of HBzT

Enamine Formation is Not the Rate-Limiting-Step in Fragmentation

Our studies of proton exchange at $C_{2\alpha}$ of NMHBzT show that exchange is more rapid than fragmentation. Therefore, formation of the conjugate base of NMHBzT occurs prior to the rate determining step for fragmentation. The results of our exchange studies are also similar to Washabaugh's studies of $C_{2\alpha}$ proton exchange in several related compounds: 2-hydroxyethyl-3,4-dimethylthiazolium chloride, 2-(1-hydroxyethyl)-thiamin and 2-(1-hydroxybenzyl)-oxythiamin. [35,36,37] Washabaugh and coworkers observed large β values (> 0.90) for these reactions, as we do (β = 0.90 in Figure 2-16) in our NMHBzT exchange studies.

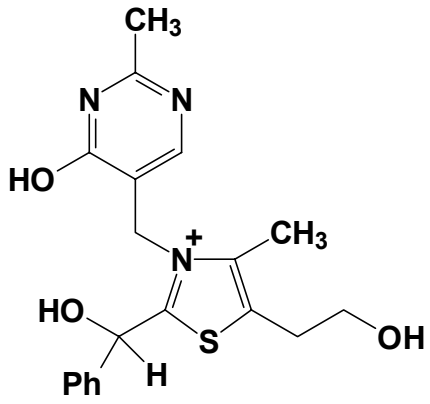

Figure Chapter Three -3: 2-1-(hydroxybenzyl)-oxythiamin (HBzOT)

We interpret the large Brönsted β value in the conventional way[40], as indicating a late or product-like transition state (Figure 3-4) for a thermodynamically unfavourable proton transfer. It also suggests that the rate-limiting step of the proton transfer is diffusion-controlled separation of the products.

Such a large β value is unusual for carbon acids since it suggests that there is a very

small barrier to protonation of the conjugate base.[19] Most carbon acids generate highly delocalized carbanions, such as the thiamin enamine in this case. Where such delocalized carbanions exist, the accompanying structural and solvation changes that are responsible for the large intrinsic barriers for proton transfers from the carbon acids that lead to these delocalized carbanions result in β values near 0.5.[41] On the other hand, carbon acids that give highly localized carbanions as conjugate bases, such as cyanide and the thiamin ylid, behave like 'normal' acids. [19,21,42] The Brönsted plots for these normal acids follow Eigen curves with slopes of 0 and ±1 in the favorable and unfavorable directions respectively.[43] Although large β values suggest localized carbanions, the carbanion in this reaction is clearly delocalized. Therefore, these large β values suggest that resonance interactions with the thiazolium ring of the HBzT enamine do not result in a significant increase to the intrinsic barrier.

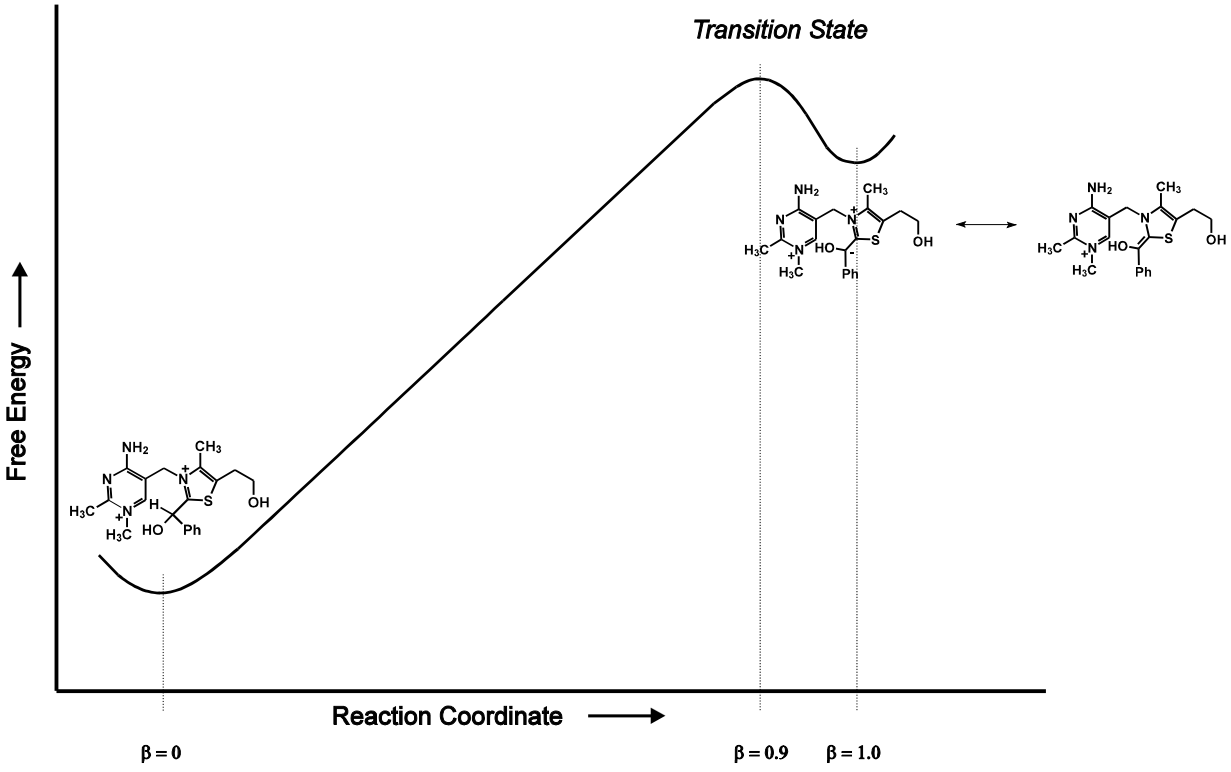

Figure Chapter Three -4: Reaction coordinate diagram for removal of $C_{2\alpha}$ proton from NMHBzT

We also see the effects of resonance interactions of the $C_{2\alpha}$ carbanion with the thiazolium ring in biological systems. Benzoylformate decarboxylase (BFD) (EC 4.1.1.7) is a thiamin diphosphate dependent enzyme that converts benzoylformate to benzaldehyde and carbon dioxide (Figure 3-5).[44] Decarboxylation of benzoylformate presumably generates the enamine of HBzT diphosphate as an enzyme-bound intermediate (Figure 3-6). Mechanism-based inhibition of BFD is possible by using an analogue of benzoylformate: [*p*-(bromomethyl)benzoyl]formate. After decarboxylation of this compound, the resulting $C_{2\alpha}$ carbanion can be resonance stabilized as the enamine (**4**) (Figure 3-6). Alternatively, elimination of bromide is possible, and inactivation of the enzyme occurs (**5**). Interestingly, it is only in the presence of BFD that elimination of bromide occurs. In free solution, there is no detectable release of bromide,[45] and this disparity will be discussed later.

Figure Chapter Three -5: Benzoylformate decarboxylase reaction

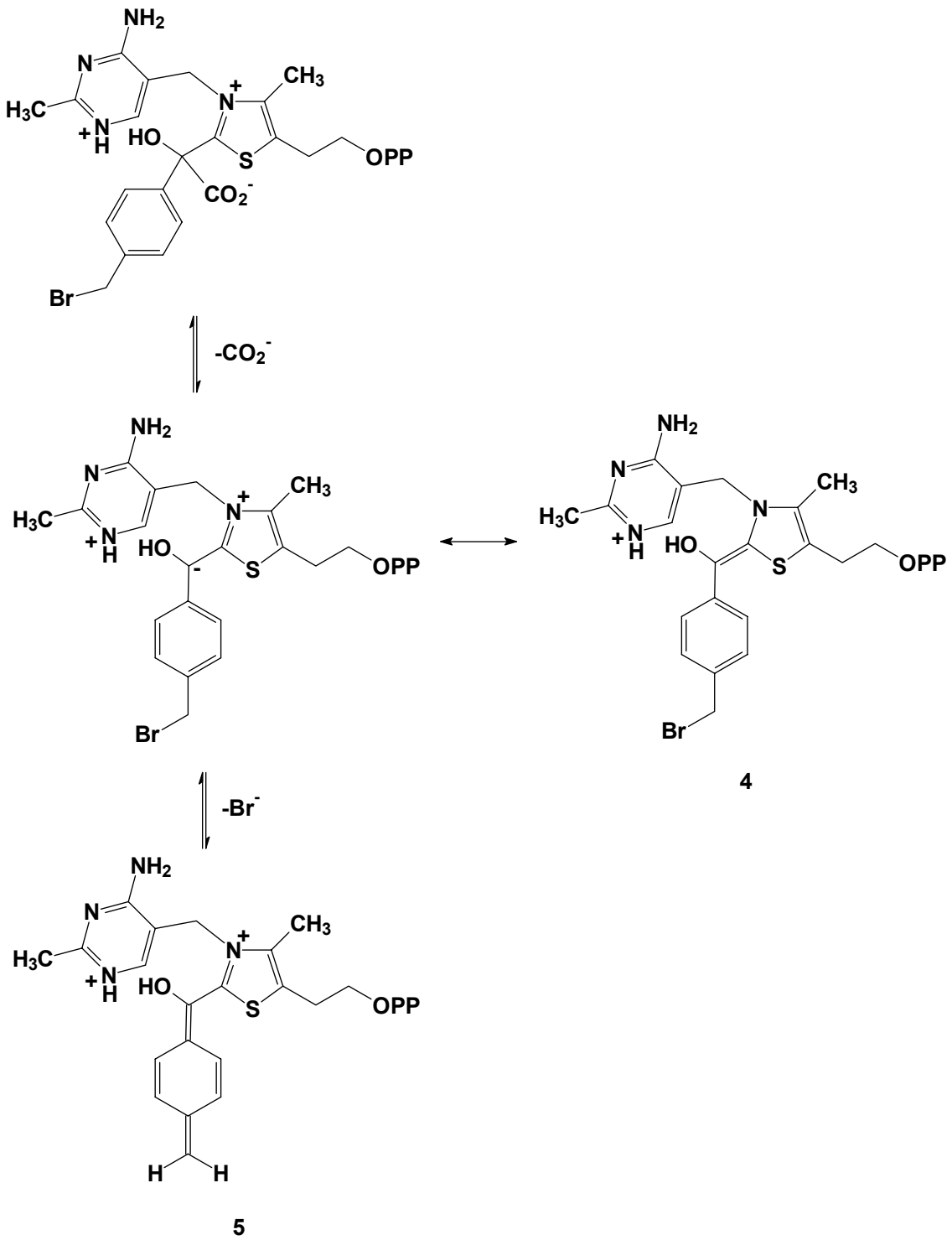

Figure Chapter Three -6: Inhibition of benzoylformate decarboxylase

Other Possibilities Must Be Considered:

What if pK_a' is not the thermodynamic pK_a associated with the $C_{2\alpha}$ proton? Recently, Washabaugh and coworkers have measured the $C_{2\alpha}$ pK_a (15) in a model compound: 2-(1-hydroxybenzyl)-oxythiamin (HBzOT in Figure 3-3).[37] They calculated the pK_a by assuming a diffusion-controlled rate (3.0×10^9 $M^{-1}s^{-1}$) for re-protonation of HBzOT's conjugate base. For the $C_{2\alpha}$ proton of HBzT to have a pK_a of 7.3 as seen in HBzT's fragmentation pH-Rate profile, it must have a very slow rate of reprotonation: ~1×10^{-5} $M^{-1}s^{-1}$. However, this is many orders of magnitude smaller than the rate constant for protonation of a highly delocalized system such as dimethylmalonate, which has a protonation rate constant of 4.0×10^5 $M^{-1}s^{-1}$. Such a slow rate constant for protonation of HBzT's conjugate base would also be inconsistent with the large β value for the deprotonation reaction (> 0.90), and the correspondingly small α value for the protonation reaction (< 0.10). Since the apparent pK_a' (7.3) is much smaller than the pK_a of 15 measured for the analogue, it is unlikely that what we observe is due to dissociation of the $C_{2\alpha}$ proton. Therefore, we must consider other possibilities: a pH-dependent equilibrium, or a change in rate-determining step.

Possible Explanations for the Apparent pK_a of 7.3:

The apparent pK_a of 7.3 can be due to a pH-dependent equilibrium involving the $C_{2\alpha}$ proton. Removal of the $C_{2\alpha}$ proton generates the thiamin enamine (Figure 3-7) and protonation on the $C_{2\alpha}$ carbon regenerates HBzT. However, the thiamin enamine can also tautomerize to form another intermediate: benzoylthiamin (BT). Since the ketonization reaction is a pH-independent process, the equilibrium between HBzT and BT is pH-

dependent, and can be responsible for pK_a'. By convention, the ketonization equilibrium in Figure 3-7 is usually referred to as an enolization equilibrium, defined as K_E in the reverse direction. Since our observed pK_a' is 7.3 and Washabaugh's measurement[37] of $pK_a^{c2\alpha}$ is 15 ± 1 in a related compound, it suggests that pK_E is 7.7 ± 1. This is not an unreasonable value for this pK_E since acetophenone is structurally similar (Figure 3-7), and has a pK_E of 7.96.[46]

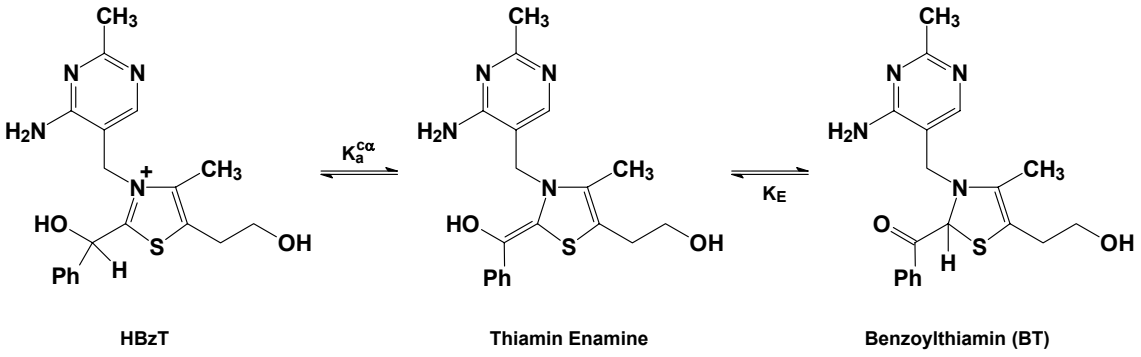

Figure Chapter Three -7: Ketonization of thiamin enamine to generate benzoylthiamin

Can pK_a' Be Due To Hydride Transfer?

Another route to the benzoylthiamin intermediate (BT) (Figure 3-7) is via the base catalyzed 1,2-hydride-shift mechanism shown in Figure 3-8. A similar mechanism is generally accepted for the base-catalyzed rearrangement of phenylglyoxal hydrate to mandelic acid. Hine and coworkers showed that under strongly basic conditions (> 1 M hydroxide), phenylglyoxal hydrate rearranges to mandelic acid via a 1,2 hydride shift, from either the monoanionic, or the dianionic intermediate (Figure 3-9).[47] This reaction is characterized by a kinetic isotope effect (k_H / k_D) of 5.0 when the substrate is deuterated on the C1 carbon, and ^{1}H NMR studies reveal that rearrangement occurs without loss of

the deuterium label to solvent. This can be contrasted to the behaviour of the system at neutral pH.

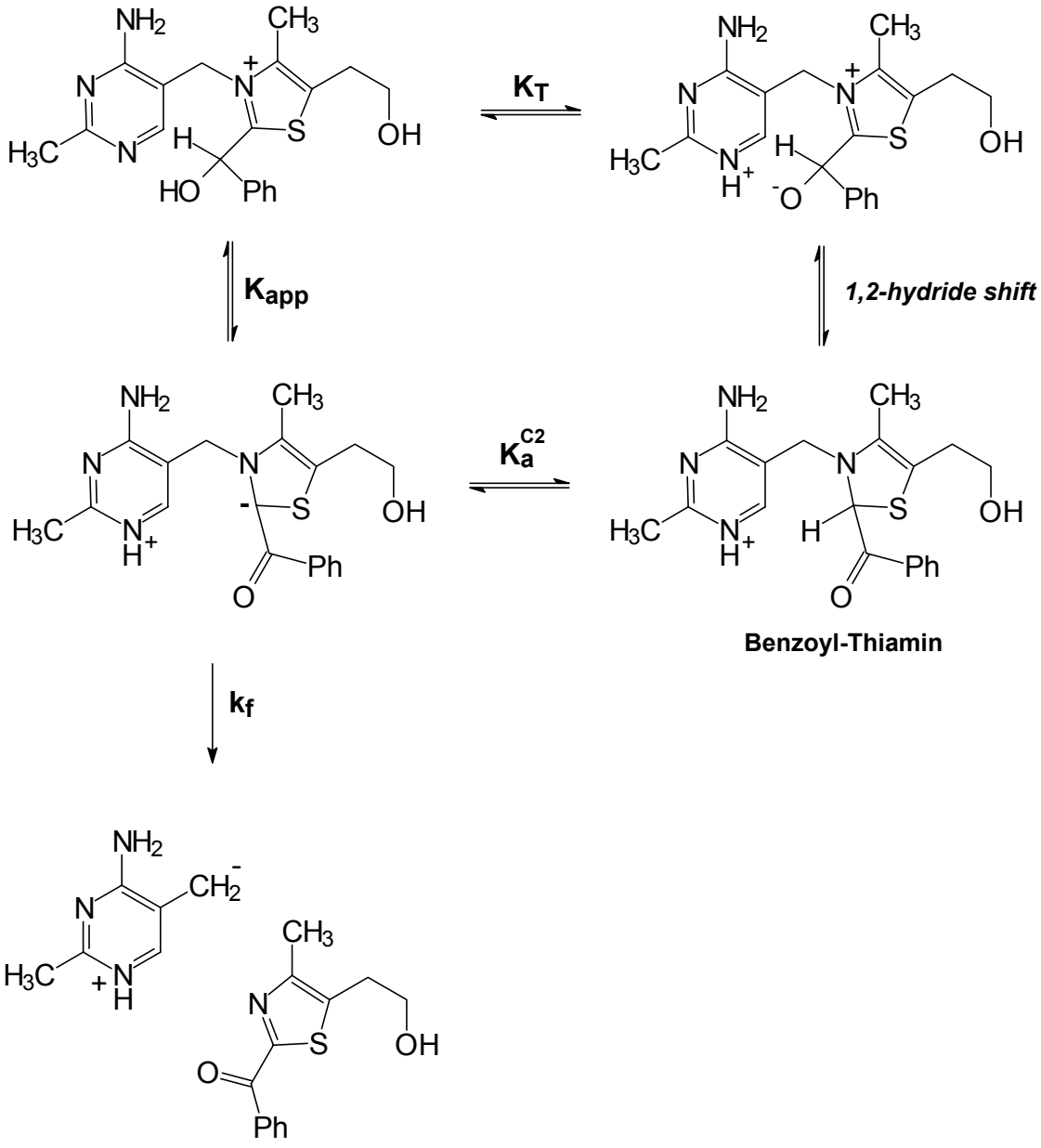

Figure Chapter Three -8: Hydride shift accounting for apparent pK_a

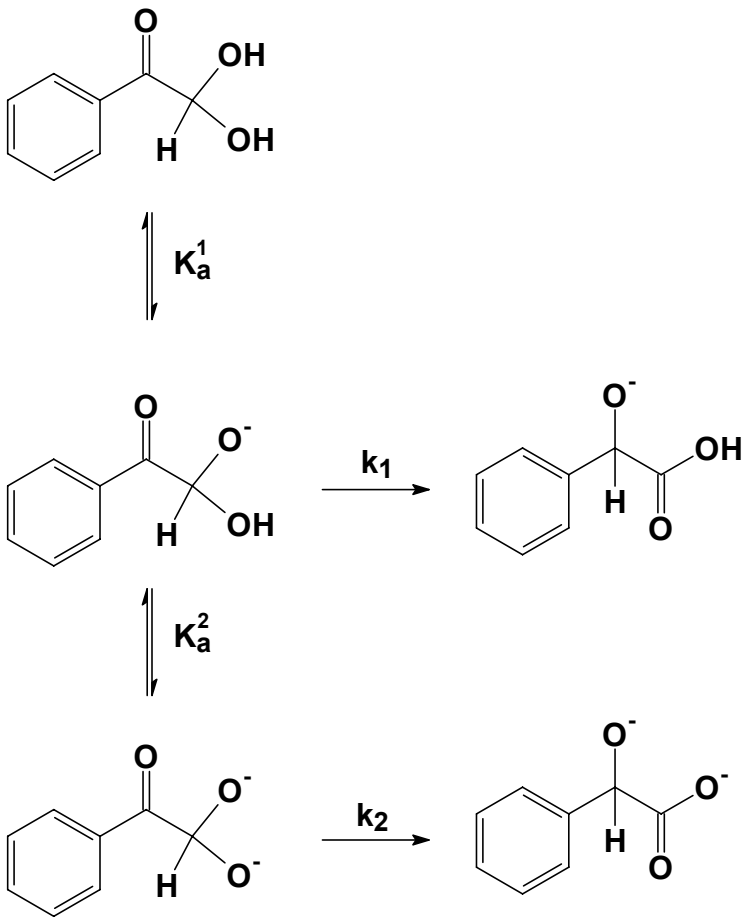

Figure Chapter Three -9: Intramolecular Cannizzaro rearrangement

The Glyoxalase I enzyme catalyzes this rearrangement, operates at neutral pH, but uses a different mechanism. Jordan and coworkers observed general base catalysis in their model studies of this reaction at neutral pH[48,49]. The reaction solutions contained glutathione, phenylglyoxal, magnesium and either phosphate or imidazole as the general base. The reaction is buffer catalyzed with a zero intercept in the rate vs. buffer concentration plot. C1-deuterated substrate displays a kinetic isotope effect (k_H / k_D) of 2.3. In similar studies with unlabelled substrate in neutral D_2O solutions, solvent deuterium was incorporated into the C_2 carbon at levels exceeding 90%. Since hydride-

shift mechanisms proceed without transfer to solvent and proton transfer mechanisms proceed with exchange, this is strong evidence for a proton transfer mechanism operating at neutral pH.[48,49] Therefore, this suggests that a similar HBzT rearrangement reaction at neutral pH would proceed via an enediol intermediate.

Benzoylthiamin (BT) and Analogues Reported in the Literature

Risinger and coworkers conducted experiments to isolate a neutral, tricyclic form of thiamin (Figure 3-10) by reacting thiamin with various aldehydes in ethanol. After 5 hours of reaction with benzaldehyde, they saw the appearance of benzoylthiamin (BT) (Figure 3-11) in addition to the expected benzoin condensation products. Similar reactions can also be found in earlier studies (Figure 3-12).[50,51] In all cases, they found that formation of acylthiamin compounds was faster than the production of benzoin by the normal catalytic process.

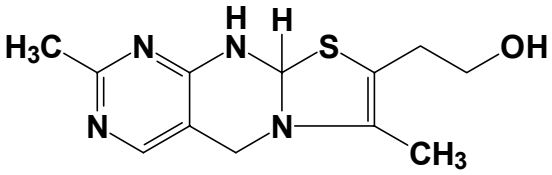

Figure Chapter Three -10: Tricyclic form of thiamin

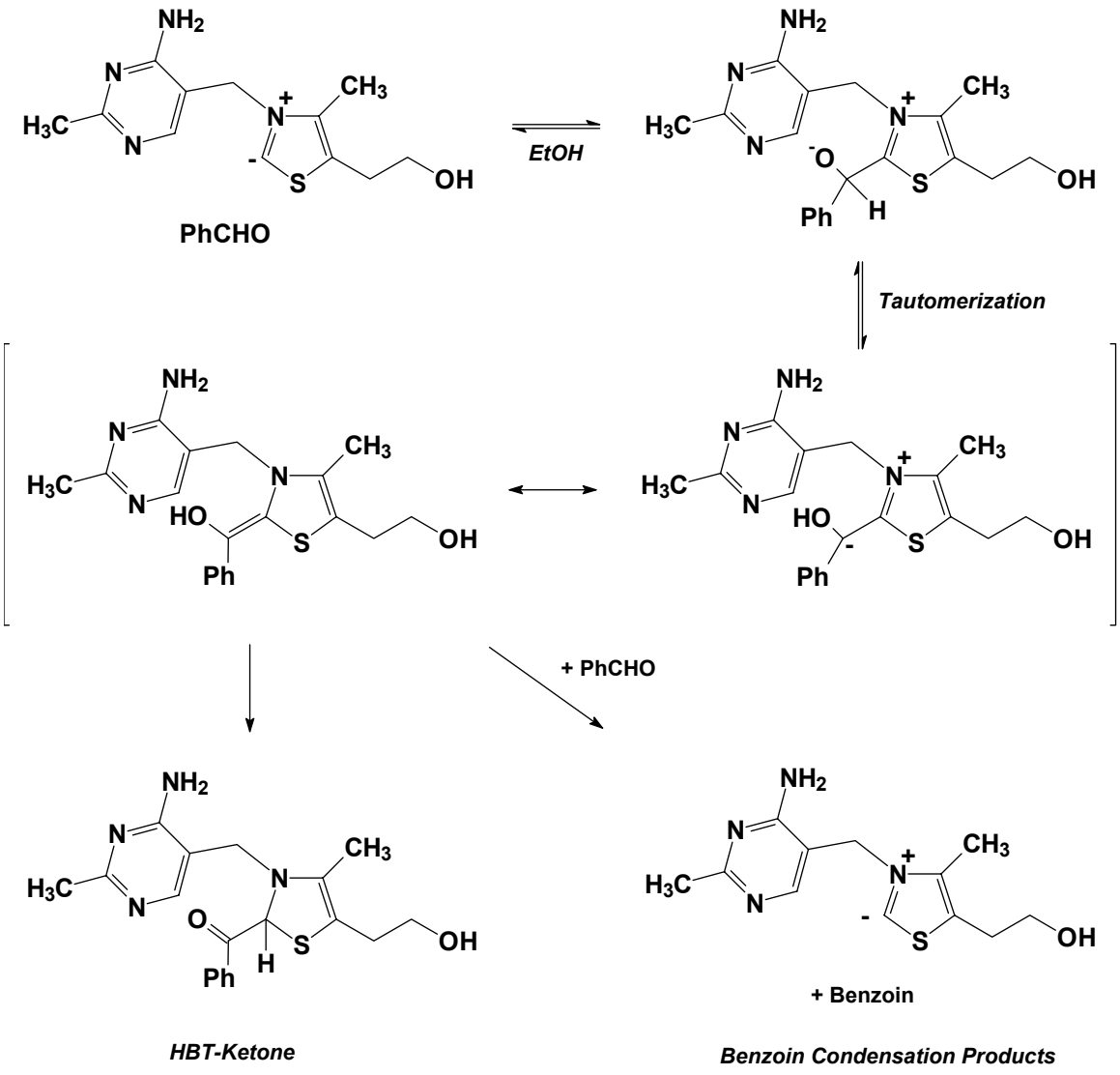

Figure Chapter Three -11: Risinger's observation of HBT-ketone (benzoylthiamin)

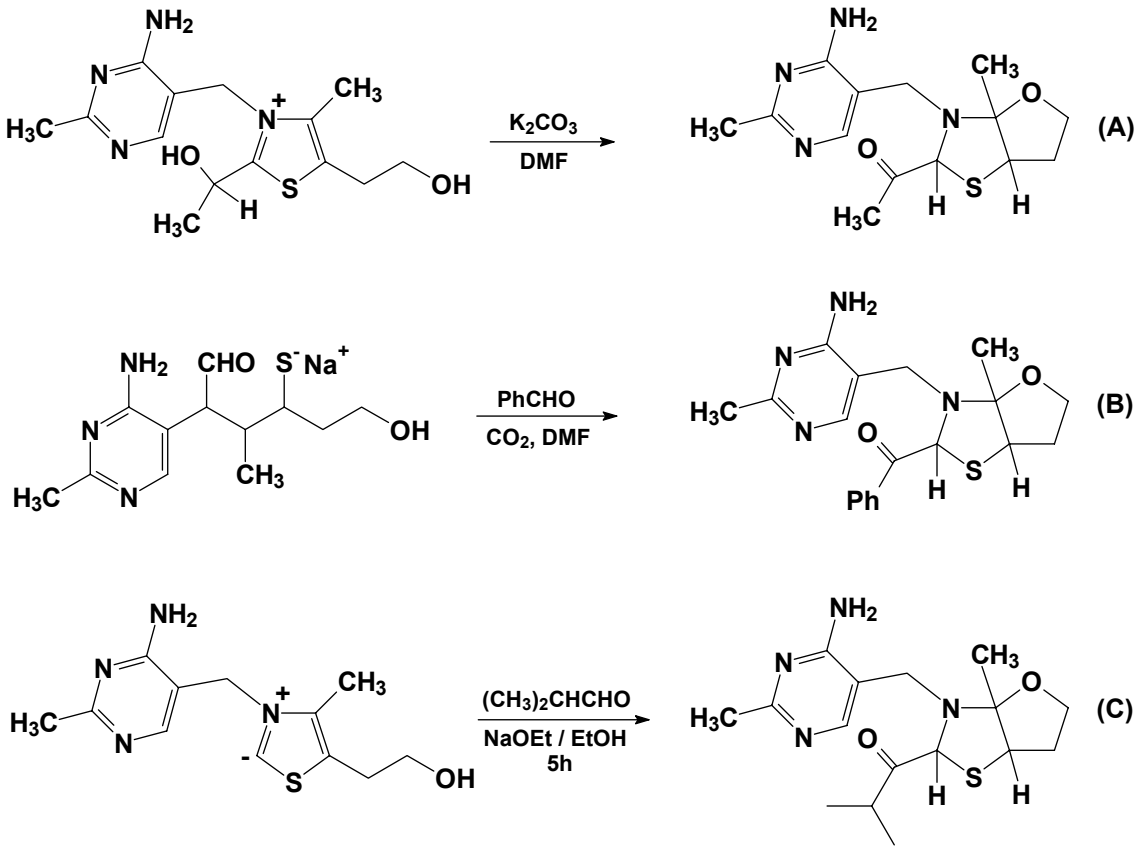

Figure Chapter Three -12: Other observations of thiamin-ketone adducts

Nucleophilic Catalysis

A mechanism similar to Zoltewicz's mechanism for nucleophilic fragmentation of thiamin might also apply to fragmentation of HBzT. Although our fragmentation reactions are run in the absence of nucleophiles such as the sulfite used in Zoltewicz's mechanism, there is the possibility of intramolecular nucleophilic catalysis. We observed that cyclization of the hydroxyethyl side chain of the thiazolium ring onto the C6' carbon on the pyrimidine ring can generate cHBzT, which accompanies the fragmentation reaction at low pH. This suggests the possibility of the hydroxyl group of the C_2 adduct cyclizing onto the C_6' carbon on the pyrimidine ring to provide another possible route for

fragmentation (Figure 3-13).

In Zoltewicz's mechanism, sulfite donates electron density into the pyrimidine ring. An ether linkage can donate electron density into the ring as effectively as sulfite (compare $\sigma_M = 0.10$ for $-OC_4H_9$ vs. $\sigma_M = 0.05$ for $-SO_3^-$).[52] The pyrimidine ring can then transfer electron density into the thiazolium ring by cleaving the bond between the bridging methylene group and the thiazolium ring nitrogen (Figure 3-13). The thiazolium ring can then leave in a unimolecular fragmentation step, followed by elimination of the pyrimidine ring to give the fragmentation products.

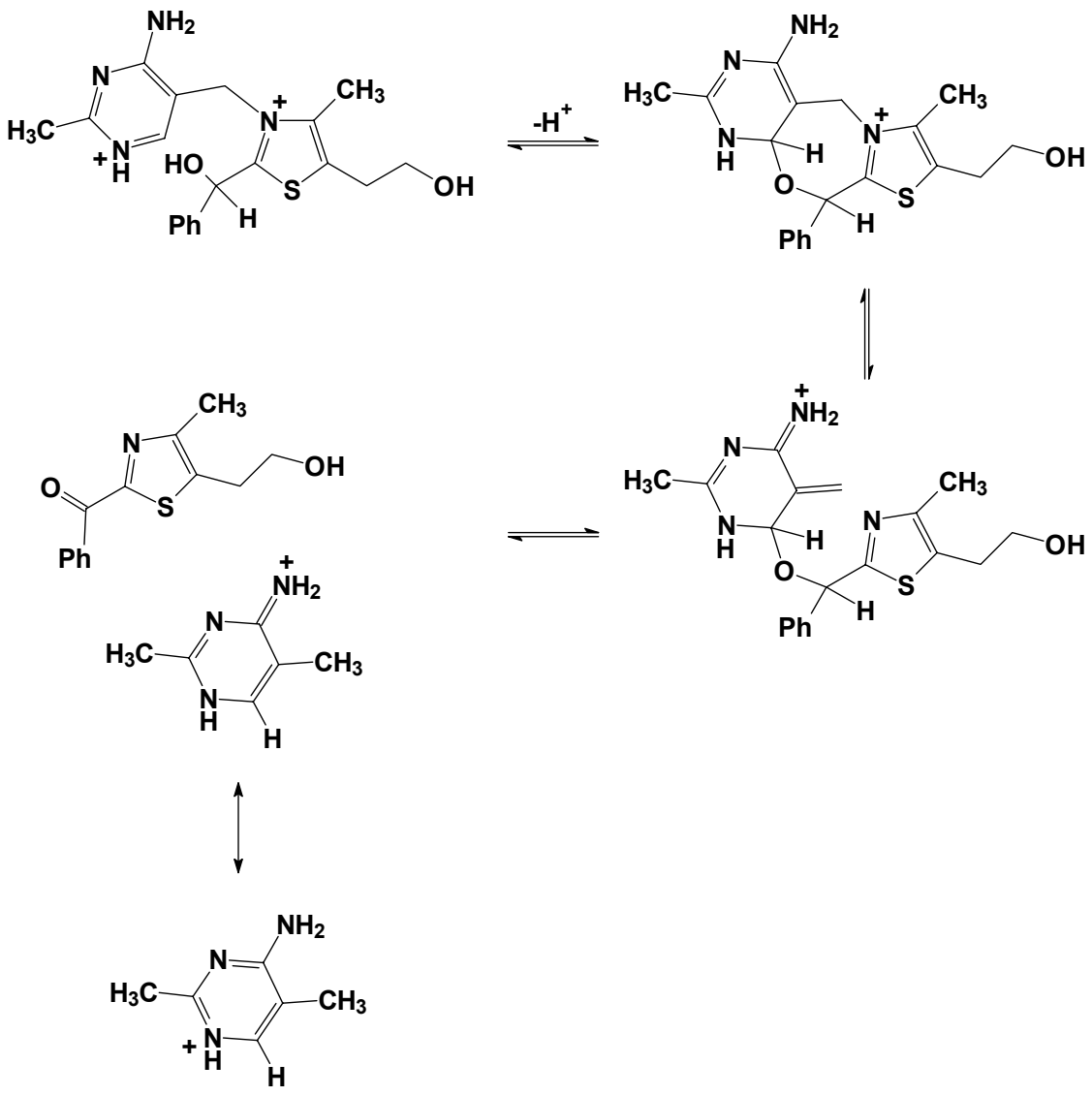

Figure Chapter Three -13: Nucleophilic catalysis fragmentation mechanism

Ruling Out Possibilities for the Two Apparent pK_a's

We can narrow down the list of possibilities since the fragmentation mechanism must account for the differences between the pH-Rate profiles for HBzT, which has several breaks, and the pH-Rate profile for NMHBzT which is linear. The data suggest that the first apparent pK_a (5.1) in the HBzT fragmentation pH-Rate profile is the thermodynamic

pK_a of the N_1' nitrogen. This idea is supported by the observation that a titration curve of HBzT is superimposable onto the pH-Rate profile for fragmentation. NMHBzT does not show this apparent pK_a since it does not have a dissociable proton on the pyrimidine ring. NMHBzT's linear pH-Rate profile also implies that it is operating by a single mechanism, with a common rate-determining step throughout the pH-range studied. Below this pK_a (5.1), the rate coefficients for the fragmentation of HBzT and NMHBzT are virtually identical, implying that there is a common mechanism operating at these pH's (Figure 3-14). Thus, NMHBzT fragments by the same mechanism as HBzT in this region, and throughout the pH range that we studied.

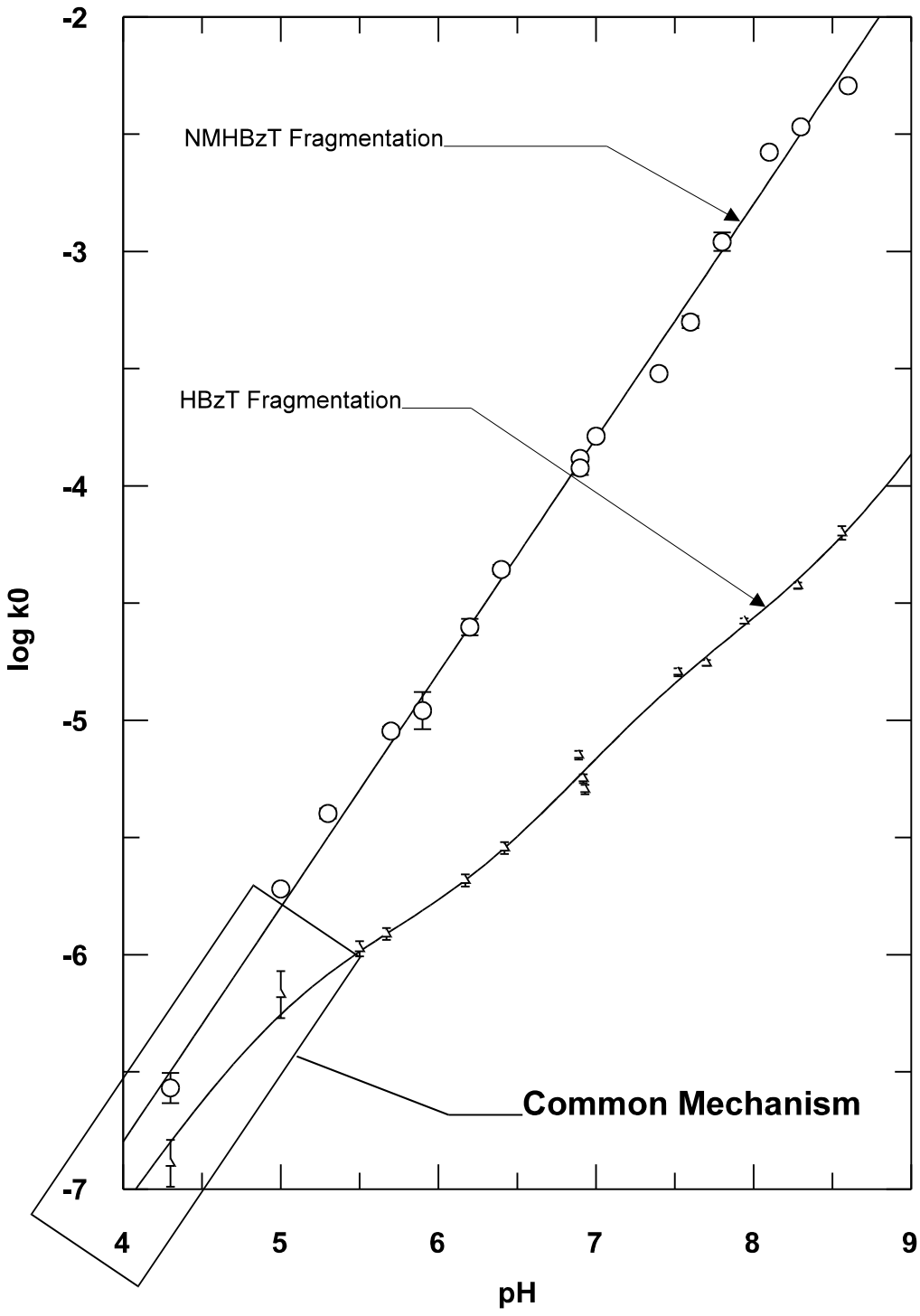

Figure Chapter Three -14: Common mechanism operating at pH's below the N_1' nitrogen's pK_a

The second apparent pK_a in the HBzT pH-Rate profile is more difficult to interpret. The nucleophilic substitution mechanism does not have a suitable explanation for the second apparent pK_a. We have already ruled out the possibility that the second apparent pK_a is the result of a titration of the $C_{2\alpha}$ proton. Finally, we considered the possibility that it is a pH-dependent equilibrium that generates benzoylthiamin as an intermediate prior to rate limiting fragmentation.

We now rule out accumulation of benzoylthiamin as an intermediate since tautomerization from the enol to the keto form would likely proceed via the enolate in Figure 3-15. The mechanism requires removal of BT's C_2 proton for the elimination across the C_2-N_3 bond that would lead to the fragmentation products (Figure 3-16). However, removal of this proton would generate the same thiamin enolate as in Figure 3-15. Therefore, if removal of this proton is also the rate-limiting step in fragmentation, fragmentation must also occur when the enolic proton is removed from the thiamin enol. This would preclude the accumulation of BT prior to fragmentation, and as a consequence, could not explain the value of the second apparent pK_a.

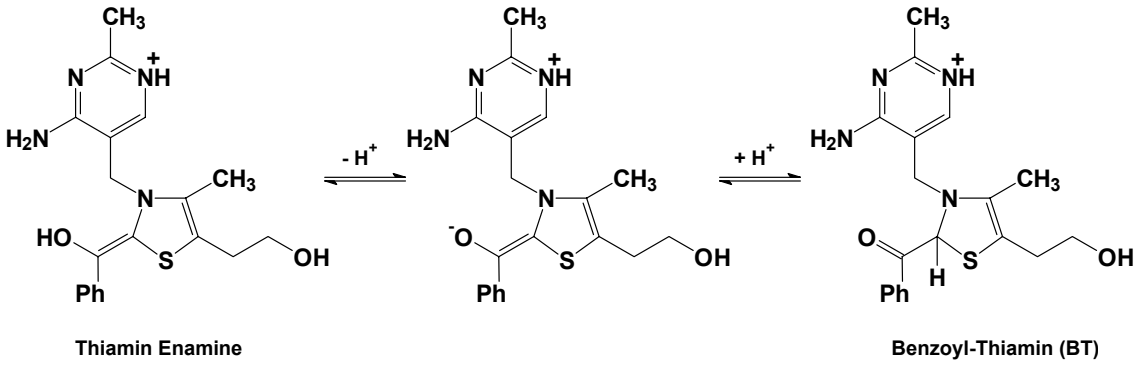

Figure Chapter Three -15: Ketonization process proceeds via the enolate

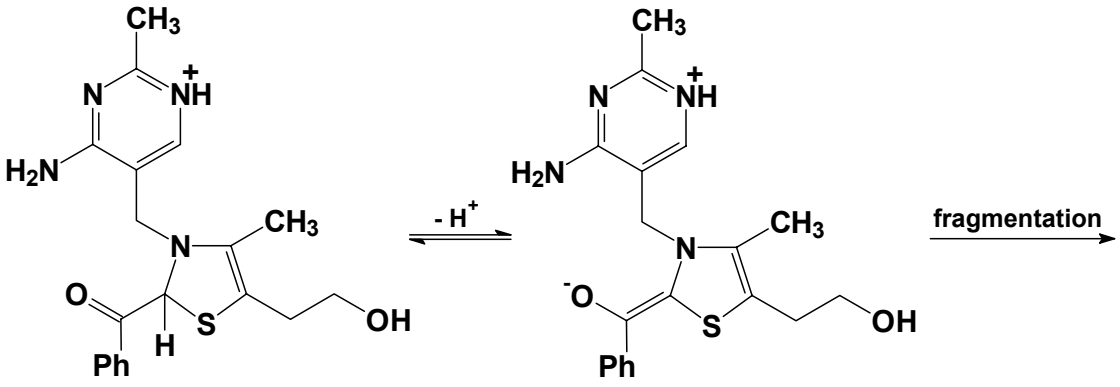

Figure Chapter Three -16: Fragmentation also proceeds via the enolate

Revised Hydroxybenzylthiamin Fragmentation Mechanism:

Figure 3-17 shows our revised HBzT fragmentation mechanism which interprets the second apparent pK_a as a change in rate-determining step. The key intermediate in this mechanism is IH_2', and is generated by two proton transfer steps from IH_2. In order for the change in rate determining step to be pH-dependent, one of the proton transfer steps must be the cause. These two steps lead into and out of intermediate IH. At pH's below the second apparent pK_a, the $k_f[H^+]$ step is rate-limiting. At pH's above the second apparent pK_a, k_{-3} is the rate-limiting step since $k_f[H^+]$ is smaller than k_{-3}.

We can integrate additional observations into our revised mechanism that were not considered using our earlier models. During our kinetic investigations of fragmentation, we calculated the rate constants for elimination by using equation E-22 and our stoichiometry data. The elimination products are generated in a hydroxide-dependent reaction that likely proceeds by pre-equilibrium removal of the benzylic alcohol's proton, followed by rate-limiting elimination of the thiamin ylid (Figure 3-18). Figure 2-8 shows

the calculated rate constants for elimination in the same pH range where we studied HBzT fragmentation. Similarly, Figure 2-9 shows that the transition from fragmentation products to elimination products is in the form of a titration curve. This transition occurs because the elimination reaction has a linear pH-Rate profile in this pH region. On the other hand, the fragmentation reaction goes through several transitions: a change in rate determining step, and two changes in mechanism in this pH region. These changes prevent the fragmentation reaction from increasing in rate as fast as the elimination reaction does. Therefore, the fragmentation reaction goes from being the faster reaction to being the slower reaction in this pH range.

The low pH region of the titration curve in Figure 2-9 also never reaches 100% fragmentation products. This is because there is a partitioning between the fragmentation and elimination products at all pH's. As Figure 2-10 shows, fragmentation is faster than elimination only over certain regions of the pH-Rate profile. That we see fragmentation products generated at all is due to the fragmentation reaction being the favoured reaction over a narrow range of pH from 4.5 to 7.3.

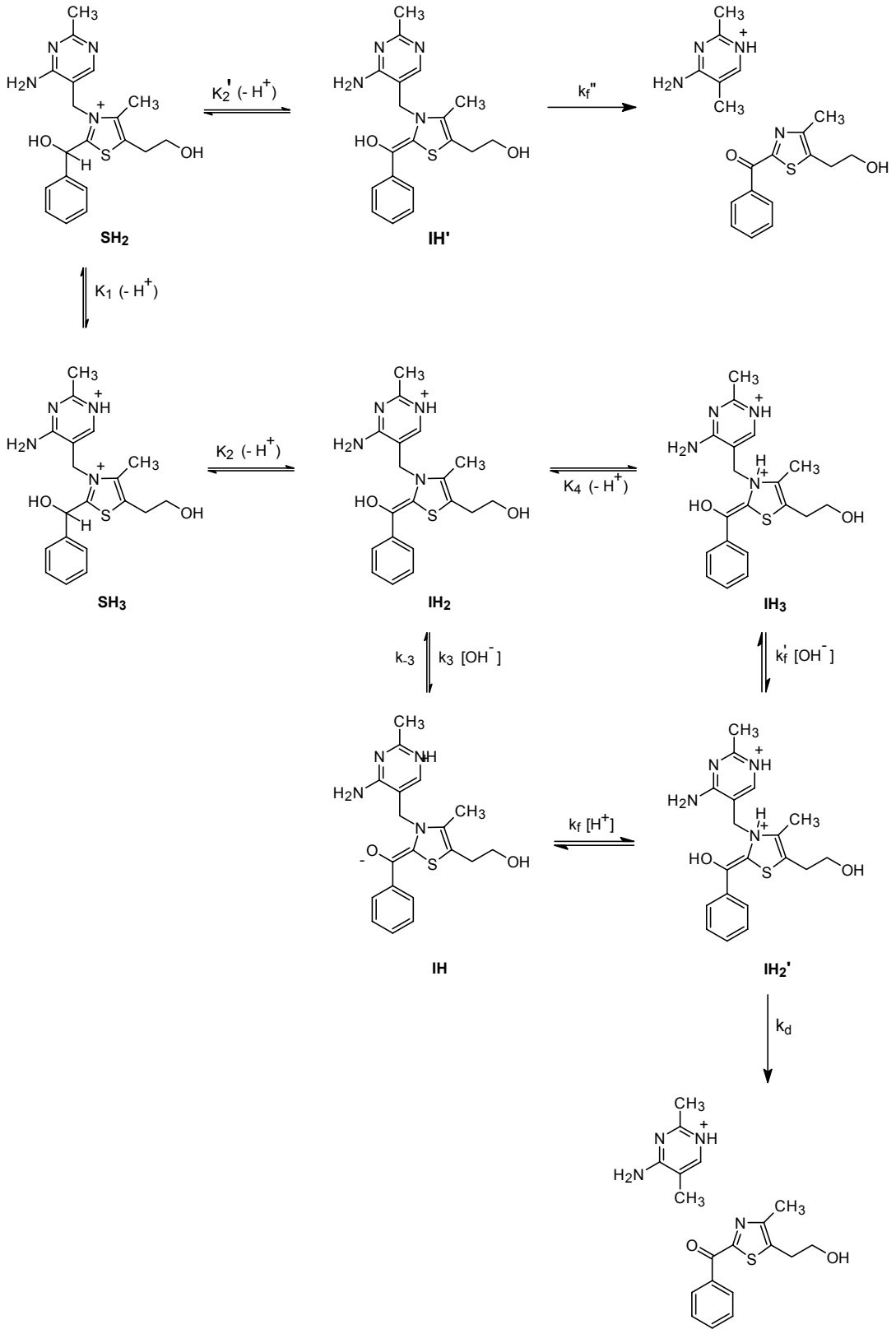

Figure Chapter Three -17: HBzT fragmentation mechanism

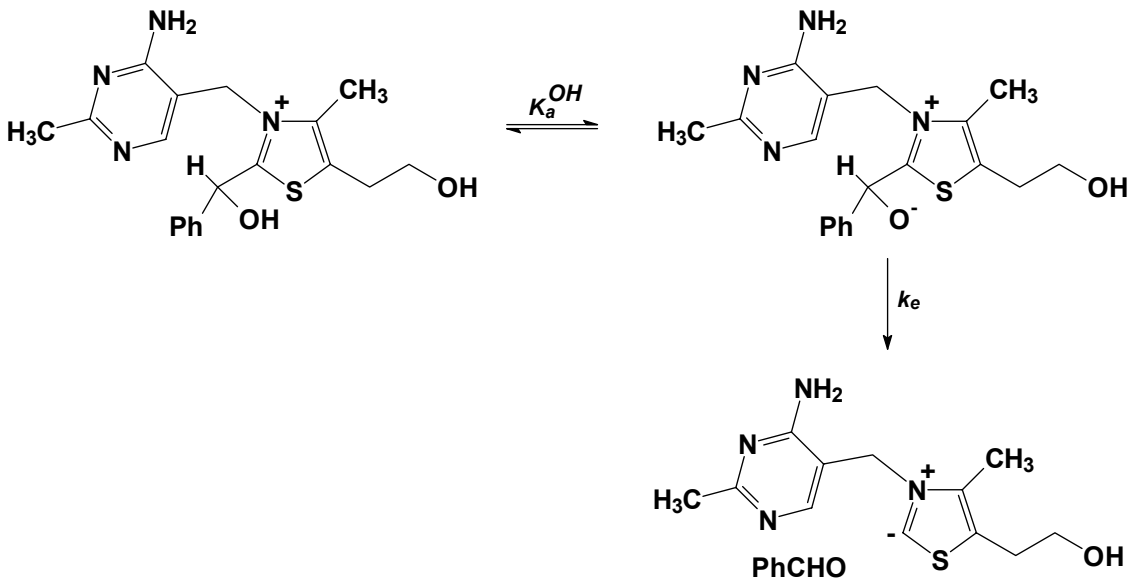

Figure Chapter Three -18: HBzT elimination mechanism

The following is a summary of the terms in Figure 3-17:

- SH_3 and SH_2 represent the major equilibrium species in solution
- IH_3, IH_2, IH and IH' represent the minor equilibrium species in solution
- K_1 is the macroscopic pK_a of HBzT's N_1' nitrogen
- K_2 is the macroscopic pK_a for loss of HBzT's $C_{2\alpha}$ proton when N_1' is protonated, and K_2' is the pK_a when N_1' is unprotonated. To simplify our calculations, we assume that $K_2 = K_2$' since the $C_{2\alpha}$ site is remote from the N_1' nitrogen.
- k_f, k_f' and k_f" are first and second order rate constants for the fragmentation reaction
- k_3 and k_{-3} are second and first order rate constants for the removal of IH_2's enolic proton
- K_4 represents the pK_a of the thiazole ring's N_3 nitrogen.

To simplify the presentation of our mechanism, we will independently consider the fragmentation pathways via N_1' protonated and unprotonated HBzT. These mechanisms operate in two different regions of the pH-Rate profile, as indicated in Figure 3-19. As the figure shows, there are the two pathways via N_1' protonated HBzT, and a single pathway via N_1' unprotonated HBzT.

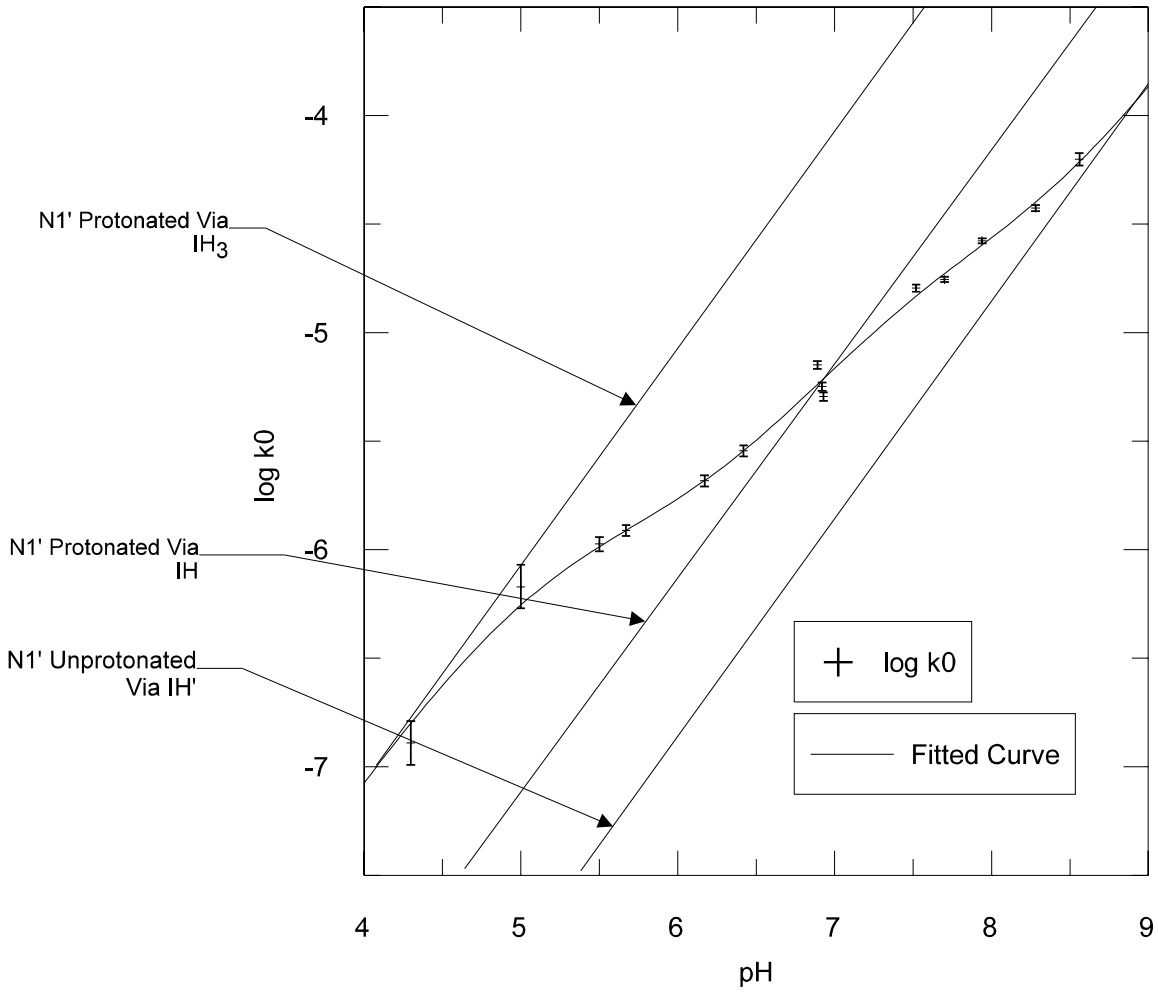

Figure Chapter Three -19: Regions of the pH-Rate profile where different mechanisms are operating

Considering the N_1' protonated pathways first, the rate expression for production of the fragmentation products is:

$$\frac{dP}{dt} = k_f[H^+][IH] + k_f^{'}[OH^-][IH_3] \qquad \textbf{E- 28}$$

The mass balance equation is:

$$[HBzT] = [SH_3] + [SH_2] \qquad \textbf{E- 29}$$

The expressions for the acidity constants by K_1 and K_2 are:

$$K_1 = \frac{[SH_2][H^+]}{[SH_3]} \qquad \textbf{E- 30}$$

$$K_2 = \frac{[IH_2][H^+]}{[SH_3]} \qquad \textbf{E- 31}$$

The key intermediate from Figure 3-17 is IH_2, so by arranging equations E-29, E-30 and E-31 above, we obtain:

$$[IH_2] = \frac{[HBzT]K_2}{[H^+] + K_1} \qquad \textbf{E- 32}$$

The expression for the acidity constant K_4 is:

$$K_4 = \frac{[IH_2][H^+]}{[IH_3]} \qquad \textbf{E- 33}$$

Therefore, the route via the IH_3 intermediate may be defined by combining equations E-

32, E-33, and E-28:

$$\frac{dP}{dt} = \left(\frac{k_f' K_W}{K_4}\right)\left(\frac{K_2}{[H^+] + K_1}\right)[HBzT] \qquad \textbf{E- 34}$$

The IH intermediate may be treated as a steady-state intermediate:

$$\frac{d(IH)}{dt} = k_3[OH^-][IH_2] - k_{-3}[IH] - k_f[H^+][IH] = 0 \qquad \textbf{E- 35}$$

and

$$[IH] = \frac{k_3[OH^-][IH_2]}{k_{-3} + k_f[H^+]} \qquad \textbf{E- 36}$$

Therefore, the route via IH may be defined by combining equations E-36 and E-28:

$$\frac{dP}{dt} = \left(\frac{k_f k_3 K_W}{k_{-3} + k_f[H^+]}\right)\left(\frac{K_2}{[H^+] + K_1}\right)[HBzT] \qquad \textbf{E- 37}$$

Combining equations E-34 and E-37, we obtain the overall expression for the fragmentation reaction via the N_1' protonated pathways:

$$\frac{dP}{dt} = \left(\frac{k_f' K_W}{K_4} + \frac{k_f k_3 K_W}{k_{-3} + k_f[H^+]}\right)\left(\frac{K_2}{[H^+] + K_1}\right)[HBzT] \qquad \textbf{E- 38}$$

and

$$k_{obs} = \left(\frac{k_f' K_W}{K_4} + \frac{k_f k_3 K_W}{k_{-3} + k_f[H^+]}\right)\left(\frac{K_2}{[H^+] + K_1}\right) \qquad \textbf{E- 39}$$

Equation E-39 can be interpreted as four distinct regions. The route via intermediate IH_3 is significant at pH's below pK_1, and is represented by the following equation:

$$k_{obs} = \left(\frac{k_f' K_W}{K_4}\right)\left(\frac{K_2}{[H^+] + K_1}\right) \qquad \textbf{E- 40}$$

At pH's below pK_1, equation E-40 is:

$$k_{obs} = \left(\frac{k_f' K_W}{K_4}\right)\left(\frac{K_2}{[H^+]}\right) \qquad \textbf{E- 41}$$

Above pK_1, $[H^+] << K_1$, and Equation E-40 approaches the value:

$$k_{obs} = \frac{k_f' K_W K_2}{K_4 K_1} \qquad \textbf{E- 42}$$

The route via intermediate IH is significant at pH's above pK_1 and below pK_2. It can be interpreted by the following equation where C represents Equation E-42:

$$k_{obs} = \left(\frac{k_f k_3 K_W}{k_{-3} + k_f [H^+]}\right)\left(\frac{K_2}{K_1}\right) + C \qquad \textbf{E- 43}$$

At pH's below the second apparent pK_a, $k_{-3} << k_f[H^+]$, and Equation E-43 is:

$$k_{obs} = \frac{k_3 K_W K_2}{K_1 [H^+]} + C \qquad \textbf{E- 44}$$

At pH's above the second apparent pK_a, equation E-43 approaches the value:

$$k_{obs} = \left(\frac{k_f k_3 K_W K_2}{K_1 k_{-3}} \right) + C \qquad \textbf{E- 45}$$

We will now consider the production of fragmentation products via the N_1' unprotonated HBzT pathway. This involves rate-limiting fragmentation via the IH' intermediate in Figure 3-17. The production of fragmentation products P is:

$$\frac{dP}{dt} = k_f^{''}[IH^{'}] \qquad \textbf{E- 46}$$

Recall that we are assuming that $K_2 = K_2$' for the purposes of simplifying the number of variables in our calculations. Therefore, the equilibrium between SH_2 and IH' is represented by the K_2 acidity constant:

$$K_2 = \frac{[IH^{'}][H^{+}]}{[SH_2]} \qquad \textbf{E- 47}$$

Substituting the mass balance equation E-29, into equations E-46 and E-47, we arrive at the following expression for k_{obs}:

$$k_{obs} = \frac{K_1 K_2 k_f^{''}}{[H^{+}]\left(K_1 + [H^{+}]\right)} \qquad \textbf{E- 48}$$

A diagram that illustrates the contributions of each of these pathways to the overall observed fragmentation rate constant is shown in Figure 3-20.

We combine Equations E-39 and E-48 to obtain the expression that describes the observed fragmentation rate constants of HBzT:

E- 49

$$k_{obs} = \frac{K_1 K_2 k_f^{''}}{[H^+]\left(K_1 + [H^+]\right)} + \left(\frac{k_f^{'} K_W}{K_4} + \frac{k_f k_3 K_W}{k_{-3} + k_f [H^+]}\right)\left(\frac{K_2}{[H^+] + K_1}\right)$$

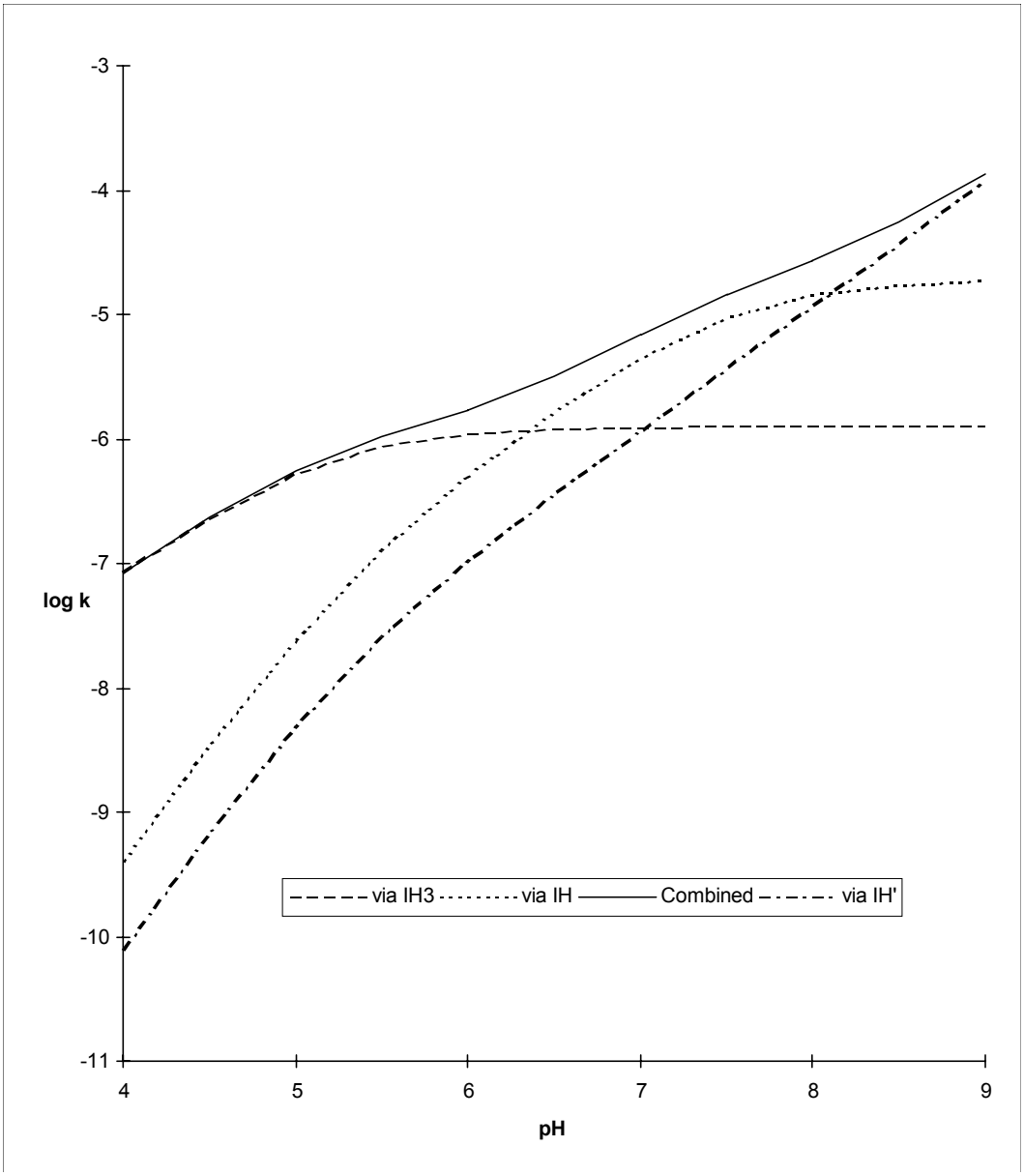

Figure Chapter Three -20: Comparison of the different fragmentation pathways and their individual contributions to the overall reaction rate

Assumptions Used in Fitting Our Parameters:

Three rate constants in our mechanistic scheme involve thermodynamically favourable proton transfers: k_3, k_f', and k_f. The first two rate constants define the transfer of a proton from an enol to hydroxide. Table 3-1 tabulates the second-order rate constants for the reaction of several nitrogen and oxygen acids with hydroxide ion. We assigned the average of these rate constants: 2.0×10^{10} M^{-1} s^{-1} to k_3 and k_f' as being representative of such a proton transfer.[54]

The third rate constant involves the protonation of the thiazole's N_3 nitrogen by hydronium ion. Table 3-2 tabulates the second-order rate constants for the reaction of several nitrogen and oxygen bases with hydronium ion. We also assign the average of these rate constants: 3.7×10^{10} M^{-1} s^{-1} to k_f as being representative of such a proton transfer.

Table Chapter Three -1: Rate constants for reactions of hydrogen ion with bases in aqueous solution

Base	*pK_a*	*log k*
H_2S	7.24	10.8
NH_3	9.25	10.6
HCO_3^-	3.77	10.7
$CH_3CO_2^-$	4.75	10.7
$C_6H_5CO_2^-$	4.17	10.5
m-Nitrophenoxide	7.15	10.6
$(CH_3)_3N$	9.79	10.4
Imidazole	6.95	10.2

Table Chapter Three -2: Rate constants for reactions of hydroxide ion with acids in aqueous solution

Acid	*pK_a*	*log k*
NH_4^+	9.25	10.6
$(CH_3)_3NH^+$	9.79	10.3
$NH_3^+CH_2CO_2^-$	9.78	10.1
Imidazolium	6.95	10.3

After fitting the parameters in equation E-49 to the HBzT fragmentation data, Table 3-3 shows the values obtained for the parameters.

Table Chapter Three -3: Measured rate and equilibrium coefficients after fitting equation E-49 to the HBzT fragmentation data

Parameter	*Value*
K_1	$7.1 \pm 0.1 \times 10^{-6}$ M
K_2	$2.1 \pm 0.2 \times 10^{-14}$ M
K_4	$4.6 \pm 0.9 \times 10^{-7}$ M
k_3	$2.0 \pm 0.1 \times 10^{10}$ $M^{-1}s^{-1}$
k_{-3}	$1.1 \pm 0.6 \times 10^{3}$ s^{-1}
k_f	$3.7 \pm 0.1 \times 10^{10}$ $M^{-1}s^{-1}$
k_f'	$2.0 \pm 0.1 \times 10^{10}$ $M^{-1}s^{-1}$
k_f''	5.6 ± 0.4 s^{-1}

Analysis of the Role of the IH_2' Intermediate:

IH_2' is the key intermediate in the fragmentation mechanism (Figure 3-21). It breaks down to form the reaction products (k_d) faster than water can transfer a proton to the enolate oxygen (k_{-f}) or than water can accept a proton from the thiazole's N_3 nitrogen (k_{-f}'). It breaks down readily since the proton on the N_3 nitrogen is positioned (Figure 3-22) to accept the negative charge generated at carbon upon breaking the bond to N_3 (Figure 3-23). Therefore, k_d must be larger than either k_{-f} or k_{-f}'. Our kinetic expressions treat IH_2' as a steady-state intermediate since the only kinetically significant steps to or from IH_2' in Figure 3-21 are k_f and k_f'.

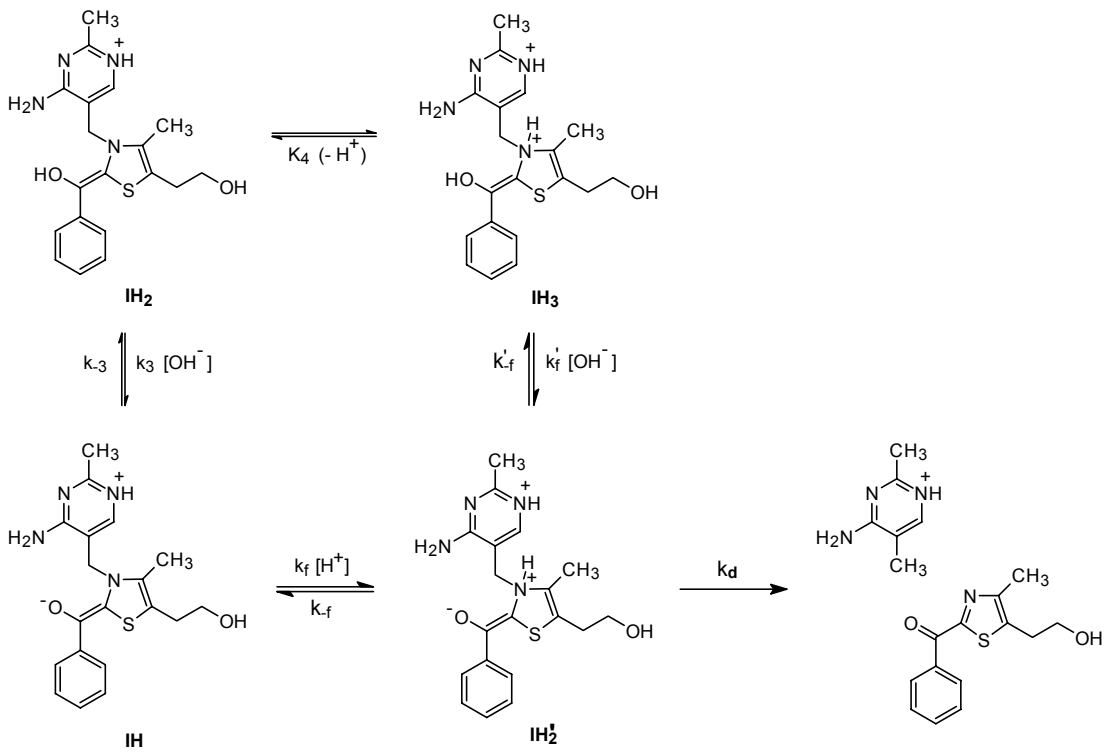

Figure Chapter Three -21: Steps Involved in generating IH2'

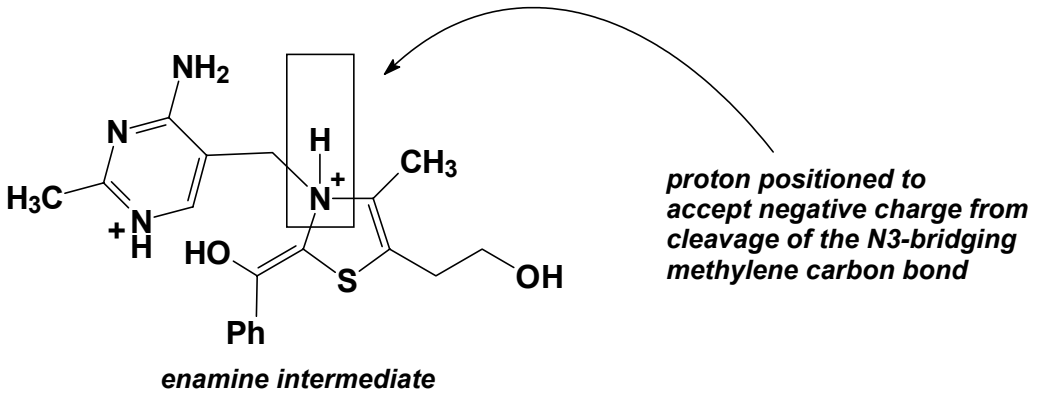

Figure Chapter Three -22: Reactivity of IH_2' results from a pre-positioned proton.

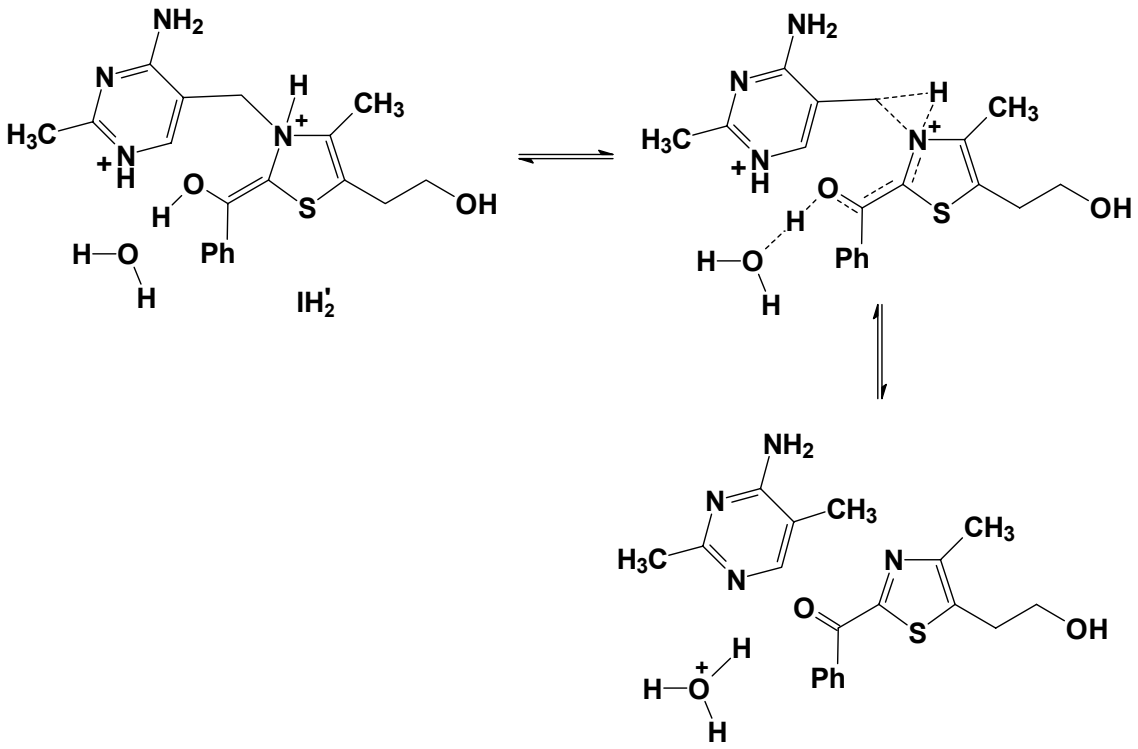

Figure Chapter Three -23: Fragmentation step, showing proposed structure for the transition state

The rate expression for formation of the fragmentation products is:

$$\frac{dP}{dt} = k_d[IH_2^{'}] \qquad \textbf{E- 50}$$

IH_2' may be treated as a steady-state intermediate:

$$\frac{dIH_2^{'}}{dt} = k_f[H^+][IH] + k_f^{'}[OH^-][IH_3] - k_{-f}[IH_2^{'}] - k_{-f}^{'}[IH_2^{'}] - k_d[IH_2^{'}] = 0 \qquad \textbf{E- 51}$$

and

$$[IH_2^{'}] = \frac{k_f[H^+][IH] + k_f^{'}[OH^-][IH_3]}{k_{-f} + k_{-f}^{'} + k_d} \qquad \textbf{E- 52}$$

By combining Equations E-50 and E-52, we obtain:

$$\frac{dP}{dt} = k_d\left(\frac{k_f[H^+][IH] + k_f^{'}[OH^-][IH_3]}{k_{-f} + k_{-f}^{'} + k_d}\right) \qquad \textbf{E- 53}$$

If $k_d >> k_{-f}$ and k_{-f}', then equation E-53 simplifies to:

$$\frac{dP}{dt} = k_f[H^+][IH] + k_f^{'}[OH^-][IH_3] \qquad \textbf{E- 54}$$

We can estimate the magnitude of k_d by using rate and acidity constants for which we have reasonable estimates: k_{-3} and K_4. From our results, $k_{-3} = 1.1 \times 10^3$ s^{-1}, the rate of protonation of the enolate oxygen by water. Since the enolic proton of IH_3 is more acidic when N_3 is protonated, k_{-3} must represent a lower limit for the value of k_{-f}'. Similarly, we can obtain an estimate for the upper limit of k_f. From our results, $K_4 = 4.6 \times 10^{-7}$ M^{-1}. As assumed earlier, a rate constant (k_p) for thermodynamically favourable proton transfer from hydronium ion to N_3 is 3.7×10^{10} M^{-1} s^{-1}. Thus, we calculate a value of 1.7×10^4 s^{-1} (k_p / K_4) for the rate constant for deprotonation of the N3 proton by water. The acidity of the IH_3 intermediate's N3 proton is more acidic than the IH_2' intermediate's N3 proton since the IH_3 intermediate is in the enol form whereas the IH_2' intermediate is in the enolate form. Therefore, 1.7×10^4 s^{-1} is an upper limit for the true value of the k_{-f} rate constant. From our estimates of k_{-f} and k_{-f}' we estimate a lower limit for the value of k_d (1.7×10^4 s^{-1}), since it must be faster than the either k_{-f} or k_{-f}'. The exact value cannot be measured in our study because this step occurs after the rate-determining process.

Relationship to the NMHBzT Fragmentation Mechanism:

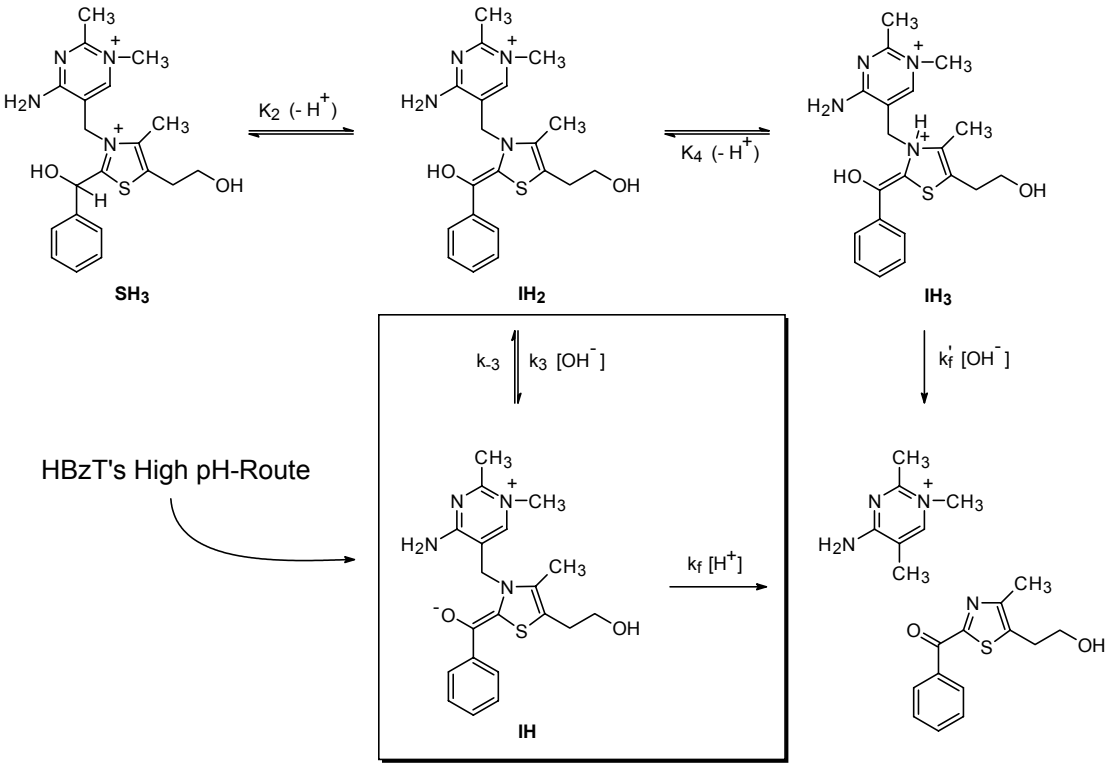

Figure Chapter Three -24: NMHBzT fragmentation mechanism details

We present a mechanism to explain the fragmentation of NMHBzT in Figure 3-24. The most important point to consider is: Why does the pH-Rate profile of NMHBzT lack the pK_a-type curvatures seen in the HBzT pH-Rate profile (Figure 2-13)? The first pK_a is absent due to the lack of a dissociable proton of the N_1' nitrogen of NMHBzT. However, the reason for the absence of the second apparent pK_a is not obvious.

There are two fragmentation pathways for N_1' protonated HBzT. The choice of pathways is controlled by the relative rates of fragmentation via IH_3 and IH which are in turn controlled by K_4 and k_{-3}. Small changes in K_4 and/or k_{-3} determine the choice of the pathway. The following series of figures shows the effect of variations on K_4 (Figure 3-

25), k_{-3} (Figure 3-27), and K_2 (Figure 3-26). Figure 3-25 shows that as K_4 increases in value, the contribution to the overall k_{obs} via the IH_3 intermediate's pathway decreases in significance (the first apparent pK_a disappears from the pH-Rate profile) relative to the IH intermediate's pathway. Figure 3-27 shows that as k_{-3} decreases in value, the contribution via the IH intermediate's pathway increases relative to the IH_3 intermediate's pathway. Finally, Figure 3-26, shows that as K_2 increases in value, both pathways increase in rate equally.

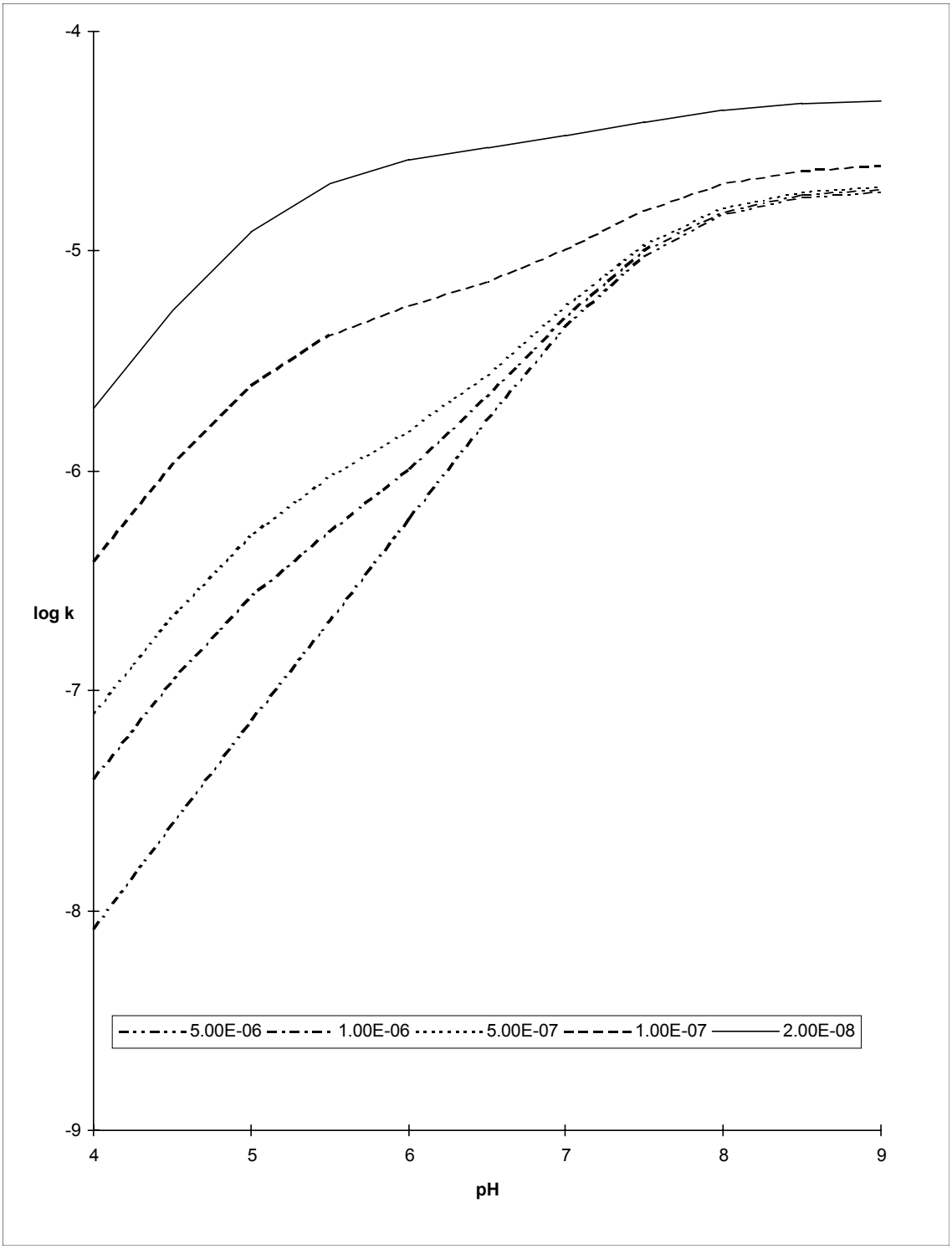

Figure Chapter Three -25: Effect of variations on K_4 on the observed rate coefficients via the N_1' Protonated HBzT pathways.

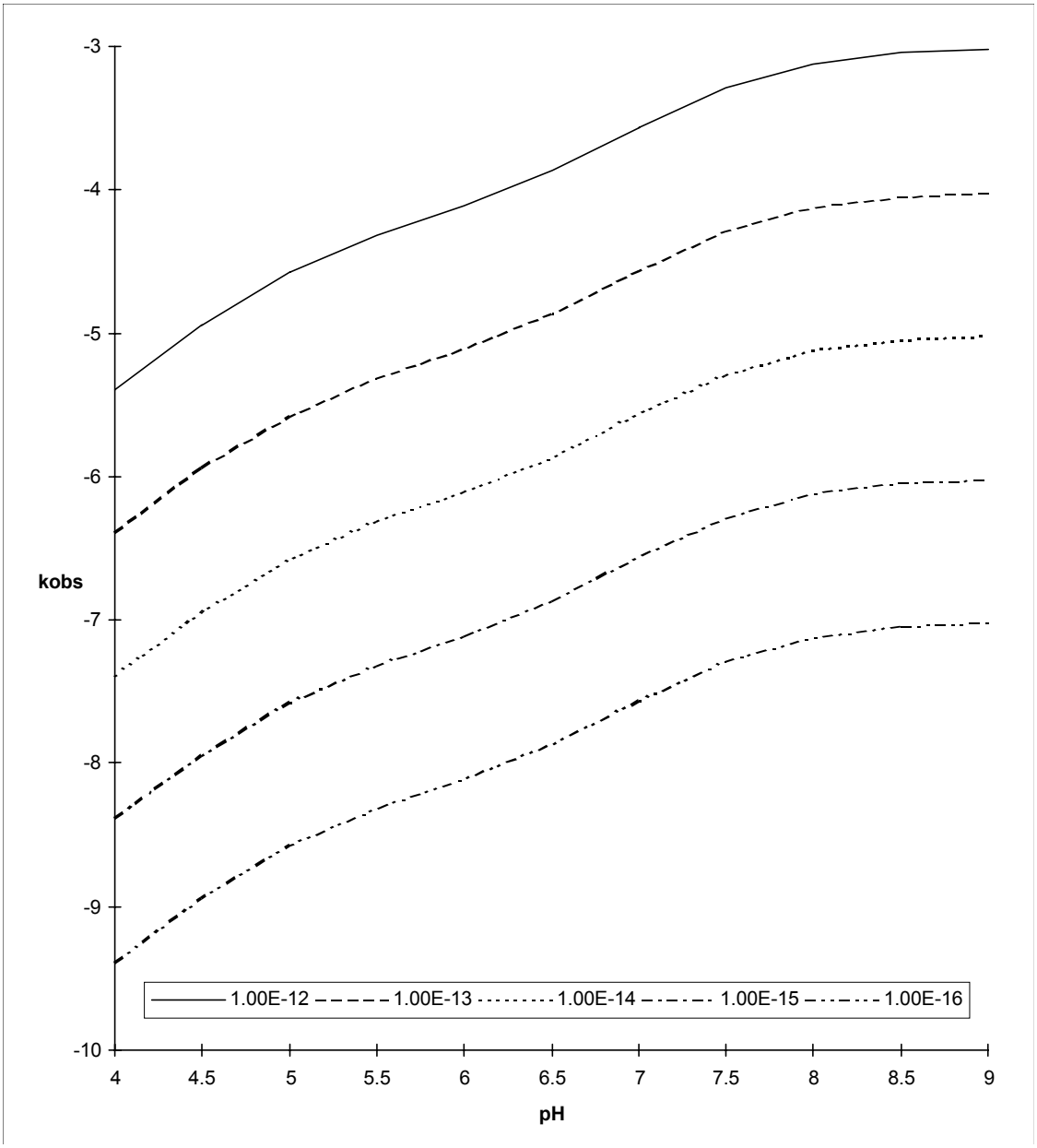

Figure Chapter Three -26: Effect of variations on K_2 on the observed rate coefficients via the N_1' protonated HBzT pathways.

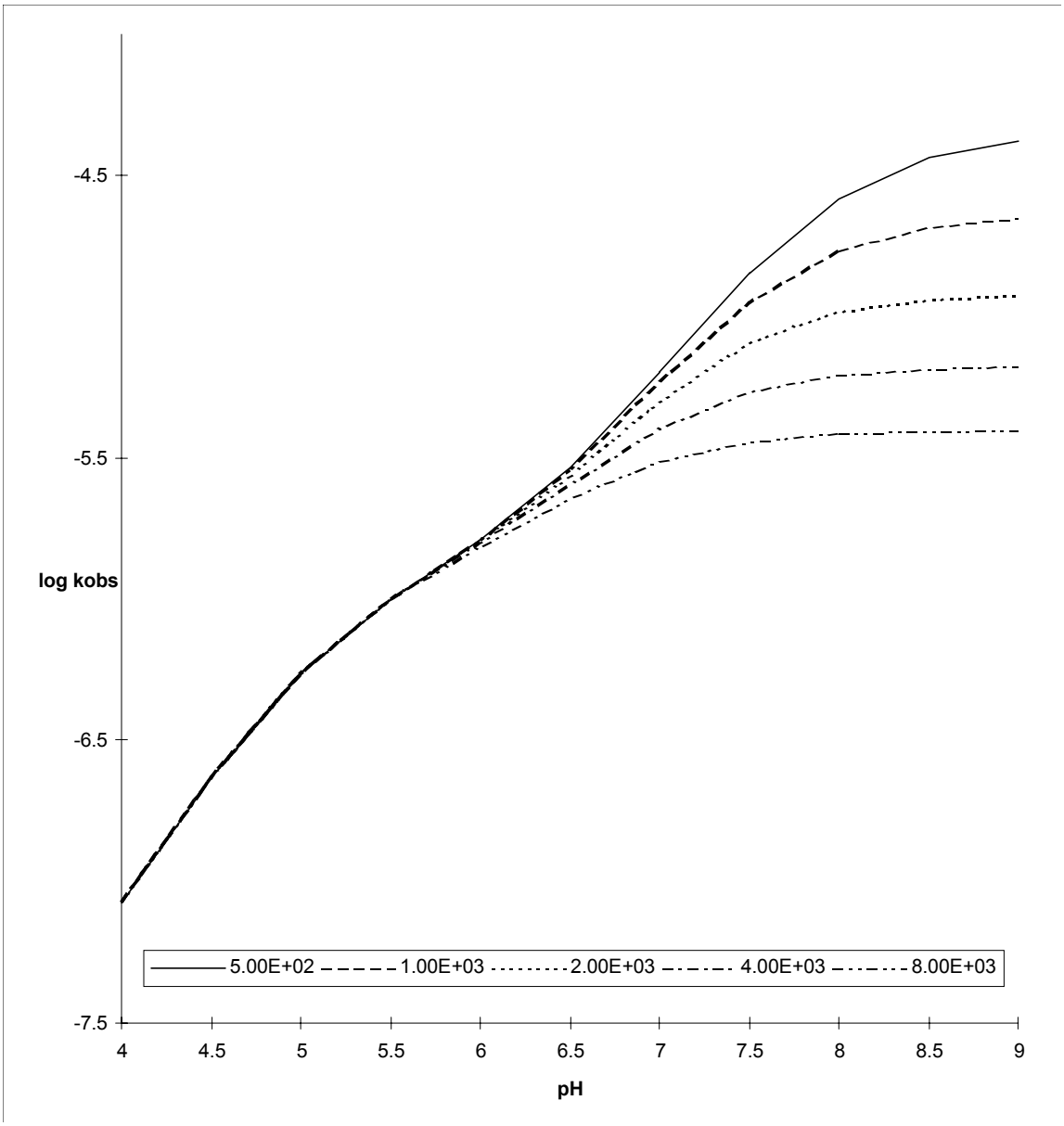

Figure Chapter Three -27: Effect of variation of $_{k-3}$ on the observed rate coefficients via the N_1' protonated pathways of HBzT.

Therefore, it is the combined effects on k_{-3} and K_4 that are responsible for the simple, linear pH-Rate profile of NMHBzT. The lack of an apparent pK_a at pH 7.3 for NMHBzT fragmentation is the result of the dominance of the route via IH_3 over that via IH.

The expression for k_{obs} in NMHBzT fragmentation is a modification of equation E-49 for HBzT fragmentation. Several terms (K_1, k_f'', K_2') can be omitted since NMHBzT lacks an acidic group on the pyrimidine.

$$k_{obs} = \left(\frac{k_f' K_W}{K_4} + \frac{k_f k_3 K_W}{k_{-3} + k_f [H^+]} \right) \left(\frac{K_2}{[H^+] + K_2} \right) \qquad \textbf{E- 55}$$

Fitting equation E-55 to NMHBzT's fragmentation data provides the following set of results listed in Table 3-4. Figure 3-28 is a plot of the observed rate coefficients and the fitted curves, showing the contribution to the overall observed rate constant via the IH and IH_3 routes.

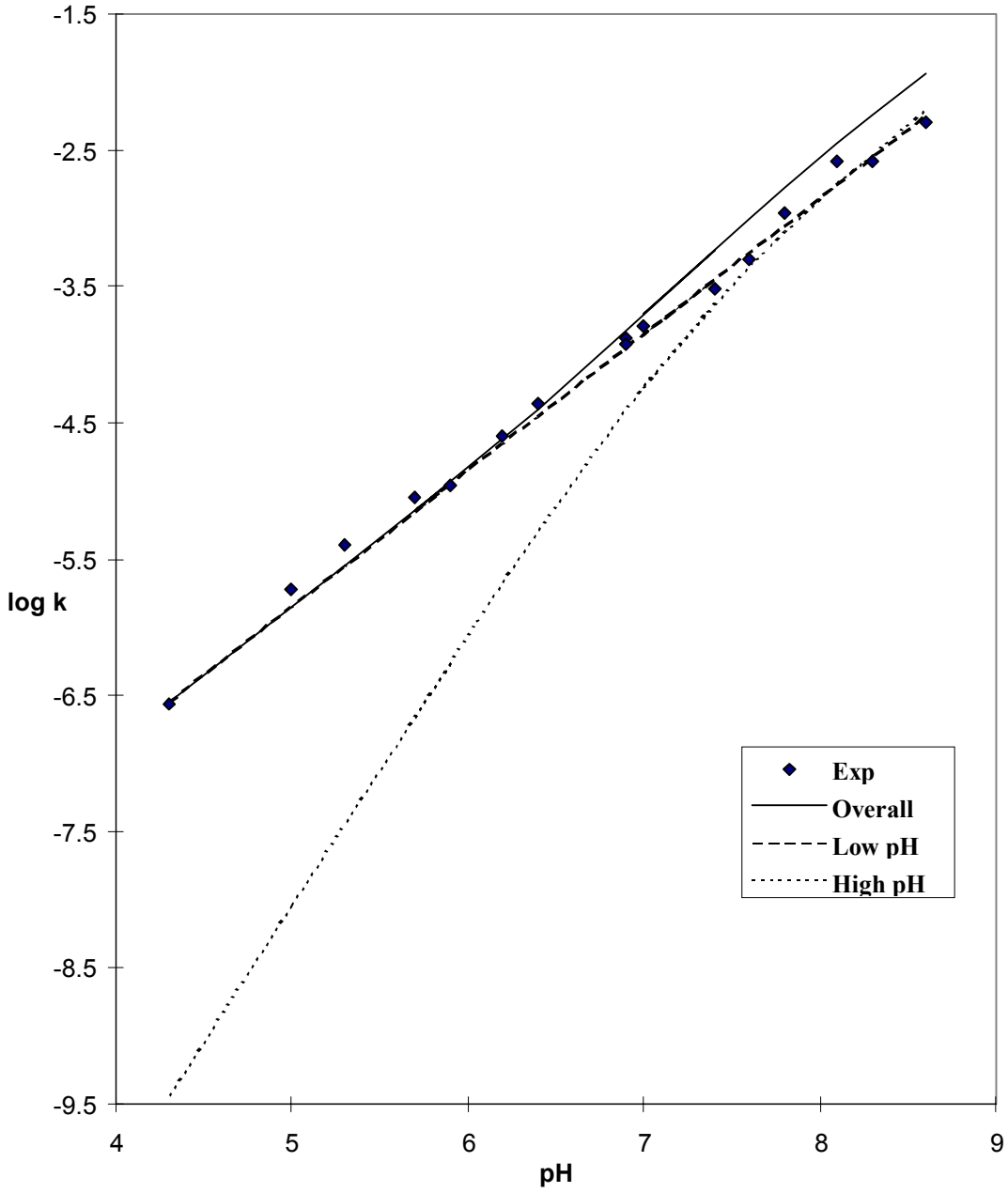

Figure Chapter Three -28: NMHBzT experimental rate coefficients and plots of calculated curves fitted to equation E-55 showing the contribution via the low pH route (the IH_3 intermediate) and the high pH route (the IH intermediate).

Table Chapter Three -4: Results obtained after fitting equation E-55 to the HBzT fragmentation rate coefficients.

Parameter	*Value*
K_2	$2.1 \pm 0.2 \times 10^{-14}$
K_4	$3.4 \pm 0.3 \times 10^{-7}$
k_3	$2.0 \pm 0.1 \times 10^{10}$
k_{-3}	$2.2 \pm 0.7 \times 10^{4}$
k_f	$3.7 \pm 0.1 \times 10^{10}$
k_f'	$2.0 \pm 0.1 \times 10^{10}$

Differences Between NMHBzT and HBzT:

The rate law for HBzT fragmentation suggests that the pK_a of the enolic proton ($pK_3 = -\log(k_3 / k_{-3})$) must decrease in NMHBzT to give a near-linear pH-Rate profile. Our curve fitting results suggest that pK_3 must decrease by at least 1.2 units to accommodate the NMHBzT experimental data. The pK_a of the N3 protonated species (pK_4) increases, but to a lesser extent, 0.2 units. The differences in the experimental parameters are summarized in Table 3-5.

Table Chapter Three -5: Differences in the pK_a of key protons

Compound	pK_3	pK_4
HBzT	7.2	6.3
NMHBzT	6.0	6.5

Our HBzT fragmentation model must explain why pK_3 decreases in NMHBzT (Table 3-5). The conjugate base of the enol (the enolate) can be stabilized by electrostatic interactions with the positively charged pyrimidine N_1' nitrogen in both HBzT and NMHBzT. However, there is a difference in the amount of electrostatic stabilization of the enolate between the two molecules. NMHBzT can more effectively stabilize the enolate since the positive charge remains permanently affixed to the N_1' nitrogen. In the case of HBzT, that same positive charge is reduced due to the existence of tautomers that remove the positive charge from the N_1' nitrogen. An important tautomerization would involve a proton transfer from the N_1' nitrogen to the thiazolium ring's N_3 nitrogen, as shown in Figure 3-30. This would reduce the net amount of positive charge on the N_1' nitrogen, and the amount of stabilization that this charge could provide for the enolate, resulting in an increase in the pK_a of the enol in HBzT over that in NMHBzT.

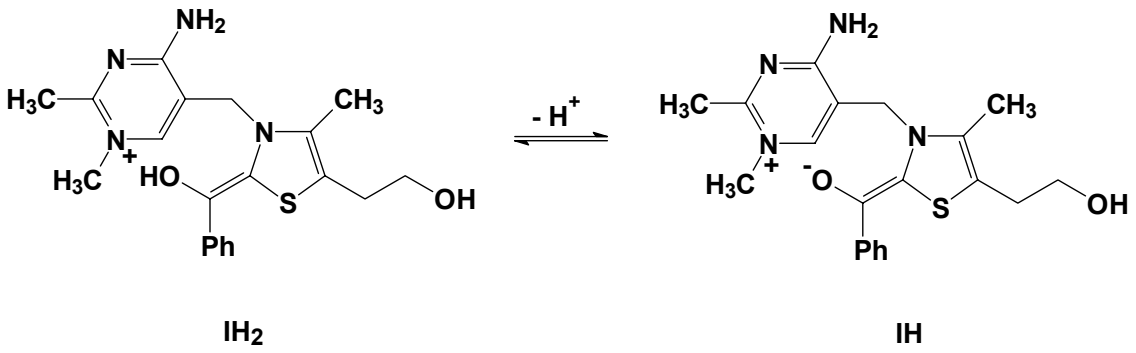

IH_2 IH

Figure Chapter Three -29: Ionization NMHBzT's enolic proton

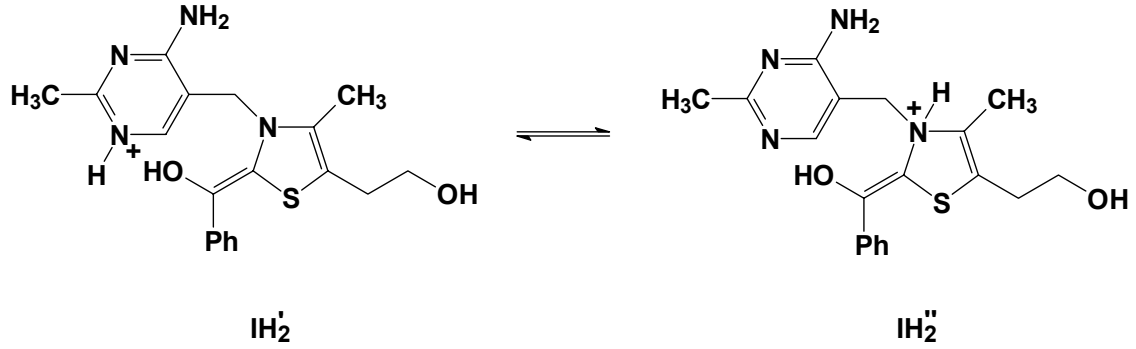

$IH_2^{'}$ $IH_2^{''}$

Figure Chapter Three -30: Tautomerization of HBzT's N1 nitrogen

Hydroxyethylthiamin Does Not Fragment to an Appreciable Extent

We found that 2-(1-hydroxyethyl)-thiamin (HET) (Figure 3-31) does not fragment under conditions where HBzT and NMHBzT readily fragment. It is likely that the pK_a of the $C_{2\alpha}$ proton is responsible for the difference in reactivity. It would be reasonable to expect that HBzT would have a more acidic $C_{2\alpha}$ proton than HET since the conjugate base of HBzT is an enamine which is conjugated with the phenyl group of HBzT, whereas HET does not have this delocalization available to it.

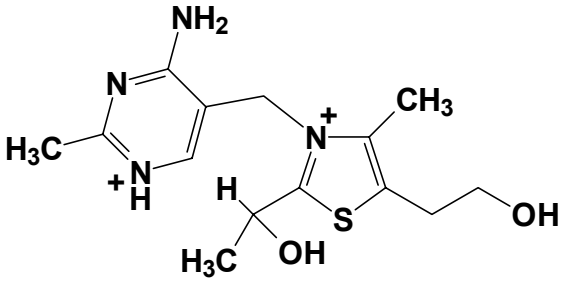

Figure Chapter Three -31: 2-(1-hydroxyethyl)-thiamin (HET)

Stivers and Washabaugh[16] studied the acidity of the $C_{2\alpha}$ proton of 2-(1-hydroxyethyl)-3,4-dimethylthiazolium ion (HETh), a compound similar to HET, except that it cannot fragment. Their studies used an iodine trapping assay and ^1H NMR exchange experiments to measure the rate coefficients for removal of HETh's $C_{2\alpha}$ proton by hydroxide. By plotting their experimental data on the same axes as our rate data for NMHBzT fragmentation (Figure 3-32), we can estimate the pK_a differences between these two compounds.

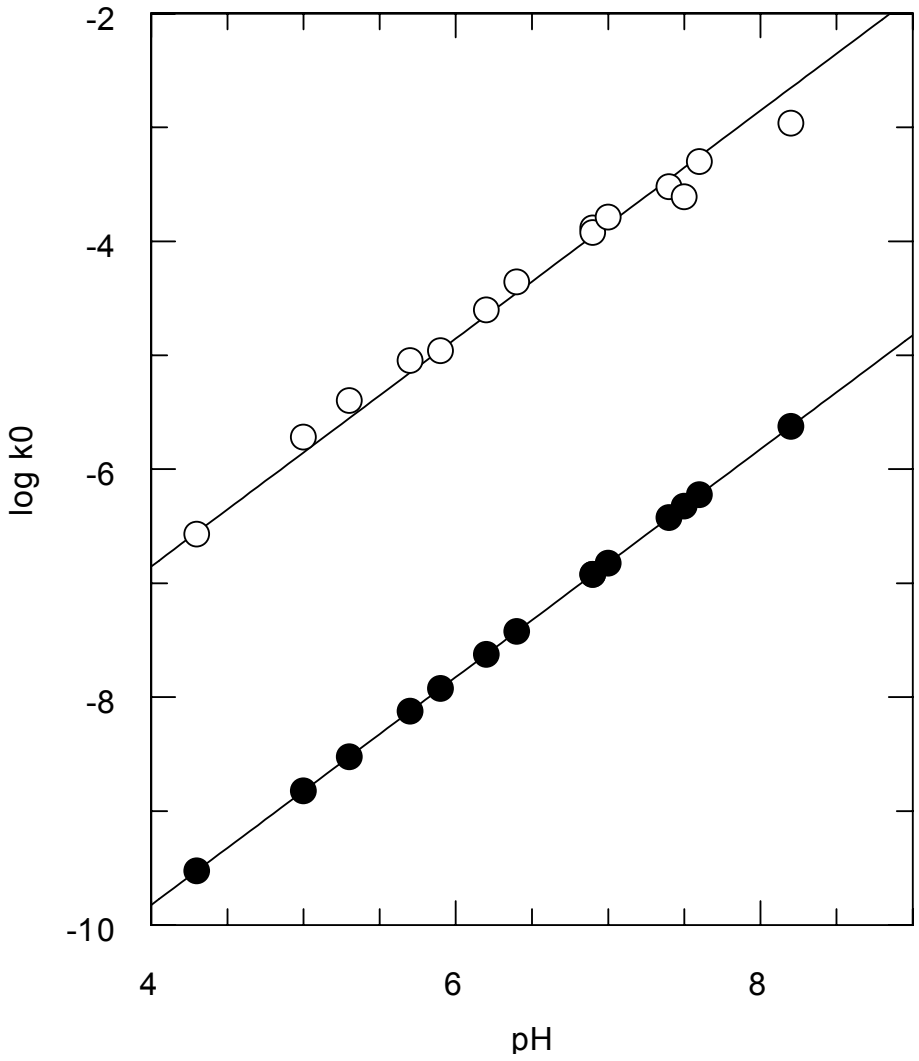

Figure Chapter Three -32: NMHBzT fragmentation (open circles) and HETh exchange (filled circles)

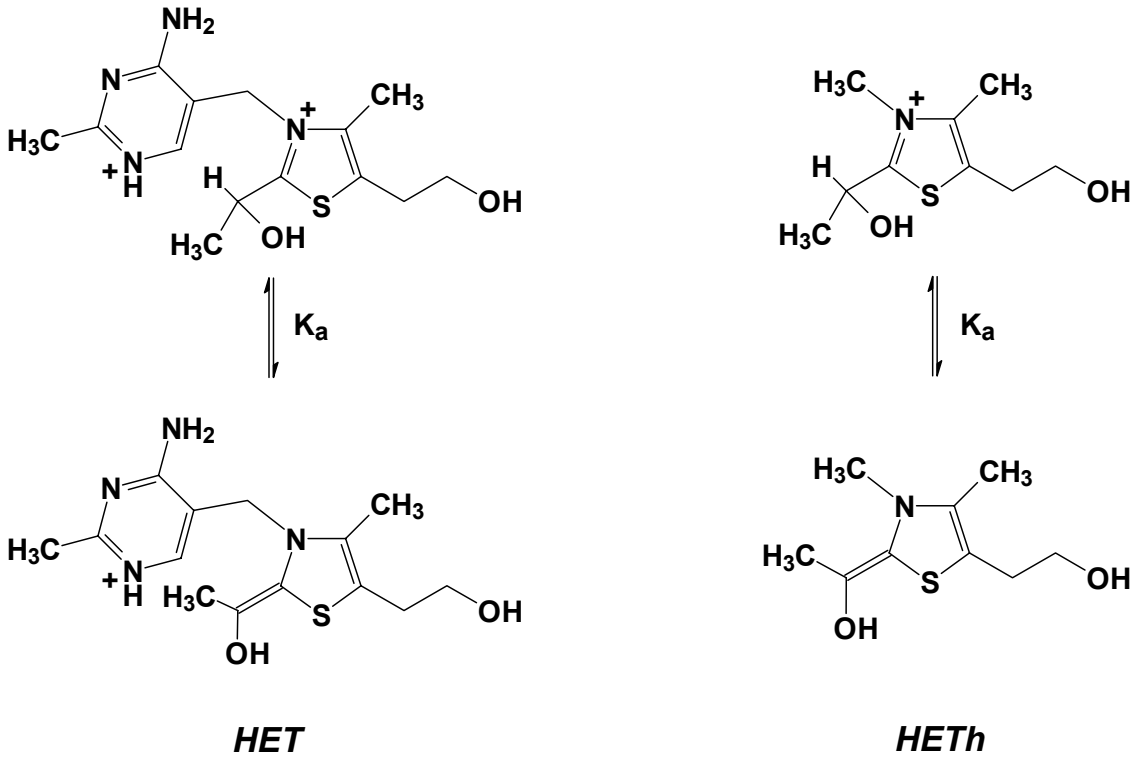

Figure Chapter Three -33: $C_{2\alpha}$ proton removal of HET vs. HETh

By using these data, we can estimate the pK_a of the $C_{2\alpha}$ proton of HET. Figure 3-32 shows that NMHBzT fragments about one hundred times faster than HETh exchanges at the same pH. The rate constant for hydroxide-catalyzed exchange of NMHBzT is $1.39 \pm 0.07 \times 10^3$ M^{-1} s^{-1} and the rate constant for hydroxide-catalyzed exchange of HETh is 1.5 ± 0.2 M^{-1} s^{-1}. If removal of the $C_{2\alpha}$ proton from NMHBzT and HETh occurs by the same mechanism, the pK_a of HET would be approximately three pK units higher than that of NMHBzT. This is confirmed by a recent measurement of HET's acidity by Washabaugh: $pK_a = 18.6$ for the N_1' protonated HET, and 19.8 for the N_1' unprotonated HET.[36]

From our earlier analysis of the HBzT mechanism, we showed that an increase in the pK_a of the $C_{2\alpha}$ proton results in a decrease in the rate of fragmentation by all

fragmentation pathways (Figure 3-26). Due to HET's slow rate of reaction, we have not undertaken a detailed kinetic study of its fragmentation.

General Base Catalysis

HBzT and NMHBzT fragmentation is catalyzed by anionic bases such as acetate, succinate, phosphate, POPSO and BICINE. However, our studies with neutral bases such as MES, HEPES and PIPES did not display any catalysis. Since the $C_{2\alpha}$ proton exchanges faster than fragmentation, the catalysis seen in fragmentation cannot be the result of the removal of this proton. It must be the result of a reaction of another acidic or basic site on the molecule.

Our proposed mechanism in Figure 3-17 shows the possibility of Brönsted base catalysis of the removal of the enolic proton from IH_3. Since IH_3 has the same protonation state as the starting material SH_3, general base catalysis is the result of removal of the enolic proton by a Brönsted base. We argued earlier that the primary pathway by which NMHBzT fragments is via IH_3 in Figure 3-24, which is analogous to IH_3 in Figure 3-17. Our observation that the fragmentation of NMHBzT is buffer catalyzed with a β of 0.98 is consistent with our proposal that the dominant pathway is via IH_3 in Figure 3-25. The large β value is consistent with proton transfer from the well-behaved enol.

Complicating Cyclization Occurs in C_2 Thiamin Adducts

HBzT cyclizes at pH's below the pK_a of N_1' to form an adduct that we call cHBzT

(Figure 3-34). Cyclization forms a carbon-oxygen bond between the 2-hydroxyethyl side-chain of the thiazole and the C6' carbon of the pyrimidine. We have deduced the structure of this compound using ^{1}H NMR.

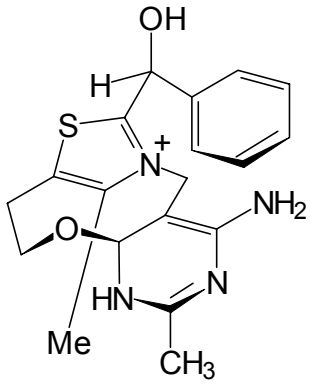

Figure Chapter Three -34: Cyclized HBzT (cHBzT)

The rate of cyclization is proportional to the concentration of N_1'-protonated pyrimidine. With increasing pH, the concentration of pyrimidine-protonated material decreases. Therefore, the rate of cyclization decreases and the relative quantity of cHBzT diminishes to an undetectable amount by ^{1}H NMR at pH's above pK_1. Identical experiments performed with thiamin as the substrate failed to produce a cyclized adduct, suggesting that the presence of a C_2 adduct on the thiazolium ring has a strong influence on the cyclization reaction.

Cyclization is significantly faster than fragmentation at pH's below the pK_a of N_1'. It remains to be seen whether the cHBzT intermediate lies on the reaction pathway to the fragmentation products. If it becomes possible to isolate cHBzT from HBzT, we can determine whether it produces the fragmentation products. An experiment which follows the fragmentation reaction under conditions where significant quantities of cHBzT

are produced is complicated by the very slow rates of fragmentation and cyclization at those pH's. Such a nucleophilic cyclization reaction provided the basis for our nucleophilic fragmentation proposal.

Implications for the Oka Rearrangement

During their studies of HBzT fragmentation in methanol, Oka and coworkers also characterized an unusual rearrangement product (Figure 3-35).[23] We can rationalize that the Oka rearrangement product is the result of a 1,3-sigmatropic migration of the bridging methylene carbon within the enamine form of HBzT. However, we did not isolate any of the rearranged product under the conditions that lead to the fragmentation products in our studies. Since Oka's original experiments involved refluxing methanolic triethylamine mixtures, it is probable that the rearrangement requires additional energy and/or the less polar environment provided by methanol for such a migration to occur.

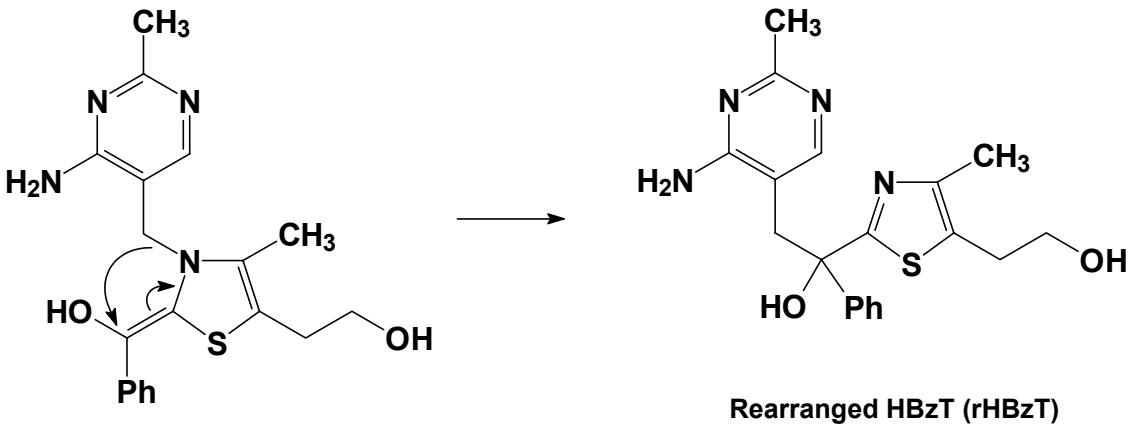

Figure Chapter Three -35: Oka's rearrangement product (rHBzT) isolated during HBzT fragmentation in methanolic triethylamine, showing a 1,3-sigmatropic migration of the methylene carbon in the enamine intermediate.

Implications for Biological Systems

Thiamin catalyzes reactions by stabilizing the generation of the HBzT enamine. This enamine has a lifetime in solution since we see exchange of the $C_{2\alpha}$ proton. Also, the HBzT enamine can be trapped if there are reactive electrophiles present. When Oka and coworkers performed their fragmentation experiments in methanolic triethylamine with an excess of benzaldehyde, they found large amounts of the benzoin condensation product in addition to the fragmentation and rearrangement products.[32] Under conditions where electrophiles are not present, the HBzT enamine can revert to starting materials, or fragment. How can an enzyme prevent the HBzT adduct from fragmenting?

For the enamine to form, the negative charge in the p orbital of the $C_{2\alpha}$ carbon would have to interact with the pi orbital system of the thiazolium ring. This requires that the enol oxygen lie in the same plane as the thiazolium ring's N3 nitrogen, as shown in Figure 3-36. The enzyme can prevent the enamine from forming by freezing the C_2 adduct in a conformation where the negative charge on the $C_{2\alpha}$ carbon cannot interact with the orbitals in the thiazolium ring (Figure 3-37). This is a reasonable explanation for the transient inhibition of benzoylformate decarboxylase by [*p*-(bromomethyl)-benzoyl]-formate (Figure 3-6).[53] In free solution there is no release of bromide since it is likely that the carbanion on the $C_{2\alpha}$ carbon is stabilized as the HBzT enamine. However, in the enzymic system there is a release of bromide ion into solution. This argues that the C_2 adduct is held in a conformation where the $C_{2\alpha}$ carbanion cannot interact with the thiazolium ring. If it interacts with the orbitals of the phenyl ring instead, the result is the elimination of bromide ion.

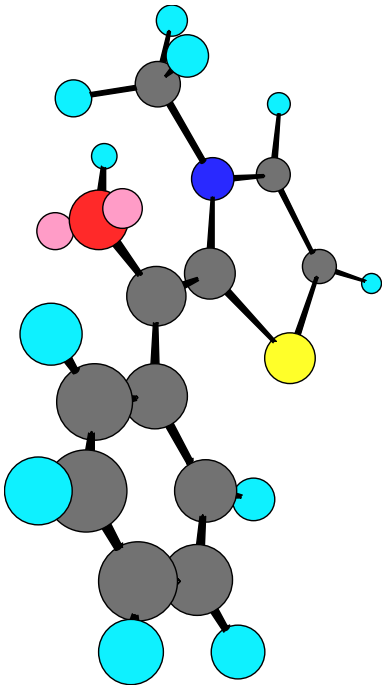

Figure Chapter Three -36: Enamine of thiazolium model compound: 3-methyl-2-(1-hydroxybenzyl)-thiazolium chloride.

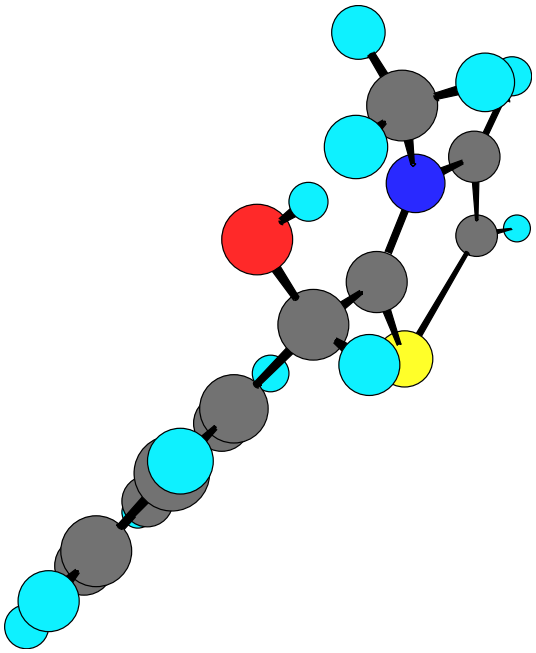

Figure Chapter Three -37: Model of thiazolium compound with phenyl ring held in a conformation where it would not be possible to form a conjugated enamine upon removal of the $C_{2\alpha}$ proton.

Conclusions

We have presented a detailed mechanism for fragmentation of HBzT that fully explains the variety of curvatures in the pH-Rate profile (Figure 3-20). Our mechanism describes fragmentation as occurring via two low barrier pathways from the N_1' protonated species, and via a single higher barrier pathway from the N_1' unprotonated species. Both of the low barrier pathways intersect at a common intermediate: IH_2' in Figure 3-21. This intermediate breaks down to form the fragmentation products faster than any reverse reaction can occur. The choice of the pathway that leads to this key intermediate is controlled by the pH of the reaction medium. At pH 7.0, the rates of fragmentation via the two pathways are equal. At pH's below 7.0, the pathway via IH_3 in Figure 3-21 is dominant. The other route is via the IH intermediate in Figure 3-21. This route is second-order in hydroxide at pH's below 5.1 (the pK_a of protonated N_1') and first-order in hydroxide at pH's above 5.1. This explains the change in mechanism that occurs at pH 7.0 since the competing route via IH_3 becomes pH-independent above pH 5.1

The rate of fragmentation via IH can also become pH-independent. This is caused by a change in rate-determining step from the $k_f[H^+]$ step being rate limiting to the k_{-3} step being rate limiting (Figure 3-21). These two rates are equal at pH 7.3. Since the rate of fragmentation via IH becomes pH-independent above this pH, a hydroxide dependent reaction on N_1' unprotonated HBzT becomes the dominant reaction pathway (Figure 3-17).

The change in the product distribution for HBzT from fragmentation products to

elimination products is also explained by our mechanism. The pH-Rate profile for the elimination reaction shows that this reaction is hydroxide catalyzed in the pH region where the product changeover occurs (Figure 2-8). On the other hand, the fragmentation reaction in this same pH region undergoes several transitions: a change in rate determining step, and two changes in mechanism. Therefore, the fragmentation reaction does not increase in rate as fast as the elimination reaction does in this pH region. This results in the fragmentation reaction changing from being the kinetically dominant reaction to being a minor reaction in this pH region (Figure 2-10).

NMHBzT fragments by the same mechanism as HBzT, but only one of the two low barrier pathways dominates its reaction. Our HBzT mechanism for fragmentation stipulates that the relative free energies of the IH_3 and IH intermediates are responsible for the choice of the fragmentation pathway. The NMHBzT pH-Rate profile lacks the complex curvature present in the HBzT pH-Rate profile, implying that a single mechanism with a common rate-determining step is operating. To explain this observation, we provide reasons that explain why the pK_a of the enamine's enolic proton in NMHBzT would be lower than the same proton in HBzT. This perturbation lowers the free energy of IH_3 relative to IH. Therefore, the majority of the fragmentation reaction occurs by the IH_3 pathway. Fragmentation via this pathway is first order in hydroxide at all pH's in our NMHBzT study. This is due to NMHBzT's lack of a dissociable proton on N_1' that leads to the saturation in the rate of fragmentation of HBzT.

Chapter Four : REFERENCES

[1] Kim, C.; Kluger, R.; Lam, J.F. Bioorg. Chem. 1993, 21, 275-283.

[2] Crane, E.J.; Washabaugh, M.W. Bioorg. Chem. 1991, 19, 351-368.

[3] Bantle, G.; Mieyal, J.J.; Rosner, I.A.; Sable, H.Z.; Votaw, R.G. J. Biol. Chem. 1971, 246, 5213.

[4] Breslow, R.; Kool, E. Tetrahedron Lett. 1988, 29, 1638-1638.

[5] Diederich, F.; Lutter, H. J. Am. Chem. Soc. 1989, 111, 8438-8446.

[6] Lapworth A., J. Chem. Soc. 1903, 83, 995.

[7] Breslow, R. J. Am. Chem. Soc. 1958, 80, 3719-3726.

[8] Breslow, R. J. Am. Chem. Soc. 1957, 79, 1762.

[9] Kluger, R. Chem. Rev. 1987, 87, 863-876.

[10] Stetter, H. Angew. Chem. Int. Ed. Engl. 1976, 15, 639-712.

[11] Seebach, D. Angew. Chem. Int. Ed. Engl. 1979, 18, 239-336.

[12] Bantle, G.; Mieyal, J.J.; Rosner, I.A.; Sable, H.Z.; Votaw, R.G. J. Biol. Chem. 1971, 246, 5213.

[13] Bordwell, F.G.; Chung, A.C.; Jordan, F.; Rios, C.B.; Satish, A.V. J. Am. Chem. Soc. 1990, 112, 792-797.

[14] Barletta, G.; Huskey, W.P.; Jordan, F. J. Am. Chem, Soc. 1992, 114, 7607-7608.

[15] Jordan, F.; Kudzin, Z.H.; Rios, C.B. J. Am. Chem. Soc. 1987, 109, 4415-4416.

[16] Stivers, J.T.; Washabaugh, M.W. Bioorg. Chem. 1991, 19, 369-383.

[17] Reference 2, pp. 353-4.

[18] Jencks, W.P. Acc. Chem. Res. 1976, 9, 425.

[19] Jencks, W.P.; Washabaugh, M.W. Biochemistry 1988, 27, 5044-5053.

[20] Reference 9, pp. 865-7.

[21] Chiang, Y.; Dahlberg, D.B.; Kresge, A.J.; Lin, A.C. J. Am. Chem. Soc. 1983, 105, 5380-5386.

[22] Hirano, H.; Kishimoto, S.; Oka, Y. Chem. Pharm. Bull. 1970, 18, 527-533.

[23] Hirano, H.; Kishimoto, S.; Oka, Y. Chem. Pharm. Bull. 1970, 18, 534-541.

[24] Buchman, E.R.; Ruehle, A.E.; Williams, R.R. J. Am. Chem. Soc. 1935, 57, 1093-1095.

[25] Williams, R.R. J. Am. Chem. Soc. 1936, 58, 1063-1064.

[26] Buchman, E.R.; Keresztesy, J.C.; Waterman, R.E.; Williams, R.R. J. Am. Chem. Soc. 1935, 57, 536-537.

[27] Kauffman, G.M.; Zoltewicz, J.A. J. Am. Chem. Soc. 1977, 99, 3134.

[28] Baugh, T.D.; Zoltewicz, J.A. Synthesis 1980, 217-218.

[29] Celotto, C.; Ibovnik, A.; Uray, G.; Zoltewicz, J.A. J. Org. Chem. 1989, 54, 3941-3945.

[30] Stirling, C.J.M. Acc. Chem. Res. 1979, 12, 198-203.

[31] Jencks, W.P. Chem. Rev. 1972, 72, 705-718.

[32] Hirano, H.; Kishimoto, S.; Oka, Y. Chem. Pharm. Bull. 1970, 18, 527-533.

[33] Bergel, F.; Todd, A.R. J. Chem. Soc. 1937, 1504-1509.

[34] Glasoe, P.K.; Long, F.A. J. Phys. Chem. 1960, 64, 188.

[35] Stivers, J.T.; Washabaugh, M.W. Bioorg. Chem. 1991, 19, 369-383.

[36] Stivers, J.T.; Washabaugh, M.W. Bioorg. Chem. 1992, 20, 155-172.

[37] Hickey, K.A.; Stivers, J.T.; Washabaugh, M.W. J. Am. Chem. Soc. 1994, 116, 7094-7097.

[38] Hirai, E.; Mizukami, S. J. Org. Chem. 1966, 31, 1199-1202.

[39] Lam, J.F.; M.Sc. Thesis; University of Toronto, 1993.

[40] Eigen, M. Angew. Chem. Int. Ed. Engl. 1964, 3, 1-19.

[41] Bernasconi, C.F. Acc. Chem. Res. 1987, 20, 301-308.

[42] Bednar, R.A.; Jencks, W.P. J. Am. Chem. Soc. 1985, 107, 7126.

[43] Reference 40, pp. 4-6.

[44] Garcia, G.A.; Kenyon, G.L.; Kozarich, J.W.; Reynolds, L.J. Biochemistry 1988, 27, 5530-5538.

[45] Dirmajer, L.J.; Garcia, G.A.; Kenyon, G.L.; Kozarich, J.W. J. Am. Chem. Soc. 1986, 108, 3149-3150.

[46] Chiang, Y.; Kresge, A.J. Science 1991, 253, 395-400.

[47] Hine, J.; Koser, G.F. J. Org. Chem. 1971, 36, 3591-3593.

[48] Doweyko, A.M.; Hall, S.S.; Jordan, F. J. Am. Chem. Soc. 1976, 98, 7460-7461.

[49] Doweyko, A.M.; Hall, S.S.; Jordan, F. J. Am. Chem. Soc. 1978, 100, 5934-5939.

[50] Hamashima, Y.; Hirai, K.; Ishiba, T.; Matsumoto, S.; Takamizawa, A. Chem. Pharm. Bull. 1968, 16, 1210.

[51] Karimian, K.; Risinger, G.E. Org. Prep. Proced. Int. 1978, 10, 45.

[52] Hansch, C.; Kim, K.H.; Leo, A.; Lien, E.J.; Nikaitani, D.; Unger, S.H. J. Med. Chem. 1973, 16, 1207-1216.

[53] Dirmajer, L.J.; Garcia, G.A.; Kenyon, G.L.; Kozarich, J.W. J. Am. Chem. Soc. 1986, 108, 3149-3150.

[54] Bell, R.P. The Proton in Chemistry; Cornell University Press: New York, 2nd Edition; 1972.